POLITECNICO DI TORINO
Repository ISTITUZIONALE

Measurement techniques for microbial corrosion assessment

Original
Measurement techniques for microbial corrosion assessment / Iannucci, Leonardo. - (2019 Dec 17), pp. 1-112.

Availability:
This version is available at: 11583/2774812 since: 2019-12-19T15:42:55Z

Publisher:
Politecnico di Torino

Published
DOI:

Terms of use:
openAccess

This article is made available under terms and conditions as specified in the corresponding bibliographic description in the repository

Publisher copyright

(Article begins on next page)

05 August 2020

ScuDo
Scuola di Dottorato ~ Doctoral School
WHAT YOU ARE, TAKES YOU FAR

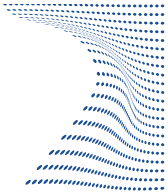

Doctoral Dissertation
Doctoral Program in Metrology (32nd cycle)

Measurement techniques for microbial corrosion assessment

Leonardo Iannucci
* * * * * *

Supervisors
Prof. Sabrina Grassini, Supervisor
Prof. Marco Parvis, Co-supervisor

Doctoral Examination Committee:
Prof. Gregorio Andria, Referee, Politecnico di Bari, Italy
Prof. Salvatore Baglio, Referee, Università degli Studi di Catania, Italy
Prof. Emma Angelini, Politecnico di Torino, Italy
Prof. Lorenzo Ciani, Università degli Studi di Firenze, Italy
Prof. Guido Perrone, Politecnico di Torino, Italy

Politecnico di Torino
December 17, 2019

This thesis is licensed under a Creative Commons License, Attribution - Noncommercial-NoDerivative Works 4.0 International: see www.creativecommons.org. The text may be reproduced for non-commercial purposes, provided that credit is given to the original author.

I hereby declare that, the contents and organization of this dissertation constitute my own original work and does not compromise in any way the rights of third parties, including those relating to the security of personal data.

. . . . . .

Leonardo Iannucci
Turin, December 17, 2019

Summary

This dissertation presents a research work related to innovative measurement approaches to study microbial corrosion. Microbial corrosion, also known as MIC (Microbiologically Influenced Corrosion), is an electrochemical process in which microorganisms are able to promote metals degradation. The main motivations for this research are related to the great relevance of this form of corrosion in many industrial applications and to the lack of specific laboratory methodologies to study it. Actually, even if electrochemical measurements can give an important insight on the involved mechanisms, traditional experimental setups for corrosion tests often are not able to reproduce conditions found in a real environment and thus the obtained results can often be not representative for a real application.

This topic has been addressed from a dual perspective: a new experimental setup specifically tailored for microbial corrosion testing has been proposed, then an imaging system to assess the effects of bacteria on sample surface has been developed. The main innovation in the new methodology is related to the use of Microbial Fuel Cells (MFCs) as environment to carry out the test. Actually they can be conveniently used to perform the experiment in controlled conditions, monitoring many of the test parameters simply measuring the current flows in the MFC. Because of this, an *ad-hoc* measuring system has been developed in order to monitor the experiment. Thanks to this new setup, the corrosion resistance of different metals can be compared, providing useful information to researchers. Moreover, one of the main advantages is that using MFCs it is possible to carry out an accelerated test without the risk of altering the microorganisms metabolism. Finally, biofilm formation on sample surface, an important information but difficult to obtain from other electrochemical techniques, can be monitored in continuum during the test.

The imaging algorithm that has been developed can be used at the end of a corrosion test in order to assess the bacteria attachment on sample surface. Using imaging techniques can be of great interest because they can provide information that can not be derived from other measurements. The main innovation in the proposed algorithm is given by the use of micrographs taken at Scanning Electron Microscope (SEM) to assess biofilm coverage. Actually, using this instrument, staining techniques are no more required and sample preparation is easier. Manifold information can be derived from the micrographs analysis, such as number of bacteria aggregates on sample surface and

their dimensional distribution.

This research work has been completed with two studies: one concerning the use of electrochemical measurements to investigate the microbial corrosion resistance of stainless steel in hypersaline environment and the other related to the characterization of innovative hybrid coatings for corrosion protection. The former aims at showing the reader an overview of electrochemical measurements and morphological characterizations used in the microbial corrosion field, presenting a real case study. It has been inserted in the same chapter where the new technique is presented in order to give a comprehensive picture of the current methodologies and of the possible ways to innovate them. Then, in the final part of the dissertation, the characterization of innovative hybrid coatings is presented. They represent one of the possible strategies to protect metals from microbial corrosion; in particular, the bacteriostatic effect of silver nanoparticles has been investigated. This characterization uses both traditional electrochemical techniques and some of those presented in this dissertation, in order to show their application.

Thus, the objective of the research work presented in this dissertation is to propose new tools to study microbial corrosion. It has been pursued developing a new experimental setup to perform corrosion tests and an imaging algorithm to characterize the material at the end of it. Future work could further investigate the possibility of having different setup for the MFCs. For example, a configuration using a dual chamber MFC could be developed, so that different conditions can be established during the test.

Acknowledgements

I would like to thank the European Federation of Corrosion (EFC) for awarding me the *EUROCORR Young Scientist Grant*. It financially supported the research period carried out in Toulouse at CNRS - Laboratoire de Génie Chimique. I also express my gratitude to Dr. Régine Basséguy for hosting me in her research group and for her support during the research activities.

I am also grateful to Dr. Pierangela Cristiani for the collaboration on the topics related to microbial corrosion and her support for the experiments involving microbial fuel cells.

Part of the study on the characterization of hybrid organic coatings was carried out in the framework of the Joint Project for the internationalization of Research between Italy and Colombia, financially supported by Politecnico di Torino and Compagnia di San Paolo (Torino, Italy), in cooperation with the Antonio Nariño University (Bogotá, Colombia).

Contents

List of Tables ix

List of Figures x

Preface xv

1 Introduction 1
- 1.1 Brief introduction on microbial corrosion . . . 1
- 1.2 Electrochemical techniques for microbial corrosion . . . 6
- 1.3 Microscopy and imaging techniques for microbial corrosion . . . 10

2 Electrochemical methods for microbial corrosion assessment 17
- 2.1 Introduction . . . 17
- 2.2 Electrochemical characterization of stainless steel in hypersaline solution 17
  - 2.2.1 Materials and methods . . . 18
  - 2.2.2 Results and discussion . . . 20
  - 2.2.3 Conclusions . . . 30
- 2.3 A novel approach for microbial corrosion assessment . . . 33
  - 2.3.1 Experimental setup . . . 34
  - 2.3.2 Measuring system . . . 35
  - 2.3.3 Experimental results . . . 38
  - 2.3.4 Conclusions . . . 46
- 2.4 Conclusions . . . 47

3 An imaging system for microbial corrosion assessment 49
- 3.1 Introduction . . . 49
- 3.2 Contours detection imaging algorithm for SEM images . . . 50
  - 3.2.1 Image acquisition . . . 50
  - 3.2.2 Image brightness and contrast normalization . . . 51
  - 3.2.3 Bacteria identification . . . 53
- 3.3 Application to metallic samples . . . 54
- 3.4 Application to non-conductive samples . . . 58

3.5 Conclusions 65

4 Hybrid organic coatings for corrosion prevention 67
4.1 Introduction 67
4.2 Materials and methods 67
4.3 Results and discussion 69
4.3.1 Electrochemical characterization 70
4.3.2 Morphological characterization 76
4.3.3 Antimicrobial behaviour of Ag-doped organic coatings 77
4.4 Conclusions 83

5 Conclusions 85

Bibliography 87

List of Tables

1.1 Summary of possible electrochemical techniques to study microbial corrosion . . . 11
1.2 Summary of possible microscopy techniques to study microbial corrosion. 14
2.1 Chemical composition of the Stainless Steels used in the study 18
2.2 Chemical composition of the electrolytic solution 19
2.3 Results from imaging analysis using epifluorescence microscopy micrographs. 26
3.1 Electrolytic Solutions Composition 55
3.2 Results from image processing of micrographs showed in Fig. 3.2. . . . 61
3.3 Results from image processing obtained for samples immersed in Artificial seawater and in Starkey medium. 61
4.1 R_{ct} and CPE_{Cdl} values obtained by fitting the impedance spectra by the equivalent circuit model of Fig. 4.3 73
4.2 R_{ct} and CPE_{Cdl} values obtained by fitting the impedance spectra by the equivalent circuit model of Fig. 4.3 79

List of Figures

1.1 Scheme showing the different stages of biofilm growth: a) Conditioning film forms on the substrate b) Planktonic bacteria attach on substrate, become sessile and produce EPS to anchor to the surface c) Bacteria form colonies d) Micro-colonies grow and biofilm thickness increases e) Portions of the biofilm detach from the surface f) The exposed areas are colonised by other planktonic bacteria 3
1.2 Equivalent circuit model for fitting EIS Spectra. 8
2.1 Open Circuit Potential (OCP) measurements carried out during the test: a) AISI 304 samples with inoculum b) AISI 316 samples with inoculum c) Comparison of AISI 304 samples with and without inoculum d) Comparison of AISI 316 samples with and without inoculum. 21
2.2 Bode plots recorded on the AISI 304 stainless steel sample immersed in Starkey Medium inoculated with salt marsh sediments. 23
2.3 Trend of the impedance modulus at 10^{-2} Hz measured on AISI 304 (a) and AISI 316 (b) samples. 24
2.4 Bode plots recorded on the AISI 316 stainless steel sample immersed in Starkey Medium inoculated with salt marsh sediments. 25
2.5 Bode plots recorded on the AISI 304 (a) and AISI 316 (b) samples immersed in Starkey Medium without inoculum. 26
2.6 Cyclic Voltammetry measurements performed on AISI 304 (a) and AISI 316 (b) samples immersed in Starkey Medium inoculated with salt marsh sediments. 27
2.7 Trend of the inverse of the polarization resistance for AISI 304 and AISI 316 samples. 28
2.8 Micrographs for AISI 304 (a) and AISI 316 (b) samples taken using epifluorescence microscopy on the left and identified bacteria using the imaging algorithm on the right. Bacteria clusters having dimension above 200 μm^2 are labelled in red, otherwise in green. 29
2.9 SEM micrographs taken on AISI 304 before (a) and after (b) removing the biofilm. Yellow arrows highlight the presence of bacteria. 30
2.10 SEM micrographs taken on AISI 316 before (a) and after (b) removing the biofilm. Yellow arrows highlight the presence of bacteria. 31

2.11 SEM micrographs taken on AISI 304 (a) and AISI 316 (b) samples after immersion in abiotic Starkey Medium. 32
2.12 Picture of the Single Chamber Microbial Fuel Cell: a Pyrex®bottle of 0.125 L volume equipped with the air-breathing cathode on the opening on the left side, the anode connected through the small opening on the right side and the big opening on the top for positioning the sample electrode. [28] 36
2.13 Block diagram of the measuring system: the SCMFC with the carbon cloth anode, the air-breathing cathode and the sample as the third electrode; the three resistors, the LM35 temperature sensor and the Digital Acquisition board (DAQ) connected to a PC. [28] 36
2.14 Current evolution in the microbial fuel cell during a test performed on a mild steel sample for 14 hours. I_A, I_C and I_S trends as a function of time are shown. The microbial corrosion attack starts immediately after the exposure of the sample to the electrolyte, as confirmed by the immediate increase of all current values (as can be observed in the expanded plot). [28] 40
2.15 FESEM image of the mild steel surface after 1 day of immersion in the operating SCMFC. Red arrows indicate cracks at grain boundaries, green ones biofilm and yellow ones highlight the presence of sulphides. The test results are shown in Fig. 2.14 41
2.16 Current evolution in the microbial fuel cell during a test performed on an AISI 304 sample for 17 days. 42
2.17 I_S trend as a function of time recorded in the same test of Fig. 2.16; the current values are normalized to the surface area of 1 cm^2. I_S increases after any addition of acetate highlighting the bacteria activity on the sample surface. [28] 43
2.18 Currents sum (I_A + I_S + I_S) from the test in the SCMFC of Fig. 2.16 and temperature trend during the experiment. 43
2.19 SEM images of the AISI 304 sample surface after 17 days of immersion in the operating SCMFC. 44
2.20 Bode plots recorded on the AISI 304 stainless steel sample immersed in the electrolytic solution containing the bacteria inoculum for three weeks. [28] 45
2.21 SEM images of the AISI 304 sample surface after the test in the operating SCMFC (on the left) and after the immersion test (on the right). [28] . . 46
3.1 SEM image of a metallic surface affected by microbial corrosion (on the left) and identified elements on the micrograph (on the right): polishing lines are highlighted in yellow, single microorganisms attached on the surface are labelled with green arrows, larger bacteria clusters are identified by red circles and salt crystals by blue circles. 56

3.2 Results from the image processing for a sample immersed in Starkey Medium (on the left) and in Artificial Seawater (on the right). Bacteria clusters having dimension above 200 μm^2 are labelled in red, otherwise in green. 59
3.3 Histograms showing dimensional distribution (expressed as agglomerate area) for the samples immersed in Starkey medium (a) and artificial seawater (b). 60
3.4 Value and uncertainty for different parameters related to bacteria attachment on stainless steel samples after immersion in Starkey Medium (S) and artificial seawater (M). 60
3.5 SEM micrograph of a metallic sample (on the left) and of a polymeric sample (on the right) after immersion in a solution containing bacteria. Microorganisms are pointed out with circles. 62
3.6 Results from the image processing for a metallic sample (on the left) and a polymeric sample (on the right). 64
4.1 Picture of the samples under study: A) Steel without coating B) Epoxy coating C) Epoxy coating with addition of silica nanoparticles D) Epoxy coating with addition of graphene oxide nanoplatelets E) Epoxy coating with addition of silver nanoparticles. 70
4.2 Bode plots recorded on the three typologies of coating after 24 hours and 96 hours of immersion in 0.1 M NaCl aerated solution 71
4.3 Equivalent circuit model used for fitting the EIS spectra. 72
4.4 Nyquist plots recorded on the different coatings after 96 hours of immersion in 0.1 M NaCl solution and results from fitting: a) Epoxy coating b) Epoxy coating + 15 wt% of TEOS c) Epoxy coating + 30 wt% of TEOS d) Epoxy coating + 0.05 wt% of graphene oxide e) Epoxy coating + 1 wt% of $AgSbF_6$ f) Epoxy coating + 3 wt% of $AgSbF_6$ 74
4.5 SECM measurement on a) Epoxy-TEOS and b) Epoxy-Graphene Oxide coatings after 1 hour and 48 hours. [71] 75
4.6 FESEM micrographs of the Epoxy-TEOS coating as deposited (on the left) and after 96 hours of immersion in 0.1 M NaCl aerated solution in the electrochemical cell used for the EIS measurements (on the right). [71] 77
4.7 Silver-Epoxy nanocomposite (1wt% $AgSbF_6$) after 96 hours of immersion in the 0.1 M NaCl solution. 78
4.8 Nyquist plots recorded on the different coatings after 240 hours of immersion in raw wastewater and results from fitting: a) Epoxy coating b) Epoxy coating + 1 wt% of $AgSbF_6$ c) Epoxy coating + 3 wt% of $AgSbF_6$. 79
4.9 Bode plots recorded on the coatings containing silver nanoparticles during immersion in raw wastewater: a) Epoxy coating b) Epoxy coating + 1 wt% of $AgSbF_6$ c) Epoxy coating + 3 wt% of $AgSbF_6$ 80

4.10 SEM micrographs showing samples surface after immersion in raw wastewater: a) Epoxy coating b) Epoxy coating + 1 wt% of $AgSbF_6$ c) Epoxy coating + 3 wt% of $AgSbF_6$. 82
4.11 SEM micrographs and identified bacteria on three samples after immersion in wastewater: a) Epoxy coating b) Epoxy coating + 1 wt% of $AgSbF_6$ c) Epoxy coating + 3 wt% of $AgSbF_6$. 83
4.12 Histograms showing dimensional distribution of bacteria aggregates on different samples: a) Epoxy coating b) Epoxy coating + 1 wt% of $AgSbF_6$ c) Epoxy coating + 3 wt% of $AgSbF_6$. 83

Preface

This PhD thesis addresses the topic of microbial corrosion from the perspective of new possible measurement approaches to study this phenomenon. Motivations for this research work can be found in the lack in scientific literature of specific methodologies to study this kind of corrosion, despite its importance in many environments and industrial applications.

The introductory chapter presents a state of the art about the most important electrochemical and imaging techniques commonly used in the field of microbial corrosion. In Chapter 2, a new experimental setup to perform microbial corrosion tests is proposed. An in-depth description of the system is provided, presenting also the results from the characterization of two different materials. Then, a second contribution of this PhD thesis is the development of an imaging algorithm to assess the effects of bacteria attachment after a corrosion test and it is described in Chapter 3. Also in this case, the proposed system has been used in different case studies to show the results that can be obtained. Eventually, in Chapter 4 the characterization of coatings for corrosion protection is presented.

Chapter 1 - This chapter provides an overview of the different methodologies used to study microbial corrosion. After a brief introduction on microbial corrosion, electrochemical and imaging techniques used for the study of this phenomenon are reviewed.

Chapter 2 - This chapter deals with electrochemical methods to assess microbial corrosion. In the first part, a case study concerning the characterization of two stainless steels is presented. It makes use of both electrochemical techniques and morphological characterizations in order to show how they are applied in the field of microbial corrosion. The second part of the chapter describes a new technique, proposed for the assessment of microbial corrosion behaviour of different metallic alloys.

Chapter 3 - This chapter presents the development of an imaging algorithm to assess the effects of microbial corrosion both on metallic surfaces and non-conductive samples.

Chapter 4 - This chapter reports the characterization of different typologies of hybrid coatings for corrosion protection, using some of the methodologies presented in the previous chapters.

Chapter 5 - This last chapter summarises the results obtained during the study, reporting the main contributions to the development of new measurements techniques for microbial corrosion.

Chapter 1

Introduction

This dissertation focuses on the development of new techniques to assess microbial corrosion, a degradation process that can affect metals in many industrial and biomedical applications. Even though this corrosion phenomenon has been studied since the beginning of last century [1], only in last decades the questions arising from this topic have been addressed using a real interdisciplinary approach. In this way, it has been possible to combine knowledge and expertise from different disciplines like biology, electrochemistry and material science to reach a deeper understanding of the mechanisms underlying microbial corrosion. At the same time, in scientific literature there is a lack of methodologies specifically tailored for this corrosion phenomenon, so this is one of the motivations for this research work.

The research was carried out focusing both on electrochemical methods and imaging techniques. For this reason, in this Chapter a general overview about microbial corrosion will be provided, giving then a deeper insight on electrochemical measurements and imaging tools used to study microbial corrosion.

1.1 Brief introduction on microbial corrosion

Corrosion can be defined as an electrochemical process in which a metal undergoes degradation when in contact with the environment [2]. It is a spontaneous process, because for most of the metallic elements the oxidised form is thermodynamically more stable than the reduced one. For this reason, gold is one of the few metals that can be found in the reduced form during mining, while usually metal ores are found [3].

The electrochemical processes involving corrosion can be described as the coupling of an anodic reaction, which is represented by the metal dissolution, and a cathodic reaction consuming the electrons coming from the metal [2]. These reactions can change depending on the material and on the environment, but a general classification of the main corrosion forms can be presented as follows:

- *uniform corrosion*, when the reactions proceed uniformly over the material surface. It can be easily assessed and the corrosion rate can be quantified in order to program proper maintenance.
- *localised corrosion*, when a specific part of the component or of the microstructure is preferentially attacked. This is the most dangerous corrosion form, because often it is difficult to detect and it can lead to catastrophic failures. Different types of corrosion can be classified under this category: galvanic corrosion, crevice corrosion, pitting, erosion corrosion and stress corrosion cracking.

Microbial corrosion can be generally classified as a form of localised corrosion. It is referred to also using expressions like 'Microbiologically Influenced Corrosion' (MIC), 'Microbiologically Induced Corrosion' or 'Biocorrosion' [3]. It can be defined as *an electrochemical process whereby microorganisms may be able to initiate, facilitate or accelerate a corrosion reaction through the interaction of the three components that make up this system: metal, solution and microorganisms* [4]. In particular, bacteria are able to change the interaction occurring at the interface between the metal and the electrolytic solution. Actually, colonization of any surface by bacteria can be described as an accumulation process, where microorganisms floating in the solution (planktonic population) adhere to the substrate, remaining attached on it and becoming 'sessile'. In the first stage, a conditioning film having a thickness of 20 nm - 80 nm is formed. It is composed of inorganic ions and organic compounds, which are able to change the surface electrical double layer and its wettability, promoting the following colonization. Bacteria start to attach on substrate surface, adhering to it thanks to the production of exopolysaccharidic substances (EPS), which will become the matrix of the biofilm. Increasing the immersion time in the solution, microbial growth leads to the formation of colonies, that expand on the surface forming a continuous biofilm. It is a gel containing about 95% of water and a matrix of exopolysaccharidic substances (EPS), where microbial cells and inorganic detritus are trapped in. Biofilm is able to alter the chemical reactions and the transport phenomena occurring on the biofouled surface, for example hindering the oxygen diffusion to the substratum. After this point, portions of biofilm can detach from the surface, but they are subsequently replaced by other planktonic microorganisms [3]. A scheme of the different stages representing bacteria colonization of a surface is shown in Fig. 1.1.

In natural environments, biofilm is composed not only by a single strain of bacteria, but by a consortium of bacteria. This is an important feature, because microorganisms can organise themselves developing behaviours that enables them to survive also in hostile environments [5]. An example of this ability is given by the Quorum Sensing, that is a mechanism of communication among microorganisms to coordinate their behaviour.

Biofilm can enhance the corrosion process through different mechanisms [6]:

- *Alteration of the transport of chemical species from or towards the metal surface*: metabolites produced by bacteria can accumulate near the metal and diffusion of

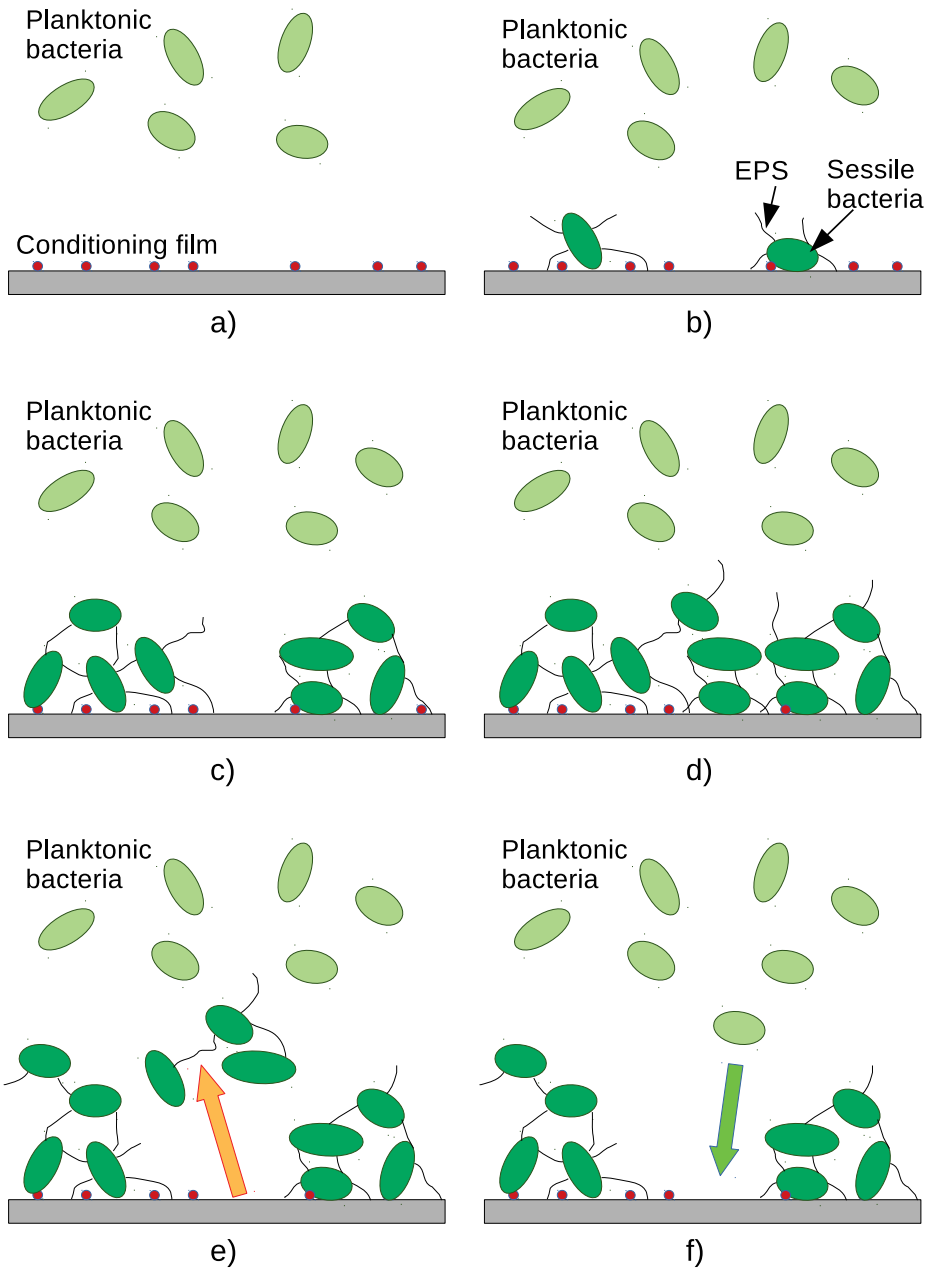

Figure 1.1: Scheme showing the different stages of biofilm growth: a) Conditioning film forms on the substrate b) Planktonic bacteria attach on substrate, become sessile and produce EPS to anchor to the surface c) Bacteria form colonies d) Micro-colonies grow and biofilm thickness increases e) Portions of the biofilm detach from the surface f) The exposed areas are colonised by other planktonic bacteria

compounds present in solution, such as nutrients or even biocides, can be hindered.

- *Facilitating the removal of protective films when the biofilm detaches*: bacteria can be entrapped in a superficial layer of corrosion products, which could detach together with the biofilm, exposing again the metal surface.
- *Inducing differential aeration effects as a consequence of a patchy distribution of the biofilm*: oxygen diffusion can be hindered by the biofilm (even with thickness of about 12 μm), so anodic sites form in areas covered by bacteria, while the other become preferentially cathodic.
- *Changing oxidation–reduction conditions at the metal–solution interface*: redox conditions can vary from bulk solution to the metal-biofilm interface because of respiration and metabolism of sessile microorganisms.
- *Altering the structure of inorganic passive layers and increasing their dissolution and removal from the metal surface*: microbial consortia can cause depassivation of the metal surface, increasing the corrosion rate of the material.

Environments in which metals can be affected by microbial corrosion include: oil and gas industry, water systems, human body, seawater, nuclear waste storage facilities, aviation fuel systems and heat exchangers [5]. Then, different are the bacteria strains involved in microbial corrosion. The most common and widely studied are: Sulfate Reducing Bacteria (SRB), Nitrate Reducing Bacteria (NRB), Acid Producing Bacteria (APB), Metal Oxidizing Bacteria (MOB), Iron Oxidizing Bacteria (IOB), methanogens, fungi and archea [7].

Electrochemical processes leading to microbial corrosion can be classified taking into account the presence of oxygen in the electrolytic solution and the mechanism used by bacteria to oxidise the metal. In anaerobic environment, the two main mechanisms are the extracellular electron transfer MIC (EET-MIC) and the metabolite MIC (M-MIC) [7–9]. In the former case, the microbes use iron as the electron donor according to the reaction:

$$Fe^0 \longrightarrow Fe^{2+} + 2\ e^- \tag{1.1}$$

This reaction occurs extracellularly, then the electrons are transported to the cytoplasm, where the reduction reaction can be catalysed by enzymes [7, 8]. In the absence of oxygen the final electron acceptor can be represented by sulfate or nitrate ions:

$$SO_4^{2-} + 9\ H^+ + 8\ e^- \longrightarrow HS^- + 4\ H_2O \tag{1.2}$$

$$NO_3^- + 8\ e^- + 10\ H^+ \longrightarrow NH_4^+ + 3\ H_2O \tag{1.3}$$

$$2NO_3^- + 10\ e^- + 12\ H^+ \longrightarrow N_2 + 6\ H_2O \tag{1.4}$$

An important parameter is also the availability of carbon source. Actually microbes need only a small amount of iron for their enzyme activities so, if available, they preferentially use organic carbon as electron donor, which can be exploited more easily. Thus, in case of carbon source starvation in the environment, corrosion rate can increase [10].

The second type of microbial corrosion in anaerobic environment is represented by Metabolite-MIC. In this case, microbes like Acid Producing Bacteria are able to secrete corrosive metabolites such as organic acids [7, 8]. Proton reduction does not need biocatalysis by microbes, so the corrosion reactions proceeds as in abiotic conditions:

$$2\ H^+ + 2\ e^- \longrightarrow H_2 \tag{1.5}$$

while the anodic reaction is represented by 1.1.

Taking in account microbial corrosion in aerobic environment, it is possible to recognize three main processes: oxygen concentration cell, corrosion induced by Iron Oxidizing Bacteria and secretion of corrosive metabolites. In the former case, aerobic bacteria in the outer part of the biofilm are able to consume the available oxygen, creating anaerobic conditions on the metal surface. If other parts of the material are not covered by biofilm, or it has a lower thickness, differential aeration can increase the corrosion rate: areas with lower oxygen concentration become preferentially anodic, while the other cathodic. Iron Oxydizing Bacteria are aerobic microorganisms that can be found in oilfield produced water. They are able to induce corrosion on steel oxidizing the ferrous iron to ferric iron, using oxygen as the final oxygen acceptor. Finally, secretion of corrosive metabolites is a further mechanism. Some bacteria, such as the Acetobacter, are able to oxidise ethanol to acetic acid during fermentation in presence of oxygen. Moreover, fungi can secrete organic acids during their growth, leading to biodeterioration of both metals and other materials [7, 8, 11].

One of the main issues in the study of microbial corrosion is also represented by the need of realistic experimental conditions in laboratory tests [12]. Actually, many factors can influence the experiment results, and often one of the main difficulties is represented by the choice of test conditions that can really simulate the 'real world'. First of all, often tests are carried out using single bacteria strains, but this is unlikely to simulate the complex microbial communities found in the environment. Single bacteria strains can be useful to investigate a specific corrosion mechanism, but the results will be hardly representative for the real conditions. As mentioned above, microorganisms behaviour changes when collaborative mechanisms like *quorum sensing* are established. Then, the test medium i.e. the electrolytic solution can select the proliferation of specific bacteria strains or promote a particular metabolism related to MIC. Presence of nutrients, such as the level of carbon sources or iron ions, can strongly influence the corrosion rate. Moreover, often in a real environment the nutrients concentration is not constant, but periods of starvation occur; this condition is not easily replicated in a laboratory setup. Then, test media can influence also the abiotic corrosion processes. Because of this, tests in sterile conditions are always needed in order to understand the real effect of microorganisms [12].

Other important parameters are represented by oxygen concentration inside the solution and test temperature. Bacteria can be divided in three categories depending on the terminal electron acceptor in their respiration process. [13] If they can use only oxygen, they are called aerobes. If they can not use oxygen as terminal electron acceptor, they are anaerobes, while facultative anaerobes are those that can use also other species as terminal electron acceptor. Then, temperature plays an important role because bacteria activity is enhanced by higher temperatures, but at the same time each bacteria strain has an optimal growth temperature. Thus, even when using a mixed inoculum, that is an inoculum containing different bacteria strains, the choice of the temperature will affect the type of microorganisms that will proliferate in the solution [3]. Moreover, if real environmental conditions should be replicated, it should be taken in account that temperature oscillations are always present and this will have also impact the test conditions. Finally, another important choice when designing an experiment is between batch or flow conditions. In the former case, stagnation is simulated, while the other case is representative of systems like heat exchangers, pipelines or ship hulls.

Case studies on microbial corrosion can be found related to different metals. Mild steel is probably one of the most widely studied materials in the field, because of the large number of applications in which it is used [5]. Other important research studies have been carried out on stainless steels, due to their applications in marine environment, where MIC is one of the most important risks as far as corrosion is concerned. Moreover, even if copper and its alloys are generally believed to have a good resistance against MIC, different studies demonstrated the presence of bacteria strains (e.g. Thiobacillus thiooxidans) with a relatively high tolerance to copper ions [3].

This general overview presented the main features that characterize microbial corrosion and the most important issues encountered in the study of this phenomenon. Following sections will focus on methodologies used in this field.

1.2 Electrochemical techniques for microbial corrosion

Electrochemical techniques are widely used to study corrosion phenomena both during laboratory tests and in-situ monitoring of materials. They can be used to derive information about reactions occurring on the metal, about the surface reactivity or the corrosion rate. Multiple advantages can derive from the use of such techniques; actually they can provide real time information about the ongoing processes and some of them, being non-destructive, can be used to assess the conservation state of a component without altering its conditions. It is possible to divide electrochemical techniques for microbial corrosion in two main categories: the traditional ones, employed also for the other corrosion phenomena, and specific setup designed to study MIC. In the first group it is possible to list: Open Circuit Potential (OCP), Linear Polarization Resistance

(LPR), polarization curves, Electrochemical Impedance Spectroscopy (EIS) and Electrochemical Noise (EN). Among the specific experimental setup designed to study MIC it is possible to account the dual cell technique, which is the most important contribution in this area, and electrochemical sensors.

Open Circuit Potential is the simplest measurement that can be performed in order to follow the changes in the sample surface reactivity. It consists in the measurement of the voltage drop between the electrode surface and a reference electrode (RE) when no voltage or current is imposed in the system. The OCP value can be analysed using the polarization curve; actually, in case of stainless steels or metals exhibiting a passive-active behaviour, it is possible to understand if the metal is in its passivity region or if, on the contrary, pitting potential is approached. Moreover, evolution of the Open Circuit Potential in a solution containing bacteria can be compared to the trend in sterile conditions in order to highlight the different changes occurring on the electrode surface. The main drawback of this technique is that little information can be derived on the corrosion rate of the metal immersed in that specific electrolytic solution [14]. Then, one of the issues is represented by the need of having a stable reference electrode. Actually, the growth of biofilm on the reference electrode can lead to a shift of its potential in the solution and thus to not accurate measurements [15]. The electrode traditionally employed as RE is the Saturated Calomel Electrode (SCE), but now in most of the laboratories it has been replaced by the Silver Chloride RE in order to avoid the use of mercury.

Linear Polarization Resistance is an important technique that can be used in order to estimate the corrosion rate of the metal under study. It is performed sweeping the sample potential in the neighbourhood of ± 10 mV or ± 20 mV around the OCP and measuring the current flowing between the sample and the counter electrode. The polarization resistance is thus defined as:

$$R_p = \left.\frac{\partial E}{\partial i}\right|_{i=0} \tag{1.6}$$

that is the slope of the potential (E) versus current (i) curve at i=0. This value is proportional to the inverse of the corrosion rate. The measurement is non-destructive, so it can performed at regular time intervals during the test without altering it. Limitations of this technique are encountered when localized corrosion is occurring, because large fluctuations in R_p can be found. Moreover, the relation between equation 1.6 and the corrosion rate does not apply if the mechanism is controlled by diffusion, but only under electron transfer-controlled conditions [15].

Changing the sample potential over a larger range, usually in the order of 0.5 V or 1.0 V, it is possible to obtain the so called 'polarization curve'. It can be used to better investigate the electrochemical behaviour of the material in that specific solution. For example, corrosion current and thus corrosion rate can be calculated using the Tafel extrapolation. Moreover, pitting potential can be measured in order to assess the

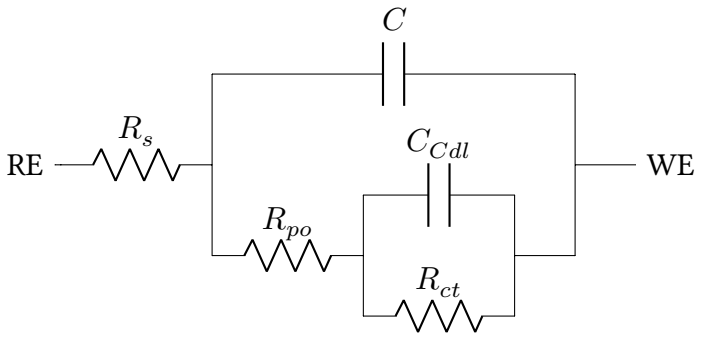

Figure 1.2: Equivalent circuit model for fitting EIS Spectra.

susceptibility of the alloy to this kind of attack [14]. These results can be used to compare the behaviour in solutions containing bacteria and in sterile conditions. As large anodic and cathodic potentials are applied, irreversible modifications are induced on the electrode surface and the measurement should be considered as a destructive one. Moreover, in MIC field it should also be taken in account that bacteria metabolism can be altered if large potentials are applied. Thus the effect of microorganisms could be underestimated [15].

Another important electrochemical technique commonly used in corrosion tests is Electrochemical Impedance Spectroscopy (EIS). A small alternating potential signal is applied to the sample, measuring its impedance over a frequency range that generally is between 10^{-2} Hz and 10^{5} Hz. The small signal does not alter the bacteria activity and does not influence the corrosion rate, so it can be considered as non-destructive [15]. Manifold information related to the superficial oxide layers can be gathered from EIS measurements. Their effectiveness in protecting the bulk material can be derived from the impedance magnitude. Moreover, impedance phase can provide important information on oxide porosity or its possible discontinuity [14]. In order to have a deeper understanding of the system, EIS spectra can be fitted using an equivalent circuit model. It can be useful in order to calculate values for physical parameters representing the system. As an example, in Fig. 1.2 an equivalent circuit typically used to model the behaviour of a metal with a superficial passive layer is presented.

The elements constituting the system are: R_s, representing the the solution resistance, C for the oxide layer capacitance, R_{po} for the oxide pores resistance, C_{Cdl} for the double layer capacitance and R_{Ct} for the resistance to charge transfer. R_{Ct} can be used in order to monitor the corrosion rate of the material, as it models the rate of the reactions occurring at the interface between the metal and the electrolyte and its trend as a function of time can help to determine the electrochemical behaviour of the alloy.

Electrochemical Noise (EN) is an effective technique to detect if localised attack is occurring on the metal. Two samples of the same alloy are immersed in the same electrolytic solution and electrically connected through a Zero Resistance Ammeter

(ZRA) [14]. Fluctuations of the current or of the potential are measured as a function of the immersion time and, as no external signal is applied, biofilm formation and development is not influenced by this measure. A statistical analysis of the noise data can thus provide information on the kind of attack. The used parameter is the ratio between the standard deviation of the current noise and the root mean square current, generally known as Localization Index (LI). If it is lower than 0.05, the corrosion process is occurring uniformly on the material, if it is between 0.05 and 0.1, a mixed morphology is present, while if this value is higher than 0.1, a localised attack is taking place [15].

As microbial corrosion is a peculiar phenomenon, determined by the activity of living microorganisms, specific setup have been proposed to investigate it. The first one was proposed by Little at the end of the eighties and is named 'Dual Cell Technique' [16]. It makes use of a cell composed of two chambers, separated by a semi-permeable membrane. They are filled with the same electrolytic solution, but in one of them an inoculum is added. Two samples of the same material are then immersed, one for each chamber, and electrically connected through a Zero Resistance Ammeter (ZRA). A galvanic current due to bacteria activity will arise, and it can be measured by the ZRA. Thus, using this technique it is possible to study the influence of bacteria on the electrochemical behaviour of a metal immersed in a specific solution. The measured current can not be related to the corrosion rate, but can provide researchers with important information on the effect of biofilm formation on the alloy, comparing biotic and abiotic conditions. Even if theoretically elegant, this technique has never been widely used, probably due to the difficulties in the realization of the experimental setup.

Other interesting tools to study microbial corrosion are represented by electrochemical sensors; they are generally used to monitor the biofilm formation on a metal when immersed in a specific environment. The sensor proposed by Licina consists of a stack of stainless steel disks (alternatively, a Titanium alloy can be used), electrically insulated from each other by means of epoxy resin [17]. It has a cylindrical shape, with a base diameter of the order of 30 mm and a length of 50 mm, so it can be even added in a plant or pipeline without altering its working conditions. One set of the metal disks is polarised respect to the remaining ones and the arising current is measured. Performing this measurement for a short period of time each day, it is possible to track the current increase due to biofilm formation, because the bacteria colonization of the disks surface favours the electron transfer to the metal. So, comparing the current value to the baseline at the beginning of the immersion (when biofilm was not present), it is possible to detect and monitor biofilm formation [6]. Thus, this sensor can be conveniently used in many industrial application, for example in order to understand if biocide treatments are effective and to put in place the necessary procedure to avoid risks related to microbial corrosion.

A theoretically similar setup was used by Angell in a research work to study microbial corrosion of AISI 304 stainless steel in anaerobic seawater [18]. In this case, the sample was a concentric electrode made of the alloy to be characterized. A small central anode was electrically insulated from a circular cathode surrounding it, using

a Teflon spacer. Electrical wires were soldered on the back of each electrode and then the embedded in resin. Using this configuration, it was possible to apply a current between the anode and the cathode, altering the bacteria colonization rate and observing the consequences on the corrosion process. Actually, after removal of the applied current, a galvanic current established between the two electrodes and this phenomenon of course was not observed in abiotic tests. Such experimental setup can also be useful to study the influence of different polarization times on the biofilm growth rate [19]. A possible drawback of this technique is that the system is sustained by the external signal applied by the potentiostat, so the bacteria metabolism could be artificially increased to non-realistic conditions.

In order to try to overcome some of the limitations related to the current experimental setup for the study of microbial corrosion, a new approach was proposed. It is presented in Chapter 2, describing its functioning and its possible applications. Main innovation is related to the use of Microbial Fuel Cell (MFC) as the environment to carry out the test. Indeed, this approach tries to combine some of the features of the Dual Cell Technique and of the concentric electrode. As explained in the next Chapter, the MFC setup enables researchers to assess the influence of bacteria on metal corrosion, as the biofilm growth can be monitored in-continuum. Moreover, unlike the concentric electrode setup, in this case the system is completely governed by bacteria activity, so unrealistic increase in reactions rate can be avoided. Characterization of different materials has been carried out in order to show the information that can be obtained from this technique and results are presented in the same Chapter.

1.3 Microscopy and imaging techniques for microbial corrosion

Electrochemical techniques are the most widely used in the corrosion field in order to study the processes involved in metals degradation. Nevertheless, morphological characterizations play an important role too, as they can help in the explanation of the behaviour of different materials. In particular, assessing the biofilm structure is an important point in order to understand the interaction between the metal and the electrolytic solution containing bacteria. Biofilm coverage, that is the surface percentage covered by microorganisms, can be an important parameter to explain the electrochemical behaviour of the material. Moreover, its structure, that is the dimension of bacteria aggregates and their three-dimensional organization, are important information that can be correlated to the solution aggressiveness. Different microscopy techniques can be taken in account, depending on the kind of information that should be derived from the characterization, and different imaging approaches can be used to obtain a quantitative assessment of the bacteria effects. Microscopy techniques can be divided in three branches: optical, electron and scanning probes.

Optical microscopy is the most widely used technique in the biology field, both for

Table 1.1: Summary of possible electrochemical techniques to study microbial corrosion

Technique	**Applied signal**	**Advantages**	**Limitations**
Open Circuit Potential (OCP)	None	Changes in the surface reactivity can be monitored in continuum during the test	Difficult to correlate to the corrosion rate
Linear Polarization Resistance	10 mV or 20 mV versus OCP in the cathodic and anodic direction	Non- destructive. Can provide an estimation of the corrosion rate	Not applicable to diffusion-controlled processes
Polarization Curve	Large polarization in the cathodic and anodic direction	Useful to predict the behaviour of a metal in a specific environment	Destructive measurement
Electrochemical Impedance Spectroscopy	Alternating voltage of 10 mV or 20 mV in amplitude	Superficial layer protective effectiveness can be assessed. Non- destructive	Data interpretation not always straightforward and unequivocal
Electrochemical Noise	None	It is able to discriminate between uniform or localised corrosion	Long mathematical post-processing to correctly interpret the data
Dual Cell Technique	None	Influence of the biofilm on the electrochemical behaviour of the material can be investigated	Information on the corrosion rate can not be derived
Electrochemical Sensors	Voltage or current	It is possible to monitor the biofilm formation	No specific information on the corrosion process

the low cost of the equipment and for the possibility to observe the biofilm without almost any alteration of its appearance and structure. In order to observe the biofilm using optical microscope, staining of the sample is required. It consists in the use of fluorescent dyes that can bind with biological macromolecules in microorganisms and then are able to fluoresce if irradiated with light at a specific wavelength [20]. Acridine Orange, DAPI (4',6-diamino-2-phenylinfole dihydrochloride) and Propidium Iodide are some of the most widely used stains. The former is able to interact with DNA and RNA, so highlighting the presence of microorganisms. Instead, using DAPI it is possible to stain only living cells, while using Propidium Iodide dead cells are stained [21]. Thus, staining a sample with both dyes, it is possible to have a representation of dead and viable cells in the biofilm under study. This is an important information if, for example, the effect of biocides is tested or if a new material with antibacterial properties is investigated.

A specific optical instrument is the Confocal Laser Scanning Microscope (CLSM), which enables researchers to obtain a three-dimensional representation of the biofilm. Also in this case, staining techniques are required in order to dye the microorganisms [20]. Main advantage of this instrument is that a direct quantification of the biofilm can be performed, measuring its thickness. Moreover, the possibility to characterize the biofilm structure is an important feature in studies related to biology. Actually, it can be associated to the involved microorganisms or to their interaction with the substratum under study.

Scanning Electron Microscopy (SEM) represents another possible technique to assess biofilm morphology, in particular when, as it often happens in studies related to microbial corrosion, the biofilm coverage is low. Using this instrument, an electron beam scans the sample surface, and the obtained image is the result of the interaction between the electrons and the outer layers of the material. If secondary electrons are analysed, a topographical reconstruction of the surface is obtained. If backscattered electrons are collected, it is possible to have compositional information about the sample. Thus a comprehensive characterization can be performed, assessing the bacteria presence and analysing also the chemical composition of the corrosion products [20]. Some disadvantages, related in particular to the demanding sample preparation, can be encountered if also the biofilm structure has to be investigated. Actually, SEM analysis must be carried out in vacuum, in order to be able to focus the electron beam on the sample. So, it is necessary to carefully dehydrate the biofilm, without altering its 3-D structure. In order to do so, generally the procedure involves first a treatment with glutaraldehyde to have cells fixation and then the immersion in different solutions with increasing concentration of ethanol in water in order to completely remove the water without making the biofilm collapse. Nevertheless, the dehydration process can lead to a shrinkage of the biofilm and to modifications in its structure [21]. From this point of view, even if electron microscopy provides a better resolution at high magnification, CLSM can reduce the presence of artifacts generated during sample preparation. Moreover, SEM can analyse only conductive samples, so if a thick biofilm covers the sample surface, or if

the sample itself is non-conductive, it must be coated by a conductive layer (usually Chromium, Gold or Carbon).

In order to overcome some of the issues related to dehydration of biofilm or non-conductive samples, a different SEM typology has been developed. Its name is ESEM (Environmental Scanning Electron Microscope) and it is able to work also at higher pressure, so allowing to analyse hydrated specimens [21]. This is a major advantage for biological samples, as their structure is not altered during sample preparation. ESEM has been extensively used in many studies about microbial corrosion, as it can combine the high resolution of electron microscopy with a simple sample preparation. Moreover, chemical composition of corrosion products can be analysed in order to better investigate the corrosion mechanism. The main disadvantage that can be accounted is that, of course, no information can be derived on cells viability when electron microscopy is used.

Atomic Force Microscope (AFM) belongs to the category of scanning probe microscopes. It is basically composed by a cantilever with a tip at its edge that scans the sample surface, measuring the interaction forces between the tip and the sample [19]. It is thus able to reconstruct the surface topography at nanometric scale, obtaining information both on bacteria presence (as singly attached microorganisms or embedded in biofilm) and on pits or corrosion products. Great advantages are related to the possibility to analyse also wet samples, so almost no preparation is required [21]. Limitations are due to the cost of the equipment, to the possible probe contamination after contact with the sample surface and to the lack of information on chemical composition of the material under study.

As briefly reviewed, different microscopy techniques can assess the surface morphology obtaining complementary information. The subsequent step is thus to derive from these analyses a measurement that can represent the samples conditions as far as the biofilm growth on it is concerned. The approach can change according to the final aim of the characterization, to the available instrument or to the measurement conditions. The use of Confocal Laser Scanning Microscope is usually assisted by specific software that is able to process the acquired images in order to obtain a 3D reconstruction of the biofilm. COMSTAT is one of the most widely used, and it can provide information on mean biofilm thickness, roughness, substratum coverage and surface to volume ratio [22]. These parameters can thus be used to compare the growth of different strains in specific environmental conditions or study the influence of the substratum on their behaviour.

An interesting approach, useful in particular to assess the biofilm growth not in laboratory but during field testing, was proposed by Larimer [23]. It consists in an image analysis of photographs taken with a commercial digital camera. First the sample under study must be stained with appropriate dyes, then the change in colour due to fluorescence is used to assess the amount of biofilm grown on the surface. The obvious advantages of such technique are the low cost and the short time required to perform the measurement. Moreover it can be performed directly in-situ when needed and is

Table 1.2: Summary of possible microscopy techniques to study microbial corrosion.

Technique	**Sample preparation**	**Advantages**	**Limitations**
Optical microscopy	Staining	Possibility to discriminate between viable and dead cells	Low magnification and low depth of field
Cofocal Laser Scanning Microscopy	Staining	3-D reconstruction of the biofilm	Same as optical microscopy
Electron Microscopy (SEM)	Sample dehydration and conductive coating	Biofilm observation at high magnification. It is possible to analyse also the chemical composition	Biofilm structure can be altered by sample preparation. It is not possible to discriminate between viable and dead cells.
Electron Microscopy (ESEM)	None	Same as SEM	It is not possible to discriminate between viable and dead cells.
Atomic Force Microscope	None	It is possible to analyse also wet samples	Expensive equipment. No information about chemical composition

completely non-destructive. Of course, obtained information are limited and only an estimation of bacteria concentration on sample surface can be performed; no information can be derived on the biofilm morphology or the degree of surface coverage.

Many are then the possible approaches to analyse micrographs taken with SEM. Heuer et al. proposed an image processing based on images acquired using backscattered electrons, where the contrast is directly related to the sample composition [24,25]. Their study was about oral implants, and the final aim was to quantify the biofilm formation. In their investigation they were thus able to quantify the biofilm coverage in different oral implants, analysing the micrograph with the ImageJ software in order to differentiate the grey areas.

Another image processing that relies on SEM images was proposed by Vyas et al. In this case, the algorithm is based on machine learning; so the software is trained to identify bacteria not relying on the simple change in pixels colour, but also according to features like edge detectors or image texture. This can be a great advantage in all those cases in which the contrast between the biofilm and the substratum is limited or the material surface has a high roughness [26].

Taking into account the possible microscopy techniques and imaging approaches, a new imaging algorithm was proposed, which is presented in Chapter 3. It analyses SEM micrographs in order to obtain information about biofilm coverage and dimensional distribution of bacteria aggregates. After an image brightness and contrast normalization, which is performed in order to limit the influence of the operator on the acquired images, the micrograph is processed identifying bacteria according to the pixel brightness. Actually the algorithm is based on the contrast between the microorganisms and the sample surface. Indeed, they appear as black spots on the bright metal surface, as they have a lower electrical conductivity. This condition is verified as long as bacteria do not completely cover the metal surface, but this hypothesis is not restrictive if the algorithm is applied to microbial corrosion tests. The image processing has also been applied to different case studies in order to assess the biofilm coverage on stainless steel coupons immersed in different solutions containing bacteria.

Chapter 2

Electrochemical methods for microbial corrosion assessment

Some of the work described in this chapter has been previously published in [27, 28].

2.1 Introduction

Electrochemical techniques are an important tool to characterize materials behaviour when immersed in electrolytic solutions and assess their corrosion resistance in that environment; a general overview of them has been presented in Section 1.2. As a matter of fact, none of these techniques can be considered comprehensive by itself, so different measurements techniques must be coupled in order to have a complete description of the system (considered as the interaction between the material and the solution). In the first section of this Chapter, the characterization of two stainless steels immersed in a hypersaline solution is presented. This represents an interesting case study for corrosion behaviour assessment, as the presence of many different salts in solution leads to complex corrosion processes, which can be investigated only using a sufficiently diversified measurement approach. In the second section of the Chapter, a novel technique for microbial corrosion assessment is described. It aims at giving a new tool for material characterization, providing information that are difficult to obtain from a simple immersion test.

2.2 Electrochemical characterization of stainless steel in hypersaline solution

This section presents the characterization of the corrosion behaviour of two Stainless Steels in hypersaline environment. A solution is defined as hypersaline if its salts

content is higher than that of ocean water. Hypersaline environments can be found in many industries, like brine mining or in the oil industry. This is an interesting case study from the material science perspective, because different research works can be found concerning the electrochemical behaviour of stainless steels in marine environment and in solutions containing bacteria [29–32], but hypersaline environments have been rarely investigated so far. Moreover, different measurement techniques must be applied in order to describe the interaction between the metal and the electrolytic solution in a comprehensive way.

2.2.1 Materials and methods

The two materials under study were AISI 304 and AISI 316 Stainless Steel; their nominal composition can be found in table 2.1. Samples have been realized cutting metal sheets to the dimension of 10 mm $\times$ 10 mm. A wire was soldered on the back of the specimen in order to have the electrical connection and then it was embedded in polymeric resin in order to expose only the desired surface area to the electrolytic solution during the test. Mirror-like surface finishing was achieved polishing the sample on emery paper until 4000 grit, then they were rinsed with distilled water and dried in air.

The electrolytic solution was hypersaline Starkey medium, whose composition can be found in table 2.2. Oligo-elements were added in order to promote the bacteria proliferation in the saline environment. The solution pH was adjusted to 8.0 ± 0.2 and remained constant during the whole duration of the test and the solution conductivity was equal to 69.2 ± 0.5 mS/cm. The inoculum for bacteria was salt marsh sediments, and it was added to the solution using a concentration of 10 vol%. Each sample was immersed in a standard electrochemical cell containing 0.5 L of solution and the inoculum was added after 24 hours after the beginning of the test. The experiments were carried out at 30 ± 3 °C in naturally aerated conditions. Five samples were tested for each material; in two of the five cases, inoculm was not added in order to characterize the alloy behaviour in abiotic conditions.

Table 2.1: Chemical composition of the Stainless Steels used in the study

	C %	**Mn %**	**P %**	**S %**	**Si %**	**Cr %**	**Ni %**	**Mo %**	**N %**
AISI 304	0.05	1.8	0.03	0.025	0.4	18.2	8.0	-	0.08
AISI 316	$\leqslant$0.07	$\leqslant$2.0	$\leqslant$0.045	$\leqslant$0.015	$\leqslant$1.0	16.5-18.5	10.0-13.0	2.0-2.5	$\leqslant$0.11

Electrochemical measurements were performed using a Princeton Applied Research VMP2 potentiostat, setting the sample as the working electrode, using Saturated Calomel Electrode (SCE) as the reference electrode and a platinum mesh as counter electrode.

Table 2.2: Chemical composition of the electrolytic solution

	Concentration [g/L]
Starkey Medium	$NaCl$ 45.00, CH_3COONa 3.00, NH_4Cl 2.00, K_2HPO_4 0.50
	Concentration [mg/L]
Oligo-elements	$MgCl_2 \cdot 6H_2O$ 55, $FeSO_4(NH_4)_2SO_4 \cdot 6H_2O$ 7, $ZnCl_2 \cdot 2H_2O$ 1, $MnCl_2 \cdot 4H_2O$ 1.2, $CuSO_4 \cdot 5H_2O$ 0.4, $CoSO_4 \cdot 7H_2O$ 1.3, H_3BO_3 0.1, $Mo_7O_2(NH_4)_6 \cdot 4H_2O$ 1, $NiCl_2 \cdot 6H_2O$ 0.05, $Na_2SeO_3 \cdot 5H_2O$ 0.1, $CaCl_2 \cdot 2H_2O$ 60

Electrochemical Impedance Spectroscopy (EIS) measurements were performed in the frequency range between 10^{-2} Hz and 10^{5} Hz using a signal amplitude of 10 mV. Cyclic Voltammetry (CV) measurements were performed polarizing the working electrode up to 20 mV versus the open circuit potential (OCP) first in anodic and then in cathodic direction; the scan rate was equal to 10 mV/min.

Epifluorescence microscopy was used to characterize biofilm coverage on samples surface at the end of the test. Carl Zeiss AxioImager M2 microscope equipped with an HXP200C light source and the Zeiss09 filter (excitor HP450r HP450200 C light source) was used to acquire the images. Staining was performed using Acridine Orange (0.01%) immediately after the end of the immersion test. The staining solution was left on the samples surface for 10 minutes and then removed by means of abundant rinsing with distilled water.

Scanning electron microscopy was used for final morphological characterization of samples surface. Images were taken with a FESEM Supra 40 by Zeiss, applying an accelerating voltage of 15 kV and using an aperture size of 30 µm.

2.2.2 Results and discussion

Samples were immersed in the electrolytic solution for 15 days and electrochemical measurements were regularly performed. A concentration of NaCl equal to 45 g/L was chosen for the hypersaline medium, because, as demonstrated in a previous publication, it represents the optimal concentration for bacteria growth in case of hypersaline environment [33]. Actually, only halotolerant strains can survive in such solutions, thus also the choice of the inoculum is not trivial. For this study, salt marsh sediments were used because, as they are directly collected from the environment, they guarantee a large biodiversity of bacteria strains [34]. In this way, results from the corrosion test will also be more adherent to the materials behaviour in real applications.

Fig. 2.1 shows the Open Circuit Potential (OCP) trend during the test. It is possible to observe the decrease after the inoculum addition, which was after 24 hours from the beginning of the test. This behaviour is similar for the two stainless steels and can be correlated to the development of the planktonic population of bacteria inside the solution. Actually, bacteria concentration was monitored measuring the solution absorbance and results show that it goes from 0.020 (value after 24 hours from inoculum addition) to 0.835 (after 112 hours from inoculum addition). Moreover, oxygen concentration measurements showed that the solution completely lacked oxygen. These three phenomena can be correlated as the development of bacteria inside the solution leads to oxygen consumption and this is highlighted also by the OCP values, that decrease to a range that is typical for anaerobic conditions. A further evidence can be derived from OCP measurements in abiotic conditions, where such trend can not be found. In this case, after an initial increase, OCP decreases to values slightly higher than those measured in solutions containing inoculum. This behaviour can be related to the extensive corrosion occurring on the material during immersion, as it will be better described

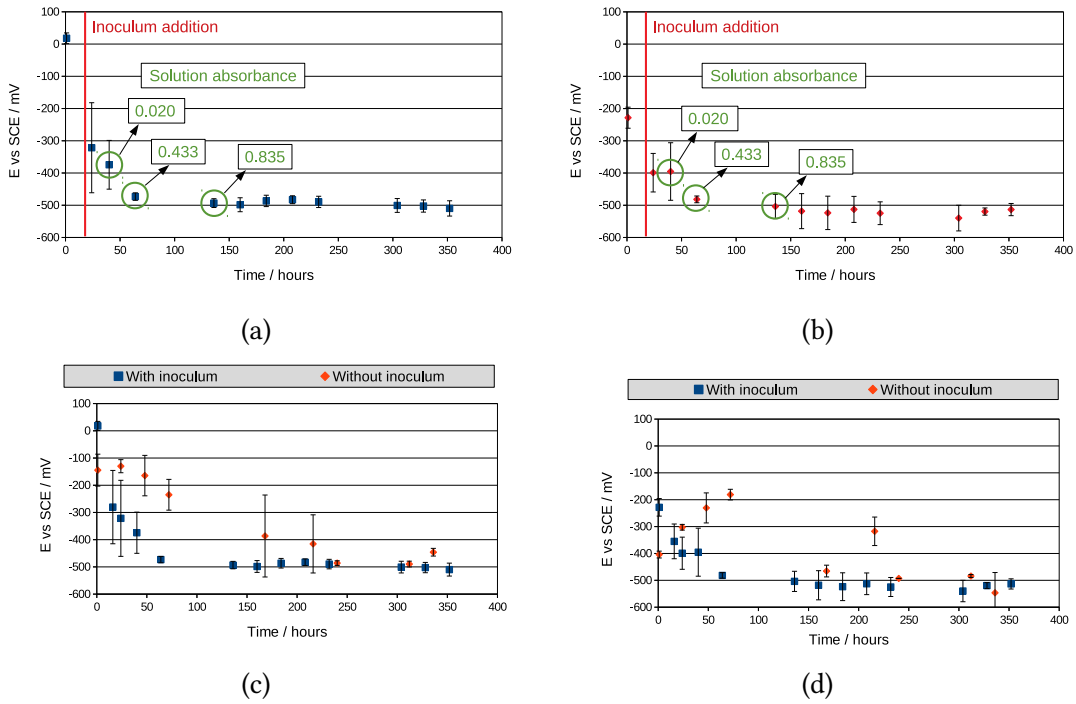

Figure 2.1: Open Circuit Potential (OCP) measurements carried out during the test: a) AISI 304 samples with inoculum b) AISI 316 samples with inoculum c) Comparison of AISI 304 samples with and without inoculum d) Comparison of AISI 316 samples with and without inoculum.

further on.

In order to assess the protective behaviour of the superficial oxide layer of the two stainless steels during immersion in the electrolytic solution, EIS measurements were carried out. Results are reported in Fig. 2.2 and Fig. 2.4 as Bode plots respectively for AISI 304 and AISI 316. In the former case, it is possible to observe that the superficial passive layer has good protective characteristics at the beginning of the test, as it can be highlighted by the modulus of impedance, reaching values above $10^5\ \Omega \cdot \mathrm{cm}^2$, and from the phase values above $80°$. Excluding the high-frequency part of the spectrum, where the solution resistance has the most important effect, the behaviour is almost capacitive in a wide range of frequencies until the last decade, in which the impedance phase values slightly decrease. Increasing the immersion time, three main modifications can be recognized in the Bode diagrams, that reveal a change in the protective capability of the superficial layer. The modulus of impedance at low frequencies decreases to values of about $4 \cdot 10^4\ \Omega \cdot \mathrm{cm}^2$; moreover, as far as the phase is concerned, its maximum value decreases below 80°and two peaks appear. The trend of the modulus of impedance as a function of the immersion time has been plotted in Fig. 2.3a . As it is possible to observe, it decreases in the first part of the test and then stabilizes at the values before mentioned.

This fairly stable behaviour can be probably related to the anaerobic conditions inside the solution, that are less detrimental for the material even if this alloy is not specifically intended for environments containing such a high chloride content. The appearance of two peaks in the phase plot after 160 hours of immersion can be related to the presence of two time constants, that is a new interface between the oxide layer and the metal.

A different electrochemical behaviour could be highlighted for the AISI 316 samples. Actually, even if a decrease in the impedance modulus can be observed in the first part of the test, it remains close to $10^5\ \Omega \cdot \mathrm{cm}^2$, showing the good protective properties of the superficial oxide. Moreover, a small decrease in the phase values can be noted, but only one time constant is present until the end of the test. The trend of the modulus of impedance for the AISI 316 samples can be seen in Fig. 2.3b. Also in this case, as already noticed for AISI 304, the modulus value decreases in the first part of the test and then stabilizes.

Tests carried out in abiotic conditions, that is without the addition of the inoculum, showed a completely different behaviour for both the alloys. In this case, as bacteria were not present, oxygen remained in the solution during the whole duration of the test and this affected the stability of the superficial oxide layer. As can be seen in Fig. 2.5a for EIS measurements on AISI 304, modulus of impedance remains almost stable (only a slight decrease can be observed), but significant modifications can be noticed in the phase plot. Actually, a capacitive behaviour is present in the first part of the test, until 72 hours of immersion, but in the second part it switches to a resistive behaviour, characterized by phase values close to zero in the low frequencies range. The same behaviour was observed for AISI 316, as can be seen in Fig. 2.5b. Also in this case a decrease in the impedance modulus is present and the phase values drop to about 20°. This behaviour can be related to an extensive corrosion occurring on the sample surface, presumably in the form of pits.

An additional electrochemical technique used to characterize the two stainless steels was Cyclic Voltammetry. As this measurements was carried out employing a small polarization of the working electrode from its OCP, the aim was mainly to derive a quantification of the polarization resistance, which is inversely proportional to the corrosion rate. In this way a further confirmation of the results from previously described electrochemical measurements could be obtained.

Results from the CV measurements of two samples are displayed in Fig. 2.6. On the abscissa the potential versus SCE is reported; in this way it is possible to notice also the shift towards lower values occurring during the test. The slope of the curve is an estimation of the inverse of the polarization resistance, so this value has been calculated for each measurement as:

$$\frac{1}{R_p} = \frac{I(OCP + 20\ mV) - I(OCP - 20\ mV)}{20\ mV} \tag{2.1}$$

in order to overcome the ambiguity given by cases in which the slope of the curve was not constant in that potential range.

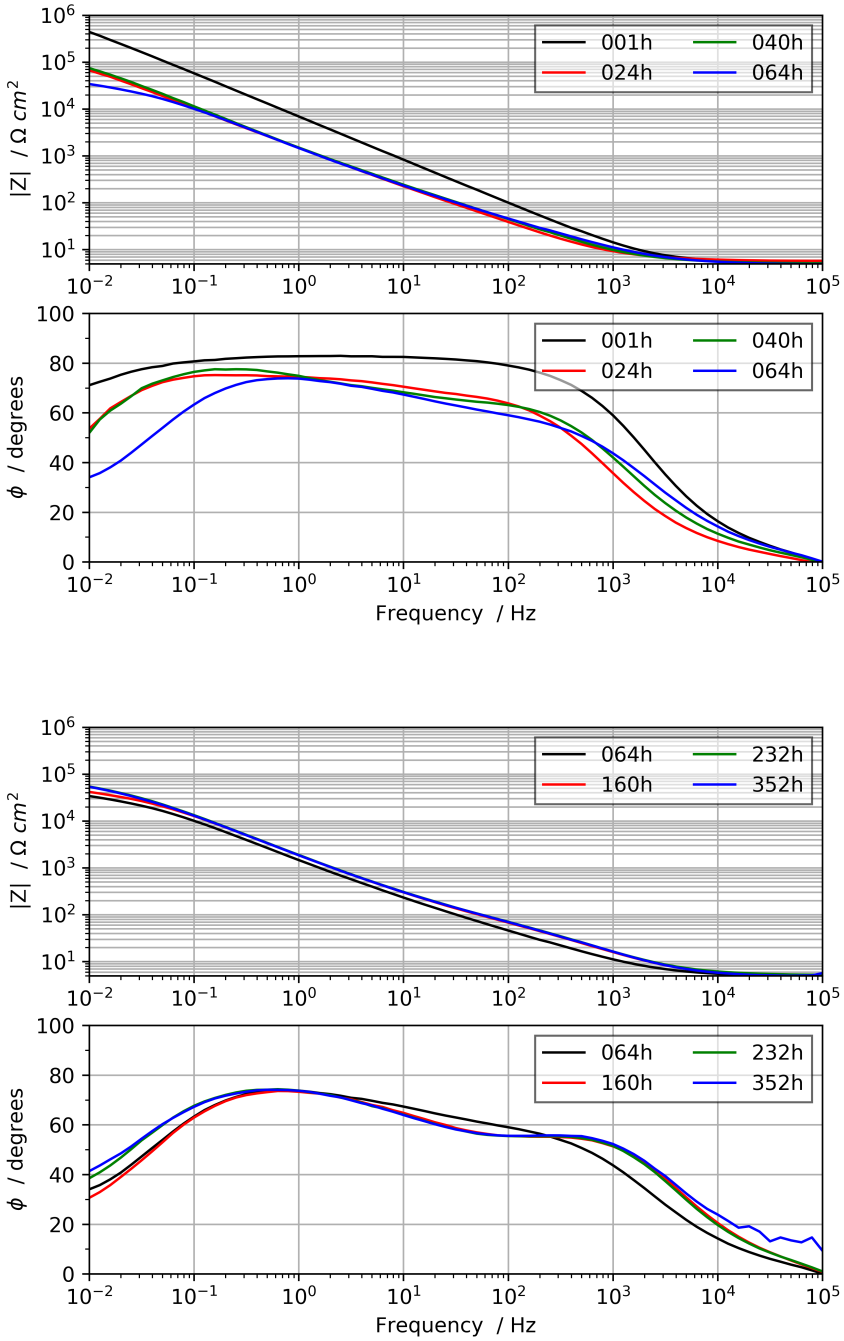

Figure 2.2: Bode plots recorded on the AISI 304 stainless steel sample immersed in Starkey Medium inoculated with salt marsh sediments.

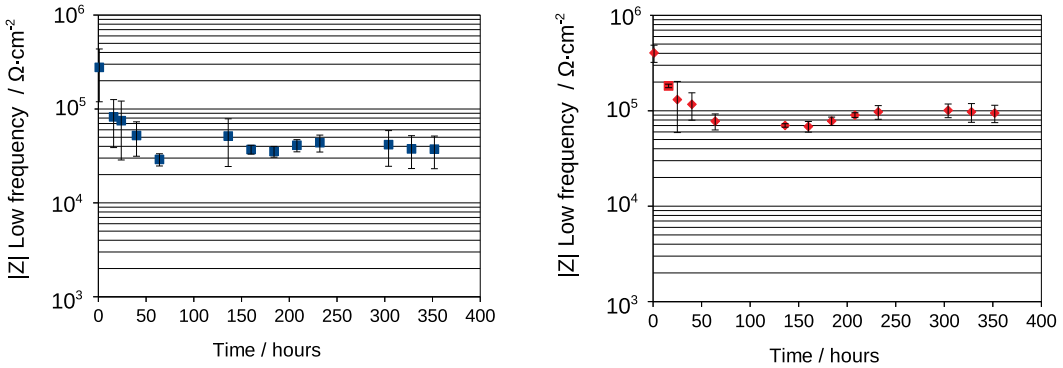

Figure 2.3: Trend of the impedance modulus at 10^{-2} Hz measured on AISI 304 (a) and AISI 316 (b) samples.

Results from calculation of $1/R_p$ are reported in Fig. 2.7. It is possible to notice that the inverse of the polarization resistance, and thus the corrosion rate, is higher for AISI 304 in comparison with AISI 316. Moreover, values remain quite stable during the duration of the test, even if in both cases a small increase in $1/R_p$ can be observed in the central part of the test, that is after 208 hours of immersion. The higher uncertainty in measurements related to AISI 304 can be possibly associated to the higher corrosion rate. Actually, when microbial corrosion is involved, large differences can be observed between samples because the corrosion reactions are linked also to the bacteria activity, which is hardly homogeneous in different batches. So this data dispersion is emphasized when the corrosion rate is higher. On the other hand, the stable behaviour of AISI 316 sample leads to more accurate measurements.

After the end of the immersion test, samples surface has been morphologically characterized in order to assess the biofilm growth. Bacteria attachment has been evaluated using epifluorescence microscopy after staining with Acridine orange. Using this compound, both the intracellular and extracellular nucleic acids are stained and thus bacteria and EPS (Extracellular polymeric substance) become visible at microscope.

Biofilm coverage was found to be similar for the two materials, as it could be expected since none of them is characterized by bacteriostatic properties. In order to assess the bacteria attachment and dimensional distribution of bacteria aggregates from a quantitative point of view, an imaging algorithm has been employed (see Chapter 4 for a complete description of the imaging system). Bacteria aggregates are identified thanks to the contrast given by fluorescence; so the imaging algorithm is able to binarize the image and then compute the desired parameters. Biofilm coverage is defined as the ratio between the number of pixels occupied by microorganisms and the total number of image pixels; then important information is related to large bacteria clusters, as they are the most dangerous as far as microbial corrosion is concerned. So, as an example,

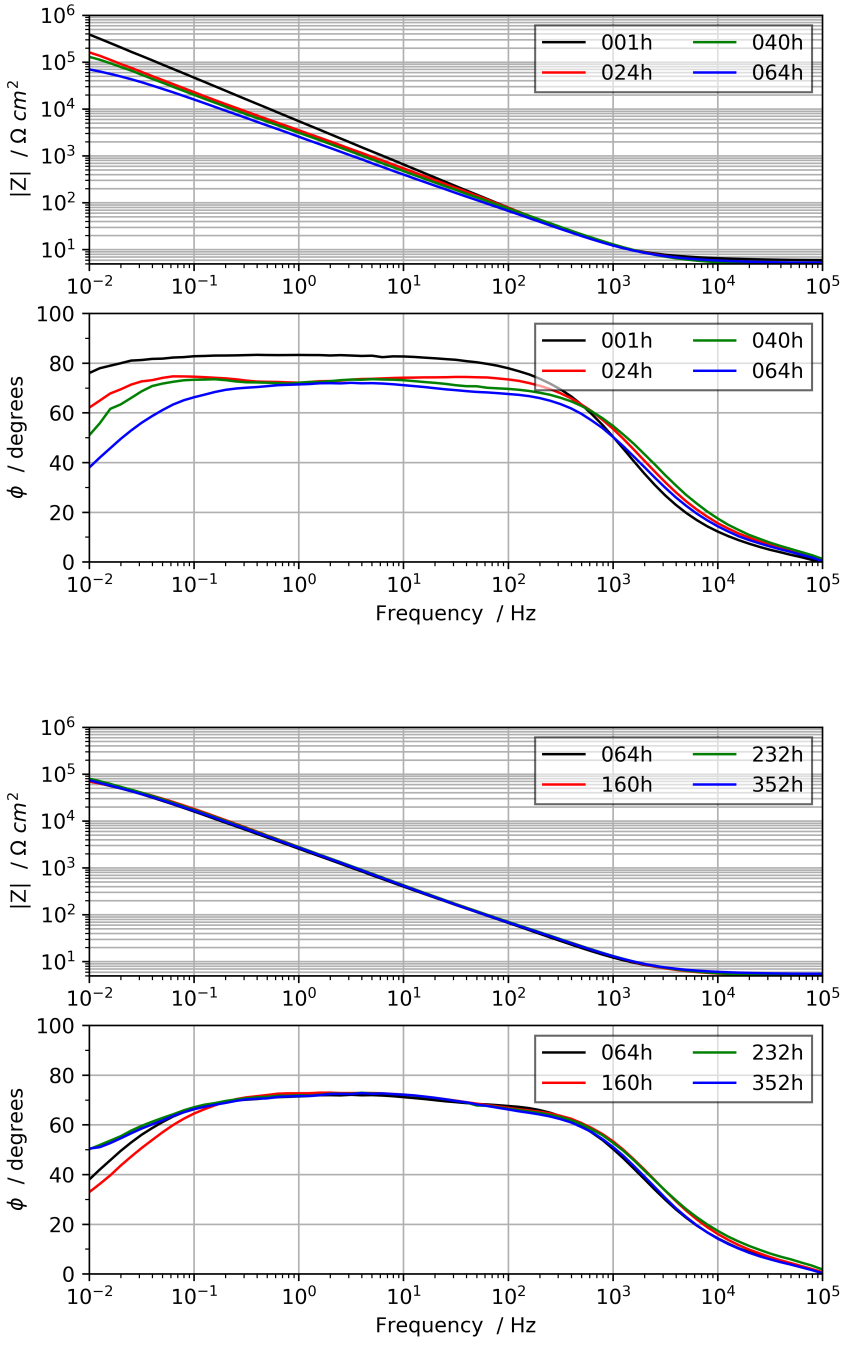

Figure 2.4: Bode plots recorded on the AISI 316 stainless steel sample immersed in Starkey Medium inoculated with salt marsh sediments.

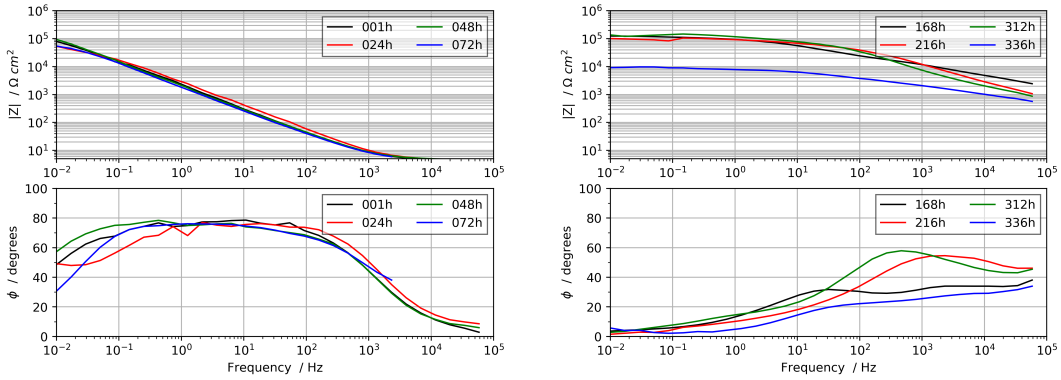

(a)

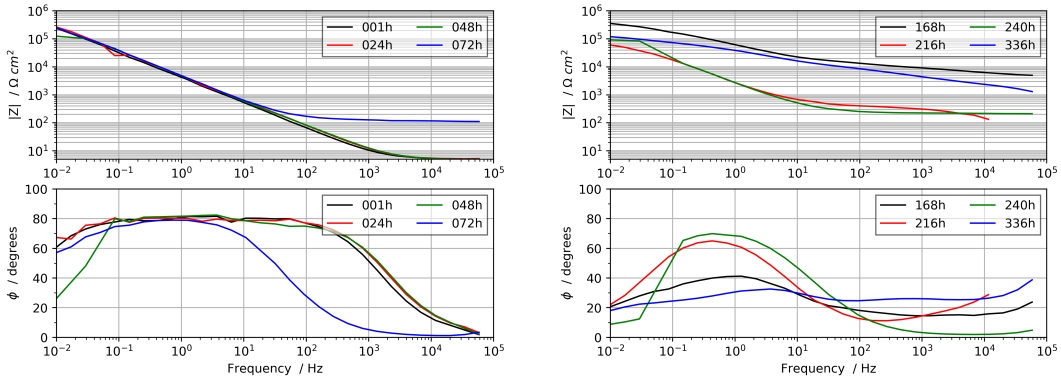

(b)

Figure 2.5: Bode plots recorded on the AISI 304 (a) and AISI 316 (b) samples immersed in Starkey Medium without inoculum.

the software is able to compute the total number of large clusters (i.e. having size above 200 μm^2) and their average size. Fig. 2.8 shows the bacteria identification on two images taken with epifluorescence microscope, while in table 2.3 further information on biofilm coverage and dimensional distribution of large aggregates are reported.

Table 2.3: Results from imaging analysis using epifluorescence microscopy micrographs.

	AISI 304	**AISI 316**
Number of large bacteria aggregates	1.8 $\pm$0.7	2.6 $\pm$1.2
Average size of large bacteria aggregates (μm^2)	196 $\pm$39	192 $\pm$37
Biofilm coverage	7.1% $\pm$2.4%	7.8% $\pm$2.9%

As it is possible to see, for both materials biofilm coverage is between 7% and 8%.

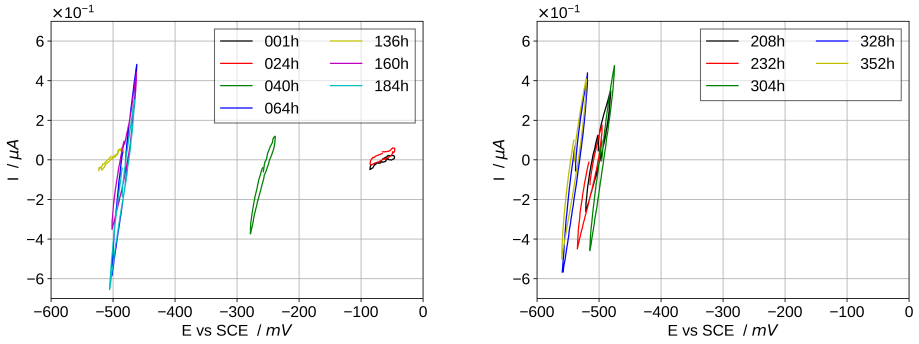

(a)

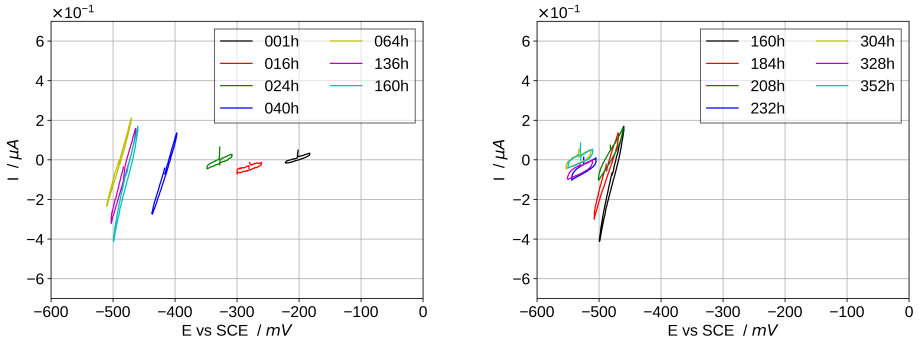

(b)

Figure 2.6: Cyclic Voltammetry measurements performed on AISI 304 (a) and AISI 316 (b) samples immersed in Starkey Medium inoculated with salt marsh sediments.

The quite high uncertainty can be related to the heterogeneity of the inoculum, as it was collected from environment. Actually, the use of this kind of inoculum can increase the results dispersion, which is always relevant when dealing with biological samples. The number and average size of large bacteria aggregates was found to be similar for the two materials. This point can be taken as an indication of the good reproducibility of the experiments.

Final morphological characterizations were carried out using electron microscopy. Thanks to the high resolution that can be achieved with the instrument, it is possible both to assess the bacteria attachment and the morphology of the corrosion attack.

Fig. 2.9 shows SEM micrographs of the AISI 304 samples. It is possible to notice the presence of both singly attached bacteria and larger aggregates. In the former case, they appear as black spots on the bright metal surface, uniformly distributed on the sample. Larger clusters develop at longer immersion time and they generally represent the most dangerous ones as far as microbial corrosion is concerned. Actually, they can create areas of differential aeration or where corrosive compounds (such as chlorides ions) can accumulate or pH changes can occur. In Fig. 2.9a it is possible to observe

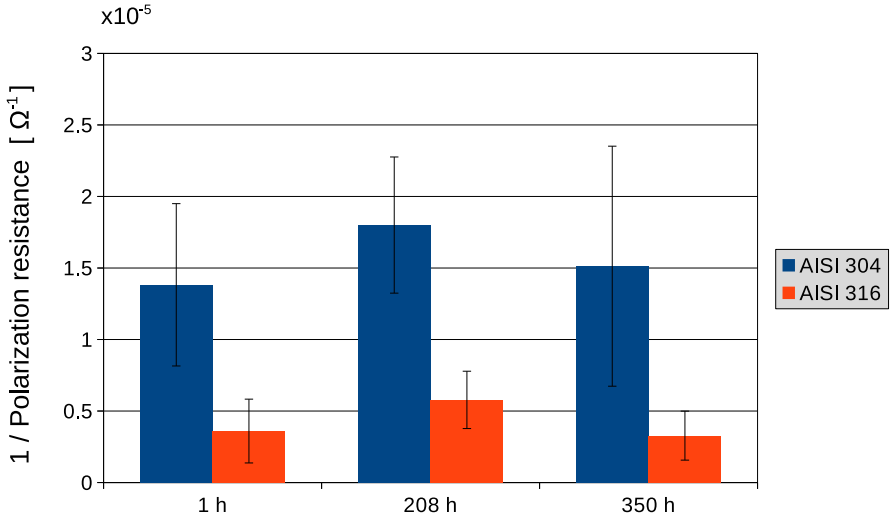

Figure 2.7: Trend of the inverse of the polarization resistance for AISI 304 and AISI 316 samples.

at higher magnification a bacteria cluster overlaying some corrosion products. Some samples have been observed at SEM after removing the biofilm, in order to reveal the corrosion morphology, which is otherwise partially concealed by attached bacteria. The superficial oxide film appears deeply damaged in many parts of the surface, both in the form of pits, and of larger discontinuities. This corrosion pattern is consistent with the electrochemical measurements, in particular the EIS spectra, which were characteristic of a discontinuous and non-protective oxide layer.

A different superficial morphology was found on AISI 316 samples. Also in this case the samples were characterized by singly attached bacteria uniformly distributed on the surface and by some larger clusters, but a different corrosion pattern could be observed after removing the biofilm. Actually, the dominant morphology was made of localized attacks and small pits. Fig. 2.10 shows some micrographs from AISI 316 samples. In Fig. 2.10a it is possible to observe the bacteria attachment and a detail at higher magnification representing a bacteria cluster. Fig. 2.10b shows some corrosion pits or localized damages present on the surface.

Samples tested in abiotic conditions showed the same corrosion pattern found in the tests using inoculum, but the attack was more extensive. AISI 304 samples exhibited large areas of the oxide layer damaged by the chlorides attack, in good agreement with EIS measurements. Actually electrochemical measurements highlighted the breakdown of the passive layer, demonstrated by the transition, in particular at lower frequencies, from a capacitive behaviour to a resistive one.

In AISI 316 samples, the corrosion morphology was characterized by pits, whose dimension was larger than those found in tests using inoculum. For both materials, this

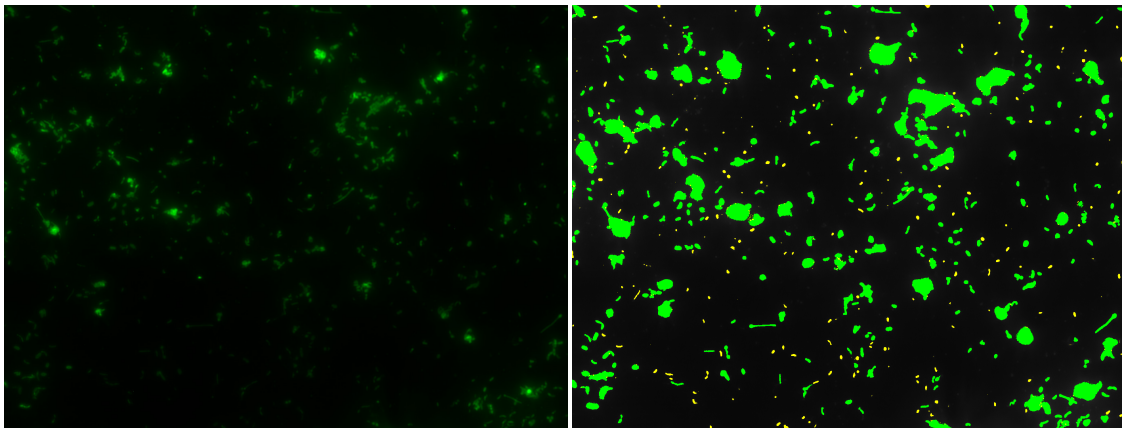

(a)

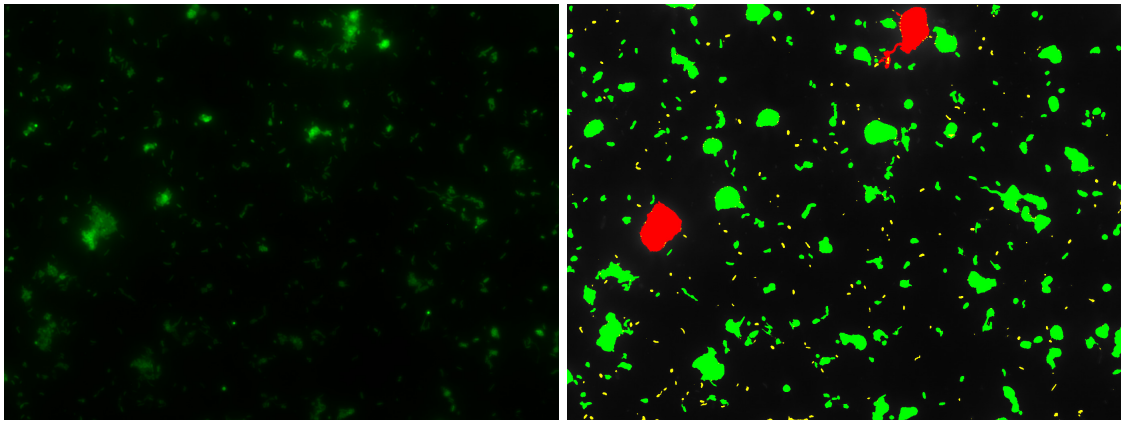

(b)

Figure 2.8: Micrographs for AISI 304 (a) and AISI 316 (b) samples taken using epifluorescence microscopy on the left and identified bacteria using the imaging algorithm on the right. Bacteria clusters having dimension above 200 μm^2 are labelled in red, otherwise in green.

behaviour in abiotic conditions can be explained considering the solution oxygen concentration during the immersion test. Development of planktonic population of bacteria in the solution leads to oxygen consumption and so anaerobic conditions, which are less aggressive for the two stainless steels.

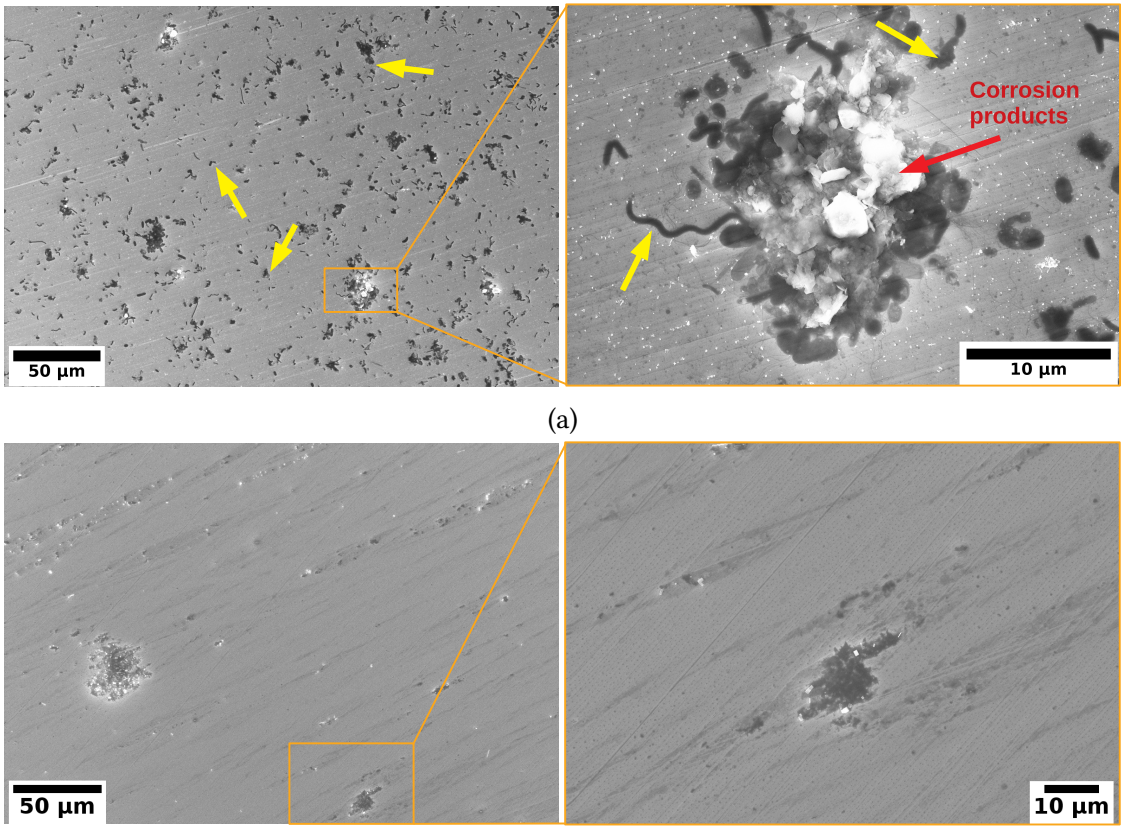

(a)

(b)

Figure 2.9: SEM micrographs taken on AISI 304 before (a) and after (b) removing the biofilm. Yellow arrows highlight the presence of bacteria.

2.2.3 Conclusions

This study presented the characterization of the corrosion behaviour two stainless steels in hypersaline solution. The use of both electrochemical measurements and morphological characterizations allowed to fully describe the behaviour of the two materials, highlighting a different corrosion mechanism. During the experiments involving bacteria, great influence was given by anaerobic conditions, that established after about 140 hours from the beginning of the test. Actually these are less aggressive for the two stainless steels, that were able to partially preserve their superficial passive layer, despite the high amount of chlorides inside the solution. The superficial oxide layer was found to be more stable and protective for AISI 316 if compared to AISI 304, as demonstrated by electrochemical measurements and morphological characterization with SEM. Moreover, biofilm coverage was similar for the two materials after immersion in the electrolytic solution, so this parameter did not influence the corrosion rate.

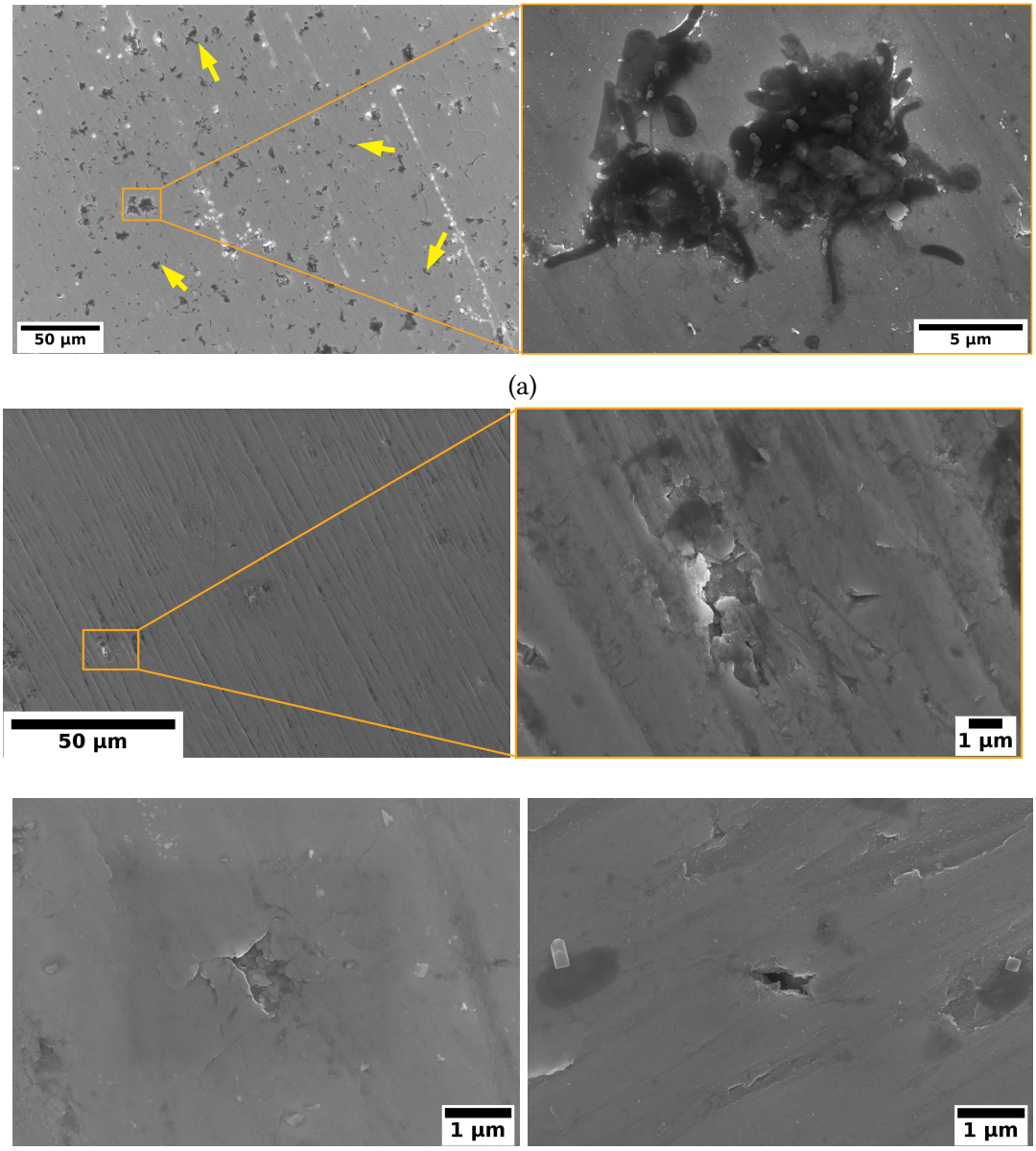

Figure 2.10: SEM micrographs taken on AISI 316 before (a) and after (b) removing the biofilm. Yellow arrows highlight the presence of bacteria.

Performing the tests without inoculum addition, a different electrochemical behaviour was found for both alloys. Actually, without the microorganisms inside the solution, oxygen concentration remained constant during the experiment and this affected the stability of the passive layer in the hypersaline environment. Both materials were characterized by an extensive corrosion attack, under the form of pits for AISI 316

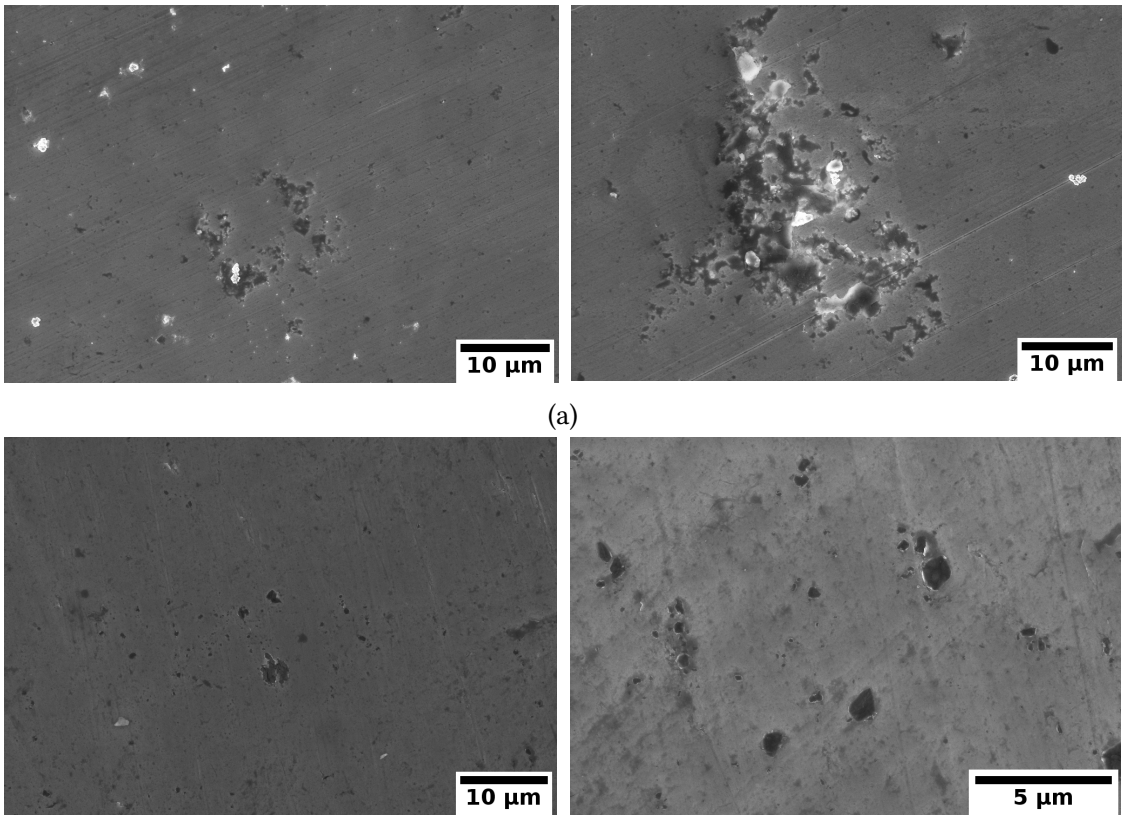

Figure 2.11: SEM micrographs taken on AISI 304 (a) and AISI 316 (b) samples after immersion in abiotic Starkey Medium.

and of a more general attack for AISI 304.

This case study represents an interesting example of corrosion inhibition caused by bacteria activity. Actually, their metabolism changed the environmental conditions inside the electrolytic solution, making them less aggressive for the materials under study. Further work could better characterize the different superficial oxide layer in the two alloys, for example by means of X-ray Photoelectron Spectroscopy (XPS), in order to understand more in depth the corrosion mechanism.

2.3 A novel approach for microbial corrosion assessment

"Methodologies commonly employed to study MIC can be divided into two major groups: field tests and laboratory tests. In the former case, the material is tested directly in the environment where it is used; this provides the advantage of having results directly applicable to the system under study, but, on the other hand, leads to long experiments and to great difficulties in discriminating the effects of individual parameters during the test [35] [36].

Laboratory tests are usually based on electrochemical measurements, such as metal open circuit potential monitoring, Electrochemical Impedance Spectroscopy (EIS), polarization resistance and Electrochemical Noise Analysis (ENA) [37]. Main limitations of these approaches are connected to the difficulty in carrying out accelerated tests avoiding any alteration of the microbial activity in order to not get to misleading conclusions [3].

In addition, another issue in MIC testing is the choice of using a single bacterial strain or an inoculum containing a wide variety of bacteria. In the former case, studies on the effect of specific types of bacteria on metal corrosion can be performed, but generally it is difficult to derive information about the overall behavior of the material. Actually in a real environment a great variety of bacteria is present and this modifies their activities and their role in the corrosion processes. Collaborative behaviors between different bacteria strains can occur inside the biofilm, leading to harsher conditions for the material under investigation [3].

A unique solution to arrange a fast and reliable methodology specifically suited for MIC is still missing in scientific literature. An interesting solution proposed by Little [16] is the Dual Cell Technique: two samples of the same material are immersed inside two identical electrochemical cells separated by a membrane and then connected to a zero resistance ammeter. Bacteria are added into one of the two cells and the galvanic current between the two specimens is monitored in order to study MIC susceptibility of the material versus the sterile conditions. This solution has the advantage of having the possibility of using real inoculum, however, despite it is a theoretically elegant experiment, this technique has been rarely used, perhaps because of the difficulty in the realization of the test.

Another interesting solution, which allows one to use real inoculum, is to use Microbial Fuel Cells (MFC), innovative tools able to convert organic matter into energy thanks to the activity of bacteria [38, 39]. Actually, mechanisms involved in the electron transfer to and from the electrode, which are at the base of the operation of a MFC, are the same responsible for corrosion processes [9]. An approach similar to that of the Dual Cell technique proposed by Little, is therefore the dual chamber MFC. In this case bacteria are added to both chambers of the fuel cell, one in aerobic conditions and one in anaerobic conditions. A current arises, due to the different biofilm present on the metal

surfaces, and mechanisms of microbial corrosion can be studied both in aerobic and anaerobic conditions. In the proposed system, a further simplification has been made, as it involves a Single Chamber Microbial Fuel Cell (SCMFC). In this case, described in the following sections, aerobic reactions take place on an air-breathing cathode [40] and the sample is immersed in the electrolytic solution in anaerobic conditions. As soon as bacteria colonize the metal surface, it is possible to measure a current flowing between the sample and the aerobic cathode, highlighting the growth of the biofilm on the sample and the reactions catalysed by bacteria." [28] ©2019 IEEE

2.3.1 Experimental setup

The proposed technique makes use of Microbial Fuel Cells (MFC) to perform corrosion tests in known and controlled conditions [27]. MFCs are innovative tools that exploit bacteria activity to catalyze chemical reactions and produce energy, chemicals or recover byproducts [41, 42]. They can be designed in different configurations, according to the working conditions and the bacteria populations living on the electrodes surfaces; main distinction can be done between Double Chamber Microbial Fuel Cells (DCMFC) and Single Chamber Microbial Fuel Cells (SCMFC). In the first case, anode and cathode are immersed in two different electrolytic solutions, separated by a semipermeable membrane. In this way, it is possible to have different conditions in each of the chambers, as an example aerated and anaerobic, and the different reactions occurring on the two electrodes will lead to a current flowing between anode and cathode. SCMFCs represent a further simplification of the whole setup. Actually, anode and cathode are immersed in the same electrolytic solution containing the bacteria inoculum. One of the electrodes acts as an air-breathing cathode, using oxygen as terminal electron acceptor; the other one, which acts as the anode, is completely submerged in the electrolytic solution and not exposed to the air, so that anaerobic reactions occur on its surface. Thus, different bacteria populations develop on each of the electrodes, colonizing its surface and leading to different electrochemical potentials [43]. Connecting anode and cathode, in presence of bioavailable products (fuel of the MFC) which can be oxidized by bacteria, the cell is able to produce an electric current circulating between the two electrodes [44, 45].

When the MFC has reached stable working conditions, that is the biofilm has covered the two electrodes surfaces, they have stabilized at different potentials and the current between them is no more increasing, the corrosion test can be performed. "A sample of the metal under study is immersed inside the solution containing bacteria and connected to circuit of the SCMFC. The current that flows in the cell is measured as a function of the immersion time in order to collect information on the bacteria-induced metal degradation and on the microorganisms activity. As a matter of fact, the anodic current measured in the SCMFC can be correlated with two phenomena whose effects are superimposed: the oxidation of the metal and the bacteria metabolism, which oxidize bioavailable organics. In both cases, electrons are transferred to the air-breathing

cathode, where oxygen is the ultimate electrons acceptor after several redox reactions of electrochemical, biotic, and abiotic character." [28] ©2019 IEEE

Using a MFC as environment to carry out a corrosion tests brings different advantages. Actually, it represents a system whose operation is totally based on the presence and activity of microorganisms; anode and cathode are made of the same material, so no current would arise without bacteria metabolism. Thus it is possible to collect the solution to fill the MFC directly in-situ from the environment that is supposed to be studied and the presence of bacteria in it would be simply demonstrated by the current output. This can be considered a great simplification if compared to usual procedure, which estimates bacteria concentration in a solution measuring its absorbance. Moreover, within certain ranges, anodophilic bacteria produce current/voltage signals proportional to the oxidation of bioavailable organics, so the concentration of nutrients in the solution can be monitored measuring the current flowing between the two electrodes [46,47]. This is an important point, as the nutrients concentration influences any microbial corrosion test, but often it is not tracked as it would require costly chemical analyses (enzymatic essay, gas chromatography, HPLC- High Performance Liquid Chromatography or colorimetric essay). Finally, stable anaerobic conditions are present in the solution and this can be monitored measuring the anode electrochemical potential.

The MFCs used in this experimentation were Pyrex bottles with an opening on the side to insert the air-breathing cathode. The anode is immersed in the solution filling the cell, which has a volume of 0.125 L. Both anode and cathode were carbon cloth with a living biofilm on them [27]. The anode is immersed in the electrolytic solution and it is colonized by anaerobic bacteria, as the solution lacks oxygen; on the other side, aerobic bacteria are present on the air-breathing cathode, which is exposed to the external environment [14]. The anode inside the solution is square shaped and has surface of about 25 cm^2; the cathode has a circular shape, with a surface of about 5 cm^2. A photograph of the used SCMFC is presented in 2.12.

2.3.2 Measuring system

An ad-hoc measuring system has been designed to monitor the experiment in the MFC. In order to measure all currents flowing in the cell, an analog-to-digital acquisition board has been used, employing the three resistors as shunts. The block diagram of the measuring system is shown in Fig. 2.13 and it is composed of the following.

- A Single Chamber Microbial Fuel Cell (SCMFC). It can be represented as a two electrodes cell, filled with the solution containing the bacteria inoculum. The sample made of the material whose microbial corrosion behaviour has to be assessed is immersed in the cell and then connected to the electrical circuit of the MFC.
- A set of resistors (R_S, R_C and R_A) which are employed as shunts to monitor the current evolution. Even though this is not the only possibility as other approaches

Figure 2.12: Picture of the Single Chamber Microbial Fuel Cell: a Pyrex®bottle of 0.125 L volume equipped with the air-breathing cathode on the opening on the left side, the anode connected through the small opening on the right side and the big opening on the top for positioning the sample electrode. [28]

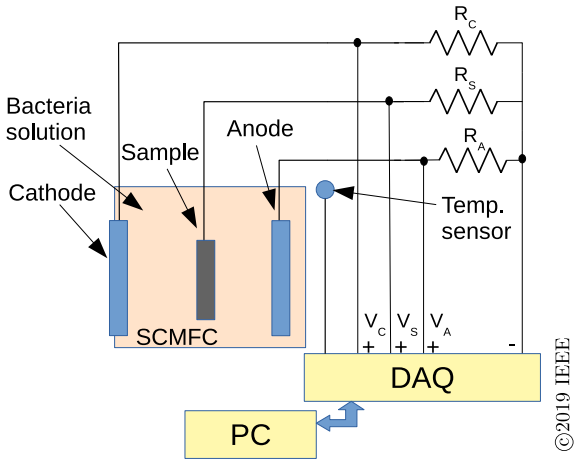

Figure 2.13: Block diagram of the measuring system: the SCMFC with the carbon cloth anode, the air-breathing cathode and the sample as the third electrode; the three resistors, the LM35 temperature sensor and the Digital Acquisition board (DAQ) connected to a PC. [28]

based for example on zero-gauss current sensors could be used, this setup is extremely cheap and can be used to arrange a simple measuring system. To perform the corrosion test, a reproducible working point must be selected for the for the

MFC, in order to be able to compare results from different experiments. Resistance values can be chosen in order to maximise the cell current or to work close to the maximum power point. In the former case, the minimum resistance values is limited only by the measuring system sensitivity.

- "An analog to digital acquisition board (ADC) which is used to measure the voltage drops on the shunts and therefore to monitor the current evolution. Several solutions can be used for this block such as digital acquisition boards or microcontroller based boards. The former are more suitable and flexible to design the system, the latter are extremely cheap using solutions as an example based on Arduino boards [48]. These solutions would also decrease the overall cost of the entire measuring system, avoiding the use of a dedicated PC. In addition to the current measurements, also the temperature has to be monitored as this is a critical parameter in microbial corrosion tests since the bacteria activity is strongly inhibited when temperature decreases.
- A PC which is either used to manage the system, in the case the ADC block requires it, or only to store the measured data."

"In the proposed measuring system, the current flowing from the sample I_S, the current flowing to the cathode I_C, and the current flowing from the anode I_A can be obtained as:

$$I_S = \frac{V_S}{R_S} \tag{2.2}$$

$$I_C = \frac{V_C}{R_C} \tag{2.3}$$

$$I_A = \frac{V_A}{R_A} \tag{2.4}$$

where V_S, V_C, and V_A are the voltage drops on R_S and R_C, and R_A, respectively. The circuit enables a simple check of the system operation since the currents have to obey the Kirchhoff's current law:

$$I_A + I_C + I_S = 0 \tag{2.5}$$

Any deviation of the current sum from zero has obviously to be considered either due to the measuring uncertainties or to a system malfunctioning. The voltage drop between anode and cathode, which is the operating point of the SCMFC, is simply:

$$\Delta V_{AC} = I_A \cdot R_A - I_C \cdot R_C \tag{2.6}$$

This voltage can be controlled by suitably choosing the value of the resistors so that any SCMFC load condition can be easily implemented. " [28] ©2019 IEEE

2.3.3 Experimental results

In order to validate the technique and the proposed measuring setup, different experiments have been performed. In this section, two tests will be presented, representative for a material with a poor corrosion resistance, namely the carbon steel, and with a good corrosion resistance, namely the AISI 304 stainless steel.

The MFC was filled with an electrolytic solution containing the bacteria inoculum; the inoculum was sludge collected from an anossic tank of a wastewater plant, in order to guarantee a wide variety of bacteria and perform tests in a real condition. Sodium acetate was added at the beginning of each test as carbon source for bacteria inside the fuel cell, using a concentration equal to 3 g/L. During the experiment, bacteria oxidise this nutrient, generating the current flow between anode and cathode. As the acetate is consumed, the current flowing between the MFC electrodes decreases, reaching values close to zero [44]. This trend was used to monitor the nutrients concentration in the solution and acetate was added when the current flowing between anode and cathode dropped to about 15% of the initial value. After each acetate addition, its concentration reached about 3 g/L, a value which allows having stable conditions for more than 6 days.

Samples were prepared using the common procedure for corrosion tests. They were cut from a sheet to the dimension of 10 mm $\times$ 10 mm, an electrical wire was soldered on one of the sample faces and then it was embedded in a polymeric resin in order to expose only one side of the sample to the solution. Finally, the metal surface was polished on abrasive paper until 4000 grid, rinsed in deionized water and dried.

In order to ensure a good bacteria activity and keep reproducible conditions, all tests were carried out at 30 ± 3 °C.

The DAQ system was realized by using a National Instrument USB6216 DAQ board. This board contains a 16 bit ADC, is equipped with 16 single-ended input channels and is capable of working with an input range of ± 0.2 V.

Tests carried out on mild steels samples used a configuration in which resistors were chosen in order to maximise the power output of the MFC, as these are the most favourable conditions for a stable functioning of the fuel cell. Maximum power point was found to be $R_C = R_A = 100\ \Omega$, so an equivalent resistor was chosen for the third component of the circuit $R_S = 100\ \Omega$. "On the other hand, for tests carried out on stainless steel a configuration with anode and cathode kept at about the same voltage was chosen. In this way it is possible to maximise the bacteria activity, and so to have harsher conditions for the material under study, even though at the expense of the SCMFC output power. Therefore, R_C and R_A were selected to have a lower nominal value of 22 Ω. Since the measuring system is designed to work with samples characterized by good corrosion resistance, low I_S values are expected so that an R_S resistance with nominal value of 100 Ω has been selected. These resistors were measured with an uncertainty of 0.03% by using a calibrated HP34401. By using carbon-films resistors, a thermal coefficient of about ± 350 ppm/°C can be expected that turns out in a thermal

related uncertainty of less than 0.2% for a temperature change of ± 5 °C, which reasonably is the maximum expected change.

The reduced value of R_C and R_A leads to a slightly higher current compared to the value measured on the mild steel sample, which anyway is expected to remain of the order of 1 mA or below. In this condition, the maximum voltage difference between anode and cathode is of the order of 40 mV, which does not exceed about 10% of the open circuit voltage difference expected (i.e. 400 mV).

The voltage drops on both R_A and R_C, measured by the USB6216, are of the order of 20 mV which allows employing the USB6216 input range of ± 200 mV without the need of external amplifiers therefore having the possibility of working without external power supply. Since the USB6216 has a maximum stated uncertainty lower than 90 μV with an input range of 200 mV, this turns out in an uncertainty for anode and cathode currents, whose values are expected to be of the order of 1 mA, of about 0.45%.

Since the USB6216 has a maximum sampling rate of 400 kHz, all measurement are performed by simultaneously sampling all signals at 40 kHz and taking 8000 samples per channel; the measurement therefore requires only 200 ms, and consequently the effect of the power supply noise is negligible. The data averaging also reduces the ADC noise contribution so that the final expected uncertainty on each value is lower than the stated value.

In these experimental conditions therefore an uncertainty lower than 1% is obtained for anode and cathode current values, which are higher then 600 μA; same uncertainty is obtained also for the sample current which is about 125 μA.

A check of the correct system operation can be easily obtained by observing the current sum which has to be zero by design. By considering anode and cathode current the most important part of the sum to obtain an easy uncertainty estimation, a maximum sum of less than 2% of the current can be expected for currents of the order of 1 mA, i.e. a maximum sum current lower than 20 µA is expected.

The temperature is measured by using a simple LM35 temperature sensor connected to a dedicated input channel set to an input voltage range of 1 V. The temperature uncertainty for temperatures in the range 25 °C to 35 °C can be expected to be of the order of 0.5 °C." [28] ©2019 IEEE

Carbon steel samples

"Fig. 2.14 shows the current evolution during a test performed on a mild steel sample. As it is possible to observe, the current (I_S) starts flowing from the sample to the cathode since the beginning of the measurement, with a simultaneous reduction of the current flowing from the carbon cloth anode (I_A). An I_S sharp increase is measured immediately after test beginning, as bacteria started immediately colonizing the mild steel surface. The sample becomes the electrode preferentially providing electrons to the cathode, due to the superimposition of two phenomena: sodium acetate oxidation (related to bacteria metabolism) and metal oxidation. The I_S value is due to these two

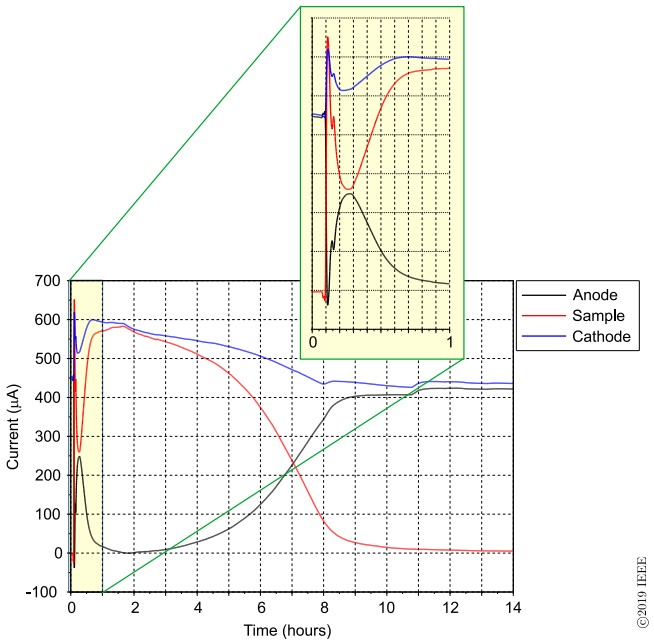

Figure 2.14: Current evolution in the microbial fuel cell during a test performed on a mild steel sample for 14 hours. I_A, I_C and I_S trends as a function of time are shown. The microbial corrosion attack starts immediately after the exposure of the sample to the electrolyte, as confirmed by the immediate increase of all current values (as can be observed in the expanded plot). [28]

contributions, which cannot be separated. The temporary decrease in I_S occurring in the first hour, with a consequent increase in I_A (see expanded plot in Fig. 2.14), can be probably related to the stabilization of the electrodes potentials after the connection of the sample in the SCMFC (of course the extensive corrosion occurring on the metal is changing its chemical composition). In the first part of the test, lasting approximately the first 6 hours, the mild steel sample remains the preferential anode of the cell and extensive corrosion occurs on its surface. Because of this, the conductivity of the sample metallic surface progressively decreased as well as the activity of bacteria on it. With the reduction of the sample current (occurring after 6 hours from the beginning of the test), the quantity of electrons provided by the cell anode increases again, leading to the last step of the test when, as the metal surface is completely covered by a corrosion products layer mainly composed of oxides and sulphides, micro-organisms are no longer able either to induce corrosion on it or to supply electrons derived from oxidation of acetate present in the solution. Thus, the fuel cell gets back to its normal operation, with current flowing almost only between anode and cathode." [28] ©2019 IEEE

After the test, which lasted about 24 hours, the sample was characterized using

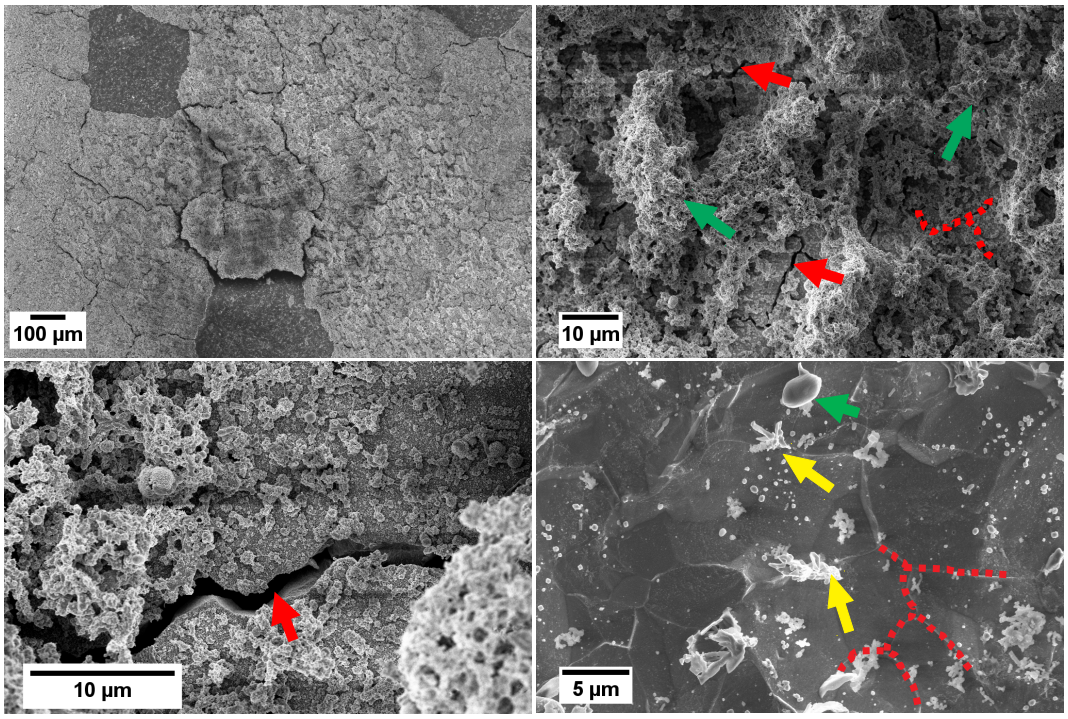

Figure 2.15: FESEM image of the mild steel surface after 1 day of immersion in the operating SCMFC. Red arrows indicate cracks at grain boundaries, green ones biofilm and yellow ones highlight the presence of sulphides. The test results are shown in Fig. 2.14

electron microscopy, in order to analyse its superficial morphology. As it is possible to see in Fig. 2.15, bacteria were able to colonize the sample surface already after only one day of immersion in the solution. Extensive corrosion can be observed on the sample, that led to cracks at grain boundaries and to the detachment of some fragments of material from the surface. At higher magnification, biofilm is clearly visible, highlighted by green arrows in the micrograph. Moreover, iron sulphide cristals (identified through Energy Dispersive X-ray Spectrometry, EDS) were found on the sample; they can be related to the corrosion reaction of iron in anaerobic environment:

$$Fe^{2+} + S^{2-} \longrightarrow FeS \tag{2.7}$$

Thus SEM characterization can confirm that the high values of current flowing between the sample and the cathode during the test can be related to the extensive corrosion occurring on its surface and to the bacteria colonization.

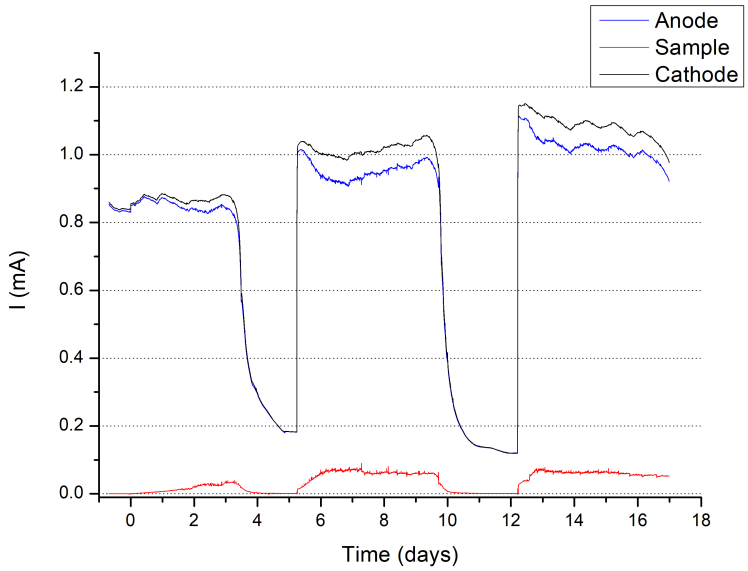

Figure 2.16: Current evolution in the microbial fuel cell during a test performed on an AISI 304 sample for 17 days.

Stainless steel samples

After characterizing a material with a poor corrosion resistance, the system was employed to test an alloy with more protective superficial oxide layer and thus a better corrosion resistance. Results for AISI 304 Stainless Steel are reported in Fig. 2.16.

In the graph, which shows the current evolution during the 17 days test, it is possible to see the main trend of I_A and I_C representing the periodical acetate consumption by bacteria. Actually, after about four days of operation, the current drops to about 0.2 mA, but, after a new acetate addition to restore the 3 g/L concentration, it increases again to the initial value. Observing the I_S current, it is possible to see that, unlike the previous case, the system is less perturbed by the connection of the third electrode to the MFC circuit. The carbon cloth remains the preferential anode during the whole duration of the experiment, even if after some hours an additional current contribution starts flowing from the sample to the cathode (see Fig. 2.17 for an expansion of the I_S trend).

I_S increases since the beginning of the test, as bacteria attach on sample surface and colonize it, providing also to this electrode the electrons coming from acetate oxidation. It is possible to state that this current value is directly related to bacteria activity because it decreases when the organic matter is consumed in the MFC, as it happens for I_A and I_C. Moreover, after an initial increase, I_S stabilizes to about 60 µA, presumably due to the complete colonization of the surface. Also in this case, the measured current sums two contributions due to microorganisms: oxidation of the metal (that dissolves in the

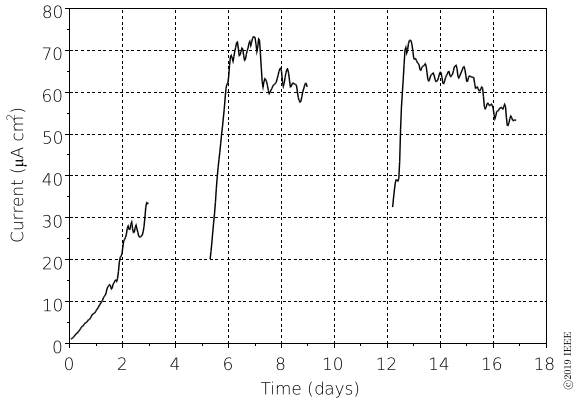

Figure 2.17: I_S trend as a function of time recorded in the same test of Fig. 2.16; the current values are normalized to the surface area of 1 cm^2. I_S increases after any addition of acetate highlighting the bacteria activity on the sample surface. [28]

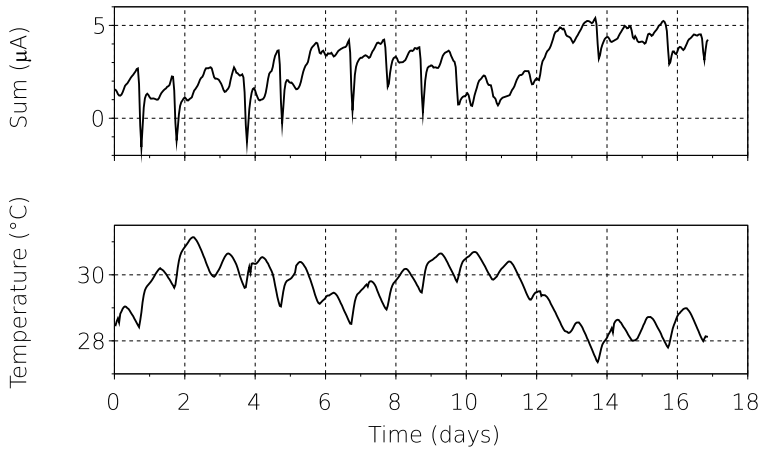

Figure 2.18: Currents sum (I_A + I_S + I_S) from the test in the SCMFC of Fig. 2.16 and temperature trend during the experiment.

solution) and bacteria metabolism, related to the oxidation of the acetate, which is the fuel inside the cell.

Fig. 2.18 also shows the current sum, which as expected remains always below $\pm$20 μA and which shows a correlation with the temperature, as expected since the resistors have a not negligible thermal coefficient. The temperature during all the tests remains between 27 °C and 32 °C.

After the test, the sample surface was characterize using electron microscopy. In this case, no signs of corrosion could be highlighted. The biofilm covered almost continuously the electrode surface, confirming the indication given by the I_S trend. Removing

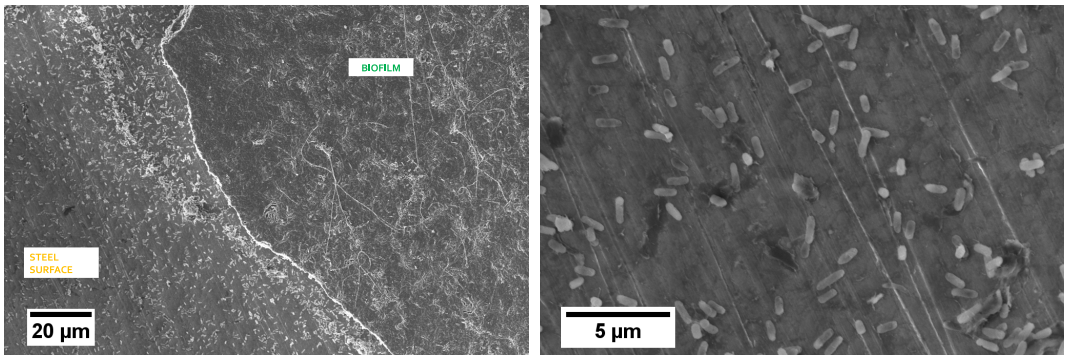

Figure 2.19: SEM images of the AISI 304 sample surface after 17 days of immersion in the operating SCMFC.

the biofilm in some part of the surface, it was possible to observe the metal surface, which appeared undamaged; the scratches are related to the polishing process.

Comparison with traditional immersion test

"The obtained test results highlight how the current I_s from the sample seems to be representative of the biofilm growth on the sample and consequently of the corrosion on the surface, enabling researchers to easily compare microbial corrosion resistance of different materials in a simple and direct way.

To confirm this correlation, the results obtained through the proposed measuring system have been compared to those of a standard immersion test where the polarization effect, due to the connection of sample inside the fuel cell, is not present.

The immersion tests were carried out in parallel with the SCMFC test, using the same electrolytic solution, wastewater, in the same temperature range of $30 \pm 3\,^{\circ}\mathrm{C}$ and adding acetate at the same time interval even though the bacteria activity in the solution is not monitored.

Results have been compared in terms of corrosion behavior of the metal assessed by means of Electrochemical Impedance Spectroscopy (EIS), as commonly done in corrosion tests [49–51]. This technique has been preferred to other possible electrochemical measurements, as it is non-destructive and does not alter the corrosion process occurring on the material. EIS measurements were performed on both samples after three weeks test by using an Ivium CompactStat, by applying a sinusoidal signal with amplitude 10 mV in the frequency range 10^{-2} Hz to 10^{5} Hz and acquiring 5 points per frequency decade. A silver chloride electrode was used as reference electrode and a platinum wire was used as counter electrode.

The morphological characterization of the metallic surfaces was performed by means of Field Emission Scanning Electron Microscopy (FESEM Supra 40 by Zeiss) collecting the images at 5 kV with a 20 µm aperture.

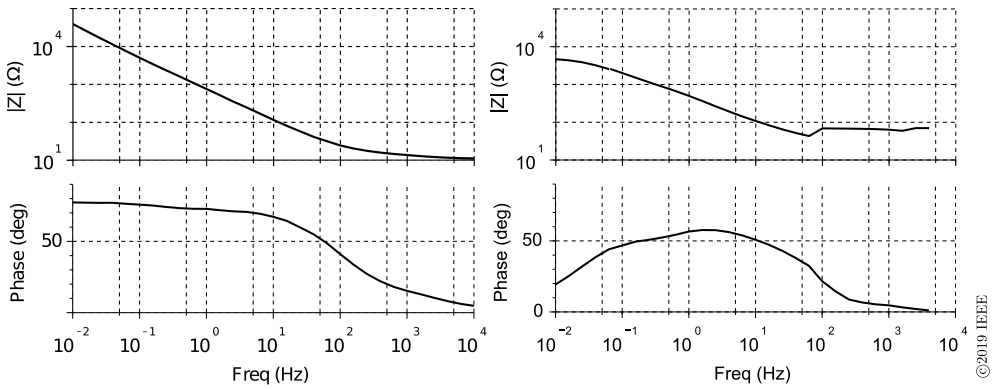

Figure 2.20: Bode plots recorded on the AISI 304 stainless steel sample immersed in the electrolytic solution containing the bacteria inoculum for three weeks. [28]

EIS spectra are presented in Fig. 2.20 as Bode diagrams. The plots show a more stable condition for the sample that underwent a simple immersion test, for which impedance modulus reaches values close to $10^5\ \Omega \cdot \mathrm{cm}^2$ and the phase reaches almost $80°$ (at low frequencies), showing a good corrosion resistance still after 20 days of immersion. This result is consistent with the good corrosion resistance of AISI 304 steel in a solution containing bacteria. As far as the SCMFC test sample is concerned, a different condition could be highlighted. Actually, the test had been more aggressive for the metal, which exhibits an impedance modulus one order of magnitude lower than the other sample (about $10^4\ \Omega \cdot \mathrm{cm}^2$ at low frequencies). The phase reaches a maximum value of $60°$, indicating a less protective nature of the superficial layer.

Observing the samples at FESEM after the two tests, it is possible to compare the different biofilm coverage (see Fig. 2.21). Images show a completely different biofilm growth between the two samples. The sample tested inside the fuel cell exhibits a continuous biofilm coverage, which conceals the metal. The presence of the air-breathing cathode, where reduction reactions are able to exploit the electrons coming from oxidation of acetate and metal, favours the colonization of the electrode surface by bacteria. On the other hand, colonization by bacteria appears at a less advanced stage for the sample that underwent a simple immersion test. Micro-organisms are present on the surface, but only discontinuously, as they have not developed a compact biofilm well adherent to the surface.

Moreover, good agreement can be found between currents I_S measured for different materials during the test in the SCMFC and EIS spectra collected after the test. Actually, alloys with poor corrosion resistance exhibited high I_S values and low modulus of impedance (for the carbon steel samples, values close to $10^2\ \Omega \cdot \mathrm{cm}^2$ at low frequencies); on the other hand, for materials with good corrosion resistance, low I_S values and higher modulus of impedance can be found (such as in the case of the stainless steel sample). As the current flowing from the sample to the cathode is related to metal

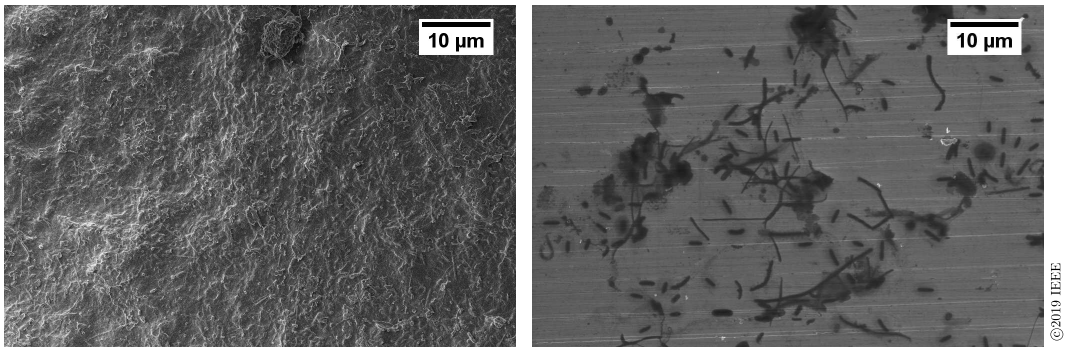

Figure 2.21: SEM images of the AISI 304 sample surface after the test in the operating SCMFC (on the left) and after the immersion test (on the right). [28]

oxidation as well as to bacteria metabolism, a direct relationship between such current and the corrosion rate can not be established. It is however possible to state that, in this specific test condition, the corrosion current is at most equal to I_S. So a comparison between different materials is possible and, as discussed for EIS measurements, supported also by traditional electrochemical methods." [28] ©2019 IEEE

2.3.4 Conclusions

"An innovative approach for microbial corrosion testing has been presented. The proposed system, that makes use of a single chamber microbial fuel cell, has been exploited in a comparative study to assess the microbial corrosion behavior of mild steel and stainless steel samples, highlighting of course the different corrosion resistance of the two alloys.

Information gained by the test are manifold. By measuring the current between anode and cathode, it is possible to monitor the bacteria activity so that it is possible to be sure to have enough nutrient concentration to have active bacteria. After sample connection inside the fuel cell, measuring the current between sample and cathode allows users to detect corrosion reactions occurring on metal surface. In the case of a material with poor corrosion resistance, large variations in the current flowing in the fuel cell can be observed, highlighting the corrosion reactions that are in progress on metal surface. On the other hand, when a material with good corrosion resistance is tested inside the cell, the current measured between sample and cathode increases slowly, until it stabilizes. This current monitoring enables to assess the progressive sample surface colonization by bacteria, which form the biofilm, and the corrosion processes ongoing on the sample surface.

The use of single chamber microbial fuel cell allows users to perform tests in conditions similar to the real ones and is faster then in the case of simple immersion test. Actually, the sample polarization obtained in the fuel cell leads to a faster colonization

of the metal surface by bacteria.

In addition, by employing the SCFMC a direct measurement of the nutrient concentration is not required since the current monitoring can be used as a direct indicator of the bacteria activity. This permits to avoid employing costly instrumentation and opens to the possibility of replicating the measuring system to several microbial cells to study the corrosion resistance of different materials at a minimum cost.

This new technique can be considered as an additional tool for researchers in microbial corrosion field. As previously discussed, test conditions are more aggressive than a simple immersion test and many important information can be easily gathered from currents flowing in the SCMFC. Compared to the Dual Cell technique, the proposed methodology has a simpler experimental setup. Moreover, information that can be derived from the two experiments are slightly different. Actually, in the SCMFC, test conditions are strictly anaerobic, allowing to study more in depth this situation. On the other hand, the Dual Cell technique is more focused on the comparison between material behaviour in sterile conditions or in an environment containing bacteria.

Advantages of this new proposed technique are then related to the test simplification in the part specifically related to biology, because bacteria cultures are not needed, as the solution can be taken directly from the environment. Eventually, performing experiments with different bacteria strains allows one to obtain results more adherent to those found in each real specific condition." [28] ©2019 IEEE

2.4 Conclusions

This Chapter presented some of the most significant electrochemical measurements that can be used for the assessment of microbial corrosion during laboratory tests. In the first part, a case study involving the electrochemical behaviour of two different stainless steel grades immersed in hypersaline solution was discussed. The use of a multianalytical approach, that exploited the results of different electrochemical and morphological characterizations, permitted to differentiate the corrosion resistance of the two different materials in the solution containing bacteria. Moreover, an interesting corrosion inhibition due to microorganisms metabolism was highlighted comparing results in biotic and abiotic conditions.

In the second part of the Chapter, a novel experimental setup for microbial corrosion study was presented. Main advantages of this technique are related to the simplification of some of the measurements needed to monitor the test. Moreover, tests conditions can be derived from the working parameters of the Microbial Fuel Cells. Results from the characterization of different materials have been presented.

Chapter 3

An imaging system for microbial corrosion assessment

Some of the work described in this chapter has been previously published in [52, 53].

3.1 Introduction

The role of electrochemical techniques in the corrosion field is of clear importance; as already discussed in Chapter 1, manifold are the information that can be derived from them to study the material-environment interaction and the corrosion mechanisms occurring. Nevertheless, most of them can not be considered as stand-alone techniques, as they must be coupled to each other or to other chemico-physical characterizations such as optical and electron microscopy, in order to investigate the mechanism and the morphology of the corrosion reactions occurring on the metallic surface. Moreover, in the specific case of microbial corrosion, an important role is played by the bacteria attachment on the sample surface. Actually, formation of biofilm can generate preferential sites for corrosion attack, as it creates areas of differential aeration or where corrosive compounds (such as chlorides ions) can accumulate or pH changes can occur. Thus, a great advantage can derive from the development of an imaging system able to quantify the microbial adhesion on sample surface.

Many approaches for imaging analysis are possible when microbial corrosion (MIC) is concerned. In particular, these techniques can be classified taking into account the instrument used for image collection or the main purpose of the characterization (corrosion assessment or biofilm growth). If surface morphology is the main concern, generally stereo-microscope, reflected light microscopy and Scanning Electron Microscopy (SEM) are used [54–57]. In order to obtain a more accurate three-dimensional reconstruction of the sample surface, white light interferometry or Fourier Transform Profilometry can be used, so that pit formation can be detected [58,59]. Most important advantages of these techniques can be related to the easy way in which corrosion pits can

be detected; their limit is related to the detection of biofilm and attached microorganisms, as the magnification is too low. On the other hand, in order to have the best morphological characterization of the biofilm, Confocal Laser Scanning Microscope (CLSM) is widely used [60–65]. This technique allows to obtain quantitative information about biofilm coverage and also its three-dimensional structure, providing important information to researchers in biology. One of the main limitations is that the sample has to be prepared using staining techniques, that often are not available in laboratories focused on materials science.

In this Chapter, an imaging system to analyse bacteria adhesion on sample surface will be presented. It is able to process micrographs taken at electron microscope in order to provide information on biofilm coverage and size distribution of bacteria aggregates present on the material after immersion in a solution containing bacteria. Even if other microscopy techniques could be used to assess the attachment of microorganisms (see Section 1.3 for the discussion about imaging techniques for microbial corrosion analysis), it was decided to use electron microscopy for different reasons. First of all, it has a sufficient resolution to analyse also samples with a low biofilm coverage, which is a common condition for corrosion field. Moreover, sample preparation for electron microscopy is easier than the one required for many optical techniques, as it does not require staining. Finally, unlike CLSM or epifluorescence microscopy, SEM is routinely used in any Material Science laboratory, so additional equipment or expertise is not required.

In the next Section, the imaging algorithm will be described in details, providing information about different steps, from image acquisition to processing. Then, two case studies will be presented, involving respectively a metallic sample and a non-conductive sample, in order to show the different parameters to use for the algorithm and the results which is possible to obtain.

3.2 Contours detection imaging algorithm for SEM images

The imaging algorithm is written in Python and employs the OpenCV opensource environment, already used in many applications involving the identification of specific objects in images [66, 67]. The whole process can be divided in four steps: image acquisition using SEM, image brightness and contrast normalization, image thresholding to obtain a binary image and finally the bacteria identification.

3.2.1 Image acquisition

Image acquisition can be performed by the operator setting proper parameters for the instrument, such as the acceleration voltage and working distance, according to the sample superficial conductivity and its morphology. Acceleration voltage can vary

typically between 1.5 kV and 30 kV. A higher value guarantees a higher signal and a lower noise in the final micrograph; moreover, increasing acceleration voltage it is possible to improve the resolution, that is the minimum-resolvable distance in the final image. At the same time, in case of insulating samples, problems related to charging effect can arise. Actually, if electrons are not able to ground properly, image artefacts can appear, generally visible as white spots. Finally, acceleration voltage influences the electrons penetration depth. Thus, using a higher voltage will lead to a larger interaction volume in the material and so the analysis will be affected also by sample inner layers.

As far as the working distance is concerned, it is generally set in the range between 1 mm to 3 mm, in order to have a good signal. Typically, choosing a smaller working distance allows to have a lower acceleration voltage, which could be favourable in case of not well conductive samples. Thus this two parameters must always be set taking in account the material under analysis and should be adapted to each other.

In this work, micrographs have been collected by means of a Field Emission Scanning Electron Microscope (FESEM - Supra 40 by Zeiss), using the In-Lens detector. As it is placed coaxial to the primary beam, it has a higher electron efficiency at low acceleration voltages if compared to the secondary electrons detector. Thus, lower acceleration voltages can be applied, avoiding charging effects and obtaining a signal coming only from interaction with the most outer layers of the sample. For the micrographs in this work, acceleration voltage was set to 5 kV, using a working distance of about 3 mm.

Magnification was chosen in order to obtain a good compromise between image resolution and dimension of the analysed area, considering that the expected size for singly attached bacteria ranges between 2 µm to 15 µm. Therefore, selecting a magnification equal to 1000X, corresponding to an analysed area of about 400 µm $\times$ 300 µm, and an image dimension of 2048 pixels $\times$ 1536 pixels, it is possible to obtain a resolution of the order of 0.2 µm/pixels. This configuration has been used for all imaging analysis described in this Chapter, unless otherwise specified.

3.2.2 Image brightness and contrast normalization

"After setting magnification and pixel size, the operator can acquire the micrograph, varying image brightness and contrast so as to obtain the best visualization of the sample morphology. Setting these parameters is a critical operation, often influenced by operator's personal decisions, which makes any automatic image processing difficult to be applied.

In addition, the image brightness can change over the scanned surface because of the different topography and roughness and as a consequence of charging effects occurring when the electron beam hits non conductive species, such as bacteria aggregates, corrosion products or salt crystals left on the sample after drying. The low voltages used by the field emission microscope and the efficiency of its detector greatly help to reduce the charging effects making them almost negligible. However, brightness can

still significantly change due to the different surface morphology in the different areas (i. e. different positions) of the scanned image, perhaps due to non planarity of the sample [68].

Therefore, an image normalization has to be performed in order to obtain SEM images whose contrast and brightness are reasonably independent from the operator. This processing involves three steps:

1. Estimation of brightness changes due to the different morphology of the surface area;
2. Correction of brightness changes in the different positions;
3. Normalization of the image contrast to eliminate the operator setting effect.

The first step requires identifying a brightness plane whose value is described by the following equation:

$$B = B_0 + \alpha_{BX}x + \alpha_{BY}y \tag{3.1}$$

where B is the brightness of the metallic surface area not interested by microbial corrosion, B_0 is the average brightness value, α_{BX} and α_{BY} are the brightness changes with position coefficients, and x and y are the position coordinates.

Since the samples have an average brightness which is almost constant in the absence of corrosion, the identification of the brightness average value could be easily performed if one is able to find on the image the areas not affected by corrosion, i.e. in the specific case of microbial corrosion, areas not affected by bacteria growth. Such a manual selection can be avoided in most cases since the area covered by the bacteria is usually limited with respect to the total scanned metallic surface, so that the image brightness as a function of the coordinates can be easily estimated by solving in the Least Square sense the matrix equation:

$$\mathbf{B} = \mathbf{U} \cdot \lambda \tag{3.2}$$

where $\mathbf{B}$ is the column vector of all pixels brightness, $\mathbf{U}$ is $n_{Pix} \times 3$ matrix in which the row is $[1, x, y]$ and accounts for the position of each line in the $\mathbf{B}$ vector and $\lambda = [B_0, \alpha_{BX}, \alpha_{BY}]'$ is the vector containing the sensitivities whose estimation is referred to as $\widehat{\lambda}$.

Of course the actual estimated brightness values depend on the way the images are acquired, i.e. on the SEM operator; however, tests performed on several images with average brightness in the range of 140 to 220 out of a maximum value of 255 led to position coefficients whose maximum value is of the order of $9 \cdot 10^{-3}$ on x axis and of $3 \cdot 10^{-2}$ on the y axis. This leads to maximum brightness changes of the order of 40 units out of 255 units.

The second pre-processing step, once $\hat{\lambda}$ has been estimated, can be simply obtained by computing the corrected brightness B_c as:

$$B_c = \frac{B}{1 + \alpha_{BX} x + \alpha_{BY} y} \tag{3.3}$$

obtaining therefore an image whose brightness is no longer affected by brightness changes in the different surface areas.

The third step can be obtained simply by changing image contrast by modifying the brightness values, so that they cover all the available gray levels. In order to avoid a normalization affected by the presence of few abnormal white and black spots, the image brightness B_{min} and B_{max} can be obtained by:

$$B_{min} = \sum_{pixelnumber} P_{xy} : B_p < B_{min}; kP_{tot} \tag{3.4}$$

$$B_{max} = \sum_{pixelnumber} P_{xy} : B_p > B_{max}; kP_{tot} \tag{3.5}$$

where P_{xy} is the generic pixel, P_{tot} is the number of pixels in the image and k is the coefficient usually in the range of 5% to 10%, which is used to define the number of pixels shown as black and white.

Once B_{min} and B_{max} have been estimated, the image brightness can be normalized as:

$$B_s = \begin{cases} 0, & \text{if } B \leq B_{min} \\ (B - B_{min}) \frac{Max_B}{B_{max} - B_{min}}, & \text{if } B_{min} < B < B_{max} \\ Max_B, & \text{if } B \geq B_{max} \end{cases} \tag{3.6}$$

where Max_B is the maximum brightness value of the image.

After image brightness and contrast normalization, the processed image appears with a uniform background, representing the sample surface, and bacteria aggregates appearing as black spots." [52] ©2019 IEEE

3.2.3 Bacteria identification

"Bacteria identification and estimation of the relative amount of attached bacteria on a surface can be performed trying to separate in the image the areas covered by the bacteria themselves. In principle this operation is reasonably easy, though questionable, when performed manually by an operator, but it is much more difficult when performed in an automatic way. The request is, for each pixel on the image, to define if it belongs to a bacterium or not, i.e. the image, which in general is a grey-scale one, must be converted into a binary one applying some form of threshold. After that, it becomes easy to estimate the relative amount of bacteria simply by counting the pixels belonging to bacteria areas with respect to the total." [52] ©2019 IEEE

The image conversion from gray scale to binary can be performed applying a proper threshold value, related to the sample morphology and so to the image contrast. Actually, the threshold process needs to be adapted to the image appearance, in particular discriminating between metallic samples and non-conductive samples. In the former case bacteria can be easily identified as dark spots, i.e. when their brightness (e.g. the black level) is at least 20% lower than the average brightness. In the case of the non-conductive sample, bacteria appear slightly brighter than the background, so the threshold process tags them if their brightness is at least 2% higher the the background. A broader discussion about this point is presented in the following two sections.

Finally, bacteria identification is performed by using the OpenCV opensource environment [69, 70] by using the `findContour` function set to identify dark spots. This function returns a list of contours which can be easily shown on the SEM image, flagging the identified aggregates. Moreover, dimensional distribution can be obtained, providing also other important information for material characterization such as number of aggregates present on the surface and biofilm coverage.

3.3 Application to metallic samples

The imaging algorithm has been used to characterize bacteria attachment on stainless steel samples after immersion in two different solutions containing bacteria. The aim was to assess quantitatively the biofilm coverage, both in terms of surface percentage covered by bacteria and as dimensional distribution of bacteria aggregates.

Two samples were prepared for the immersion test, following the usual procedure for corrosion tests. Samples dimension was 10 mm $\times$ 10 mm, they were embedded in polymeric resin, then polished on abrasive paper until 4000 grid, rinsed in deionized water and dried. The material was AISI 304 stainless steel (chemical composition can be found in Table 2.1) and the solutions used for the test were Starkey Medium and Artificial Seawater (see compositions in Table 3.1). The former is a classic growth medium for bacteria, containing mainly sulphates and chlorides ions; the latter has a more complex composition simulating marine environment, also a favourable solution for microorganisms proliferation. Different corrosion morphologies are expected for the samples immersed in the two solutions. In particular, the presence of phosphates in the Starkey Medium should accelerate bacteria proliferation both as planktonic population in the solution and attached on the sample surface. Salt marsh sediments have been used as inoculum for the two solutions; they were added in the concentration of 10 vol%. The test lasted for about 200 hours and the temperature was kept in range of $30 \pm 3\,^{\circ}\mathrm{C}$.

When the immersion test concluded, samples were rinsed in deionized water and dried. In this way, bacteria not attached to the sample surface can be washed away, avoiding to alter the following count. Moreover it is important to avoid that the electrolytic solution remains on the sample during drying, as it would lead to the formation of salt crystals on it, which would create problems during image acquisition. Actually,

Table 3.1: Electrolytic Solutions Composition

Electrolytic Solution	**Concentration [g/L]**
Starkey Medium	K_2HPO_4 0.50, NH_4Cl 1.00, Na_2SO_4 1.00, $CaCl_2 2H_2O$ 0.100, $MgSO_4 \cdot 7H_2O$ 2.00, $NaCl$ 24.53, CH_3COONa 3.00
Artificial Seawater	$NaCl$ 24.53, $MgCl_2$ 5.20, Na_2SO_4 4.09, $CaCl_2$ 1.16, KCl 0.695, $NaHCO_3$ 0.201, KBr 0.101, H_3BO_3 0.027, $SrCl_2$ 0.025, NaF 0.003, CH_3COONa 3.00

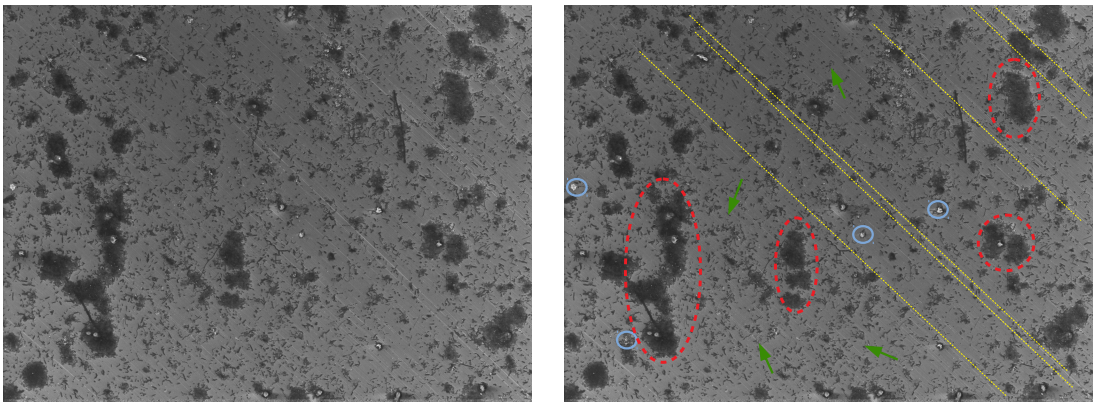

Figure 3.1: SEM image of a metallic surface affected by microbial corrosion (on the left) and identified elements on the micrograph (on the right): polishing lines are highlighted in yellow, single microorganisms attached on the surface are labelled with green arrows, larger bacteria clusters are identified by red circles and salt crystals by blue circles.

the presence of salt crystals on the sample appears at SEM as white spots surrounded by dark areas (because of the different conductivity) and this would make the micrograph difficult to process by the software. At the same time, it is important to avoid that attached bacteria detach from the sample during the washing step, so particular care should be used during this step.

After drying, the sample can be observed using SEM and micrographs can be taken. An acceleration voltage of 5 kV and a working distance of 3 mm was used to acquire the images; the magnification was of 1000X, obtaining an analysed area of about $400\ \mu m \times 300\ \mu m$. At least ten micrographs were acquired for each sample, choosing random points on the surface.

Fig. 3.1 shows, as an example, a micrograph representing one of the samples immersed in Starkey Medium. In the background, the metal surface is visible, characterized by a slightly brighter colour and some 'lines' passing on it. These are scratches related to the polishing step, which have a negligible influence on the corrosion test (as their roughness is very low), but could alter the imaging process if not correctly analysed. Then, some dark spots can be observed in the micrograph, representing the microorganisms attached on the sample surface. It is possible to see that both singly attached bacteria and larger agglomerates are present. In the former case, they have a size in the ranging from about $2\ \mu m$ to $10\ \mu m$, corresponding to an area spanning from $3\ \mu m^2$ to $20\ \mu m^2$. Bacteria aggregates can range between from $5\ \mu m^2$ up to $2000\ \mu m^2$ or $3000\ \mu m^2$. Finally, last element that can be found in a SEM micrograph after a corrosion test is the presence of salt crystals. As mentioned before, they appear as white spots on the sample surface. As the algorithm is set to identify only black objects in the image, generally they do not represent a problem for the analysis, anyway if charging effects

occur they could alter the appearance of the micrograph. In particular, if salt crystals are surrounded by a black halo, this could interfere on the bacteria identification. All the discussed elements have been identified in Fig. 3.1.

Fig. 3.2 shows the results obtained from the processing of two micrographs, corresponding to a sample immersed in Starkey Medium (on the left) and in Artificial Seawater (on the right). The former exhibits a superficial morphology characterized by the presence of large bacteria clusters and, at the same time, a high number of singly attached bacteria. This leads to a low superficial conductivity of the sample and, consequently, to a low contrast in the acquired micrograph. This effect can be mitigated thanks to the image brightness and contrast normalization, as it is possible to see in the second image. After this pre-processing, the metal surface appears brighter and a higher contrast is present between it and the bacteria aggregates. In this way, it is possible to apply the thresholding and convert the gray-scale image to a binary one: all pixels having a brightness at least 20% lower than the average are converted to black pixels, while the others become white. The pre-processing step is important in order to let the user choose a higher threshold value, so as to avoid wrong identification during the binarization. After that, bacteria identification is performed using the `findContour` function in OpenCV. In the last image of the left column of Fig. 3.2 it is possible to see the identified bacteria aggregates differentiated according to their size: the smaller aggregates are labelled in green, while the larger ones are in red. The former are generally singly attached bacteria or small clusters; they represent the early stages of bacteria colonization of the sample surface. The size that discriminates between the two categories can be set arbitrary to about 200 μm^2, which corresponds to an agglomerate of about 10 to 20 bacteria. The number of small aggregates can give an important information about the solution aggressiveness and the microorganisms concentration in it. On the other hand, large bacteria clusters can be considered the most dangerous ones, as they could create preferential sites for microbial corrosion attach. So their number and average size can give an important indication about the microbial corrosion attach occurring on the metal surface.

The sample immersed in Artificial Seawater exhibited a different superficial morphology, characterized by singly attached bacteria and only few large bacteria clusters. So in this case the influence of microorganisms on the superficial conductivity is less evident and the contrast between the metal surface and the attached bacteria is high already in the acquired image; because of this, the effect of the normalization is less evident. After the thresholding, the identification step is able to recognize the attached bacteria. In this case, a lower number of large aggregates is present. Moreover, bacteria size appears slightly higher, presumably due to different bacteria strains present in the two solutions.

Additional data derived from the processing of the two images are reported in Table 3.2. The total number of large bacteria aggregates per micrograph is 12 for the sample immersed in Starkey Medium and 8 for the other. The two samples differ also in the number of small bacteria clusters per micrograph: 18509 in one case and 7343 in the

other. The average size of large bacteria aggregates is higher for the sample immersed in Starkey Medium, indicating a more appropriate solution for bacteria proliferation if compared to Artificial Seawater. Moreover, the different average size of small bacteria clusters suggests a different shape and so, presumably, different bacteria strains present in the solution. This is a reasonable hypothesis, because using salt marsh sediments as inoculum a wide variety of bacteria is present in the solution at the beginning of the experiment and only some strains develop, depending on the solution composition. Finally, biofilm coverage can be calculated as the ratio between image pixels occupied by bacteria and the total number of pixels in the micrograph. This value is similar for the two samples, but taking in account the different number of large aggregates, which are the most dangerous, it is possible to say that the microbial corrosion attack is in a more advanced stage in the sample immersed in Starkey Medium. This information can also be derived from histograms representing dimensional distribution of bacteria aggregates; results for the two images are presented in Fig. 3.3. Immersion in artificial seawater lead to a condition in which bacteria are singularly and randomly attached on the surface with only few bigger agglomerates, which can be recognized in the histogram ranging until 3000 μm^2. On the other hand, immersion in Starkey solution induced the formation of a higher number of bigger aggregates (area above 20 μm^2).

Analysing all the acquired images, it was possible to calculate average values for all the parameters under investigation. Results are reported in Fig. 3.4 as histograms and in Table 3.3.

As it is possible to see, samples immersed in Starkey Medium present a higher number of small bacteria aggregates, characterized also by smaller dimensions. As far as the number of large aggregates is concerned, the situation is different for the two environments. The two samples immersed in Starkey Medium have an average number of large aggregates per micrograph close to 10 units, while for the samples immersed in Artificial Seawater this value is of about 5 units. The average size for large bacteria clusters is similar for the two samples.

3.4 Application to non-conductive samples

The same imaging algorithm has been applied also for the identification of bacteria on non-conductive sample. This condition can be found when, for examples, a polymeric material is being characterized. Actually, polymeric coatings are commonly used to protect metals from corrosion and some of them have bacteriostatic properties that can be exploited in environments where microbial corrosion can occur. So, even if different techniques can be used to assess the antimicrobial properties of a specific material, great advantage could arise from a software able to analyse images acquired through electron microscopy, providing information about bacteria attachment on sample surface.

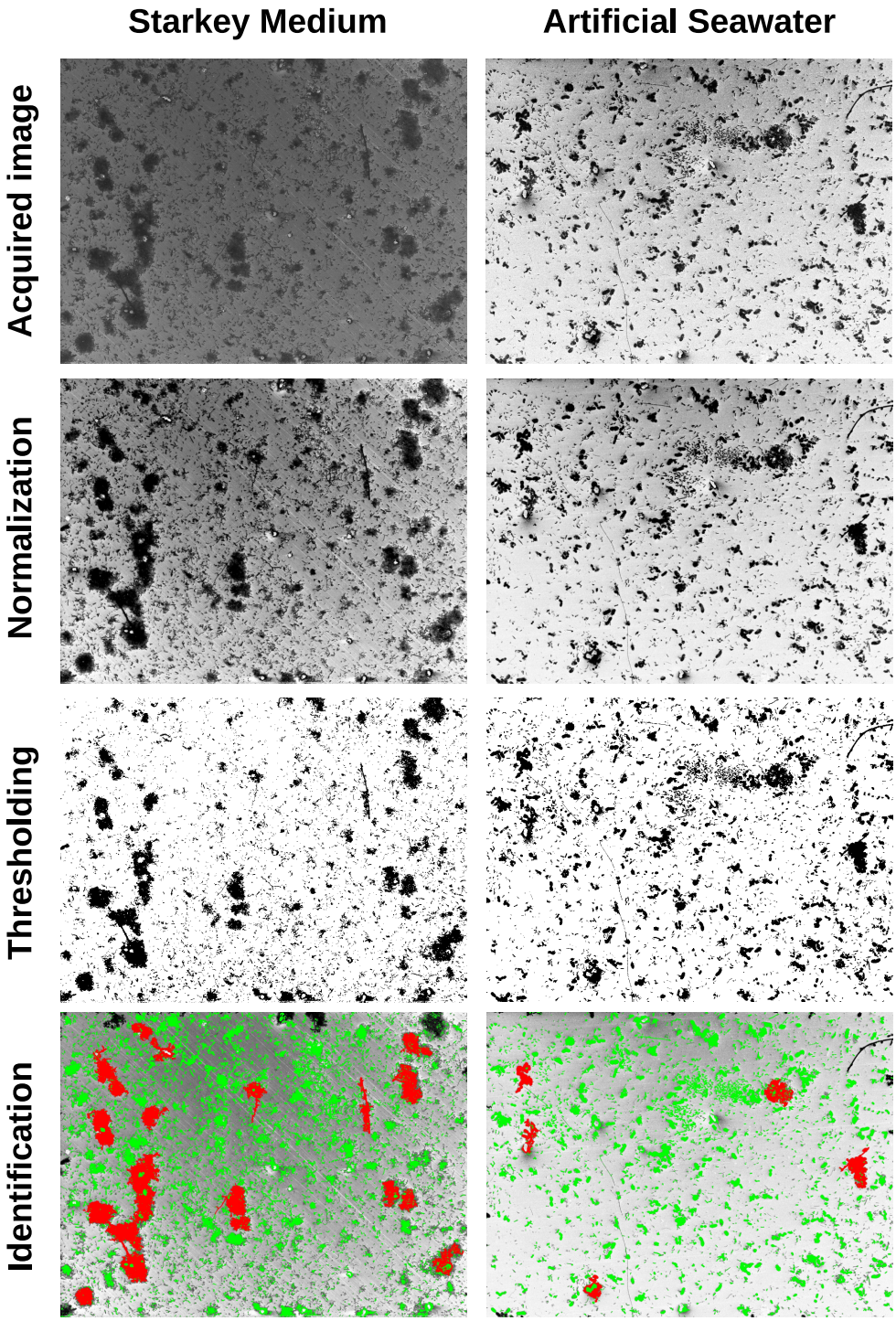

Figure 3.2: Results from the image processing for a sample immersed in Starkey Medium (on the left) and in Artificial Seawater (on the right). Bacteria clusters having dimension above 200 μm^2 are labelled in red, otherwise in green.

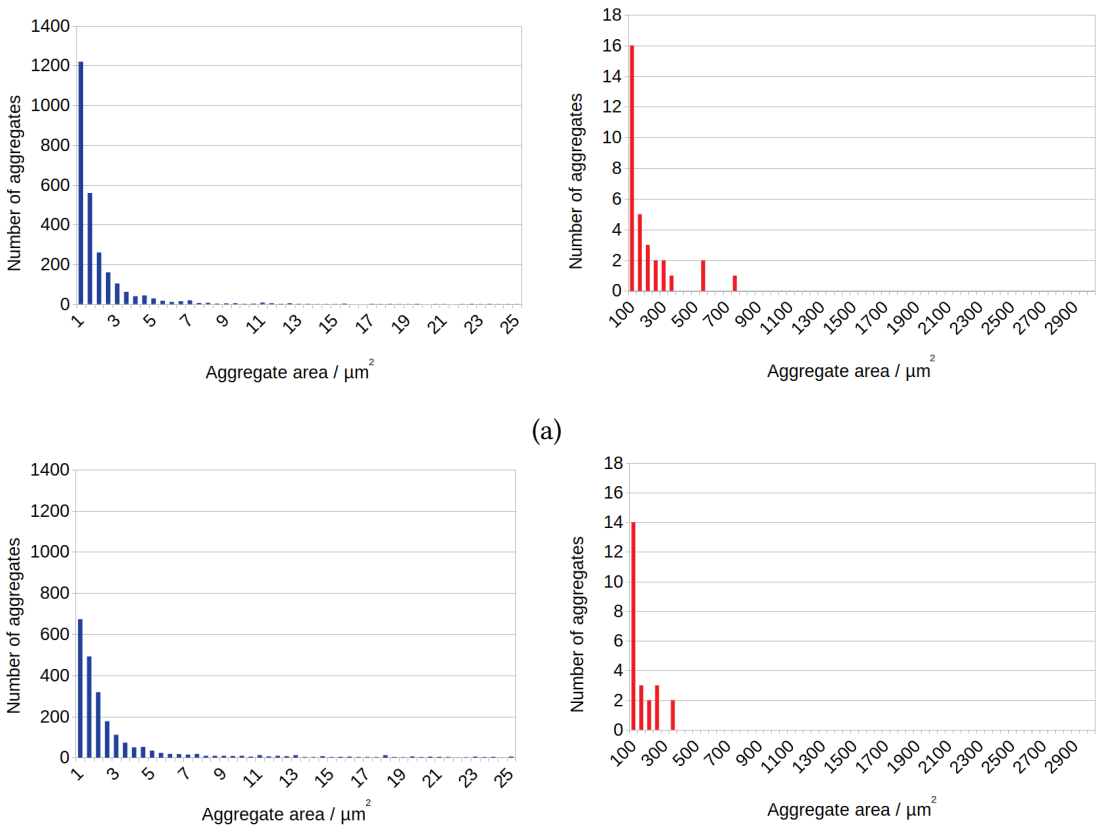

Figure 3.3: Histograms showing dimensional distribution (expressed as agglomerate area) for the samples immersed in Starkey medium (a) and artificial seawater (b).

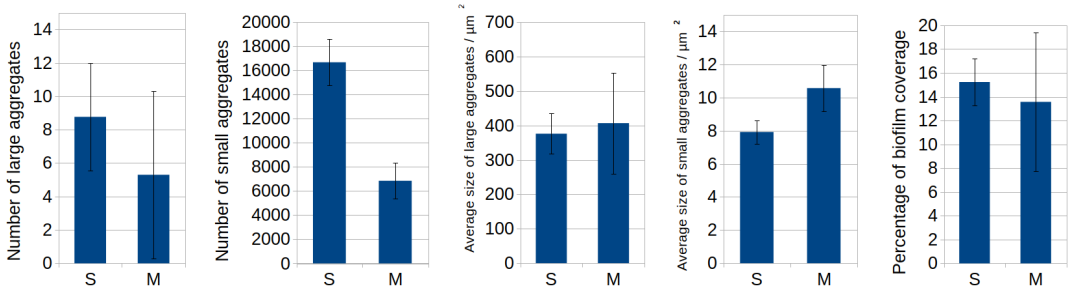

Figure 3.4: Value and uncertainty for different parameters related to bacteria attachment on stainless steel samples after immersion in Starkey Medium (S) and artificial seawater (M).

Table 3.2: Results from image processing of micrographs showed in Fig. 3.2.

Electrolytic Solution	**Number of small aggregates**	**Average size of small aggregates** $(\mu m)^2$	**Number of large aggregates**	**Average size of large aggregates** $(\mu m)^2$	**Biofilm coverage**
Artificial seawater	7343	9.7	8	316.5	14.7
Starkey medium	18509	8.5	12	438.9	15.3

Table 3.3: Results from image processing obtained for samples immersed in Artificial seawater and in Starkey medium.

Electrolytic Solution	**Number of small aggregates**	**Average size of small aggregates** $(\mu m)^2$	**Number of large aggregates**	**Average size of large aggregates** $(\mu m)^2$	**Biofilm coverage**
Artificial seawater	6852 ± 1480	10.6 ± 1.2	5.3 ± 2.2	406.9 ± 172.2	13.6 ± 2.4
Starkey medium	16686 ± 1930	7.9 ± 0.7	8.8 ± 3.2	376.2 ± 58.9	15.2 ± 1.9

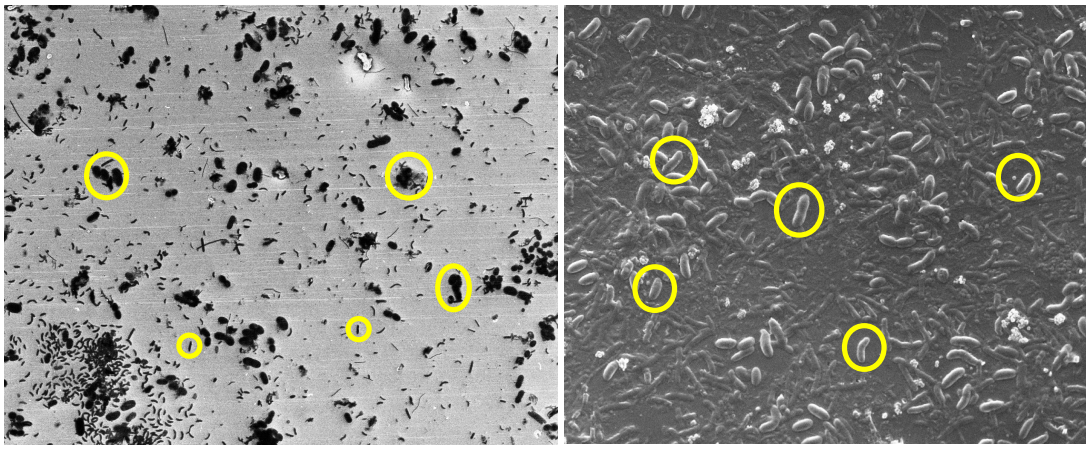

Figure 3.5: SEM micrograph of a metallic sample (on the left) and of a polymeric sample (on the right) after immersion in a solution containing bacteria. Microorganisms are pointed out with circles.

As said before, "images taken with SEM are closely correlated to the sample composition and conductivity: areas with high conductivity lead to bright areas while on the contrary areas with lower conductivity lead to dark areas on the image. This makes it easy to detect spots with low conductivity on a conductive surface, but makes it more difficult to highlight areas of different composition but similar conductivity. Actually in the case of a polymeric coating, being it non-conducting, the sample must be coated with a thin layer of a conductive material (such as Gold, Chromium or Graphite). This leads to an image in which colours are more uniform and bacteria are difficult to distinguish from the substrate. Of course, the operator can change the image contrast and brightness to adjust it for the sample, but the problem still remains. As an example, Fig. 3.5 shows side by side the images of two samples with the same magnification and taken with the same instrument. Both images refer to samples that have been immersed in a solution containing bacteria: the sample on the left refers to a bare metal (therefore a conductive material), while the sample on the right refers to a metal coated by epoxy resin (i.e. a non-conducting sample). The micrographs were acquired at a magnification of 5000X and refer to an area of about $60\ \mu m \times 40\ \mu m$, while the expected bacteria size is in the range of $2\ \mu m$ to $10\ \mu m$. The pixel resolution of the images was of about $0.065\ \mu m/pixel$.

Some bacteria can be seen attached on the surface of both samples, but the images appear quite different. On the left, bacteria appear as dark sports on a light background, as the contrast is given by the different conductivity. In the other case, as the sample has been coated by a conductive thin layer of Chromium, the contrast is limited and is only given by the morphology of the surface (i.e. by microorganisms attached on the epoxy resin).

In addition to the intrinsic difference of the images due to the sample conductivity, also the average sample brightness can change according to the position on the sample. This can be a consequence either of a not perfect sample planarity, or of the so-called charge effect [68]. In any case a correction of this effect is reasonably easy if the spot to be identified has an high contrast [52], but can be critical if such a contrast is minimal like in the case of coated samples.

A possible solution to this problem is to avoid treating the image as a whole and compute a local brightness average value according to the point and to use this value as the reference point to decide if a pixel is a candidate to be considered as belonging to a bacteria aggregate or not.

The size of the image to be considered for the local brightness average depends on the size of the expected spots: on one hand selecting a too small area might be detrimental turning out in missing some of the spots, on the other hand a too large area may lead to missing a local brightness average change. Since with the used acquisition parameters the bacterium size is expected to be of the order of 150 pixels maximum, a size of 200 pixels was selected to be considered for the local brightness estimation.

The threshold process needs also to be adapted to the image appearance, in particular in the case of a coated samples, where the contrast between the background and the bacteria is minimal. In the case of the bare metal sample, bacteria can be easily identified as dark spots, i.e. when their brightness (e.g. the black level) is at least 20% lower than the average brightness. In the case of the coated sample, bacteria appear slightly brighter than the background, so the threshold process tags them if their brightness is at least 2% higher than the background. Of course this encompasses most of the bacteria, but also some of the points which are not bacteria, but have a higher brightness.

Fig. 3.6 shows as an example the result of the threshold process on two images referring to the same samples of Fig. 3.5. It is clear how in the case of the uncoated sample the threshold process works easily, while in the case of the coated sample the resulting image is much more complex. In addition, the colour brightness inversion due to the different conductivity is clear and in the coated sample the attached bacteria appear as white areas over a dark background.

After image binarization, bacteria identification was performed using the OpenCV open source environment, as described in Section 3.2.3, but the `findContour` function was set to identify bright spots. This function returns a list of contours identified by a closed path. As the image magnification was higher than in the previous case, additional parameters were taken in consideration during the identification process. These have been used in order to remove small spots and to avoid counting areas too thin to be considered bacteria The first parameter is the area A_c enclosed by the contour, defined as:

$$A_c = \sum_x \sum_y a_{ij} \tag{3.7}$$

where the sum extend over the entire identified area. Contours with an area of less then

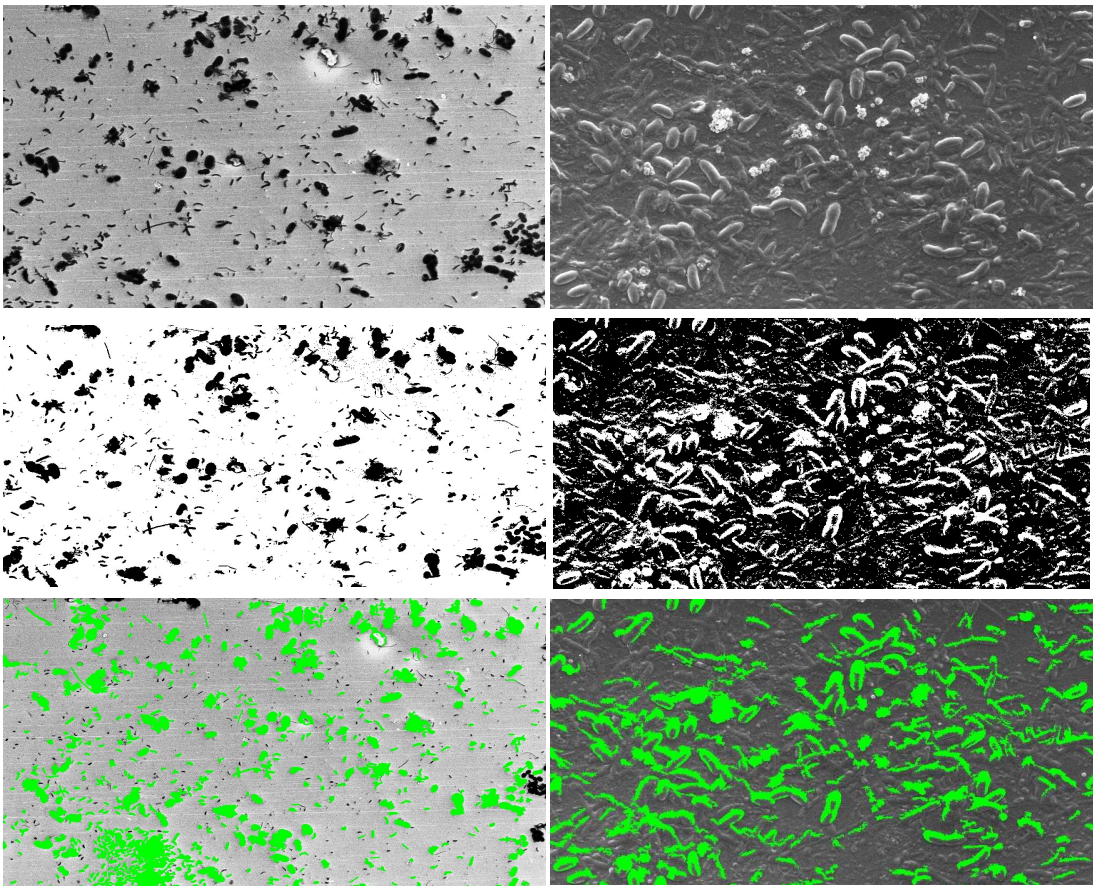

Figure 3.6: Results from the image processing for a metallic sample (on the left) and a polymeric sample (on the right).

2 μm^2 are considered spurious spots and non counted.

The second parameter used for the removal of spurious spots is the ratio between the contour area and the area corresponding to the rectangle enclosing the contour. Discarding contours with a ratio below 10% lets discarding contours which have a wire-like shape and therefore cannot be considered as bacteria.

Fig. 3.6 shows an example of the obtained results where the identified contours, both for the bare metal and for the coated one are shown in green colour." [53] ©2019 IEEE

This imaging algorithm was used to characterized the bacteriostatic behaviour of silver-epoxy nanocomposites. Results are presented in Section 4.3.3.

3.5 Conclusions

In this Chapter, an imaging algorithm has been presented. As described, it is able to identify bacteria aggregates on sample surface after a corrosion test. It has been tested both on metallic samples and non-conductive ones, discussing the different parameters that should be used to optimize the procedure. Obtained information are related to the number of bacteria aggregates attached on the sample surface, their average size and also their dimensional distribution. These data, coupled with the electrochemical measurements, can provide a deeper insight in the study of the microbial corrosion behavior of different materials.

Chapter 4

Hybrid organic coatings for corrosion prevention

Some of the work described in this chapter has been previously published in [53, 71].

4.1 Introduction

Different strategies can be undertaken in order to protect metals from corrosion. One of the most common is represented by the use of a coating that is able to act as a barrier against external environment and aggressive agents. In the field of materials science, an interesting innovation occurred in last decades has been represented by the development of 'hybrid materials'. They are a new class of materials that combines the properties of polymeric and inorganic ones. Actually, the dispersion of a nanometric filler inside the organic matrix leads to a nanocomposite in which different properties can be optimized. So it is possible for example to improve superficial hardness or barrier properties of the polymeric resin, keeping at the same time its toughness or transparency.

The aim of this study was to characterize the corrosion protection effectiveness of three different typologies of epoxy-based hybrid coatings. Three different nanofillers have been tested: silica nanoparticles, graphene oxide nanoplatelets and silver nanoparticles. The barrier properties of the coatings have been tested using Electrochemical Impedance Spectroscopy and Scanning ElectroChemical Microscopy. Moreover, bacteriostatic properties of the coatings containing silver nanoparticles have been investigated.

4.2 Materials and methods

In order to characterize the three typologies of coating, low carbon steel Q-Panel Standard Test Substrate, purchased from Q-Lab, was used as coated material. These

substrates have a superficial roughness $R_a = 0.5$ µm, as declared in the product specifications. The Q-Panel substrates were cut to the dimensions of 25 mm $\times$ 25 mm and then cleaned with acetone.

Three epoxy-based coatings have been studied, containing a different nanofiller inside the polymeric matrix: silica nanoparticles, graphene oxide nanoplatelets or silver nanoparticles. The UV-curable epoxy resin was 3,4- epoxycyclohexylmethyl - 3',4'-epoxycyclohexyl carboxylate (CE), purchased from Sigma-Aldrich. Silica nanoparticles have been produced *in-situ* inside the polymeric matrix during the polymerization process using TEOS (Tetraethoxysilane) as precursor. Two TEOS concentrations have been chosen, respectively 15 wt% and 30 wt% and Irgacure 250 (Basf) was used as photoinitiator (concentration 4 wt% respect to the epoxy resin). Graphene oxide (0.05 wt%) was dispersed in the epoxy resin using IKA Ultra-turrax at 30000 rpm for about 5 min and finally placing the mixture in an ultrasonic bath for about 60 min, as described in [72]. Also in this case, Irgacure 250 was the photoinitiator. Silver nanoparticles have been produced *in-situ* inside the polymeric matrix, following the procedure described in [73]. The epoxy resin was mixed with the silver precursor (silver hexafluoroantimonate, $AgSbF_6$) in concentration equal to 1 wt% or 3 wt% and with the photoinitiator (2,2-dimethoxy-2-phenyl acetophenone, DMPA), in concentration of 2 wt%.

"Formulations were deposited on the steel substrates using the draw-down rod coating technique in order to obtain a fixed and controlled thickness of about 60 µm± 15 µm. The used procedure is the same described in other research papers [74,75]: some coating liquid is placed on the substrate surface, afterwards a wire wound rod is rolled over the surface, so as to spread the liquid over the whole surface and doctor off the excess of coating fluid. Any other deposition technique could be applied (e.g. brushing, spraying etc.), but the draw-down rod technique assures an easy and reproducible procedure. UV-curing process was the following step and had a duration of about 180 s with light irradiance on the sample surface of about 60 mW/ cm^2. Samples coated with the TEOS formulation underwent also a heat treatment to complete the sol-gel reactions (90° C for 4 hours at 95% RH) following the procedure presented in [76]." [71] ©2018 Società Italiana di Fisica

Coated samples were characterized by means of EIS in order to investigate the protective effectiveness of the coating exposed to an aggressive solution. EIS measurements were performed in a conventional three electrodes electrochemical cell, using an Ag/AgCl electrode as the reference electrode and a NiCr wire as the counter electrode. The cell was filled with 0.1 M NaCl aerated solution for tests in sterile conditions, while raw wastewater was used for tests assessing the antimicrobial properties of the Ag-doped coatings. EIS measurements were performed in the range of 10^{-2} Hz to 10^5 Hz, with an applied voltage of 100 mV$_{pp}$. The exposed area was of about 0.8 cm^2; all results have been scaled to the equivalent area of 1 cm^2. Measurements were performed after 24 hours and 96 hours for the tests in sterile conditions and regularly until 240 hours of immersion for the tests in wastewater.

"SECM analyses were carried out in 0.1 M KCl (potassium chloride), to which 5 mM

$K_4Fe(CN)_6 \cdot 3\ H_2O$ (potassium ferrocyanide) solution was added to act as electrochemical mediator. The measuring cell was composed of a tip with diameter of 10 µm (set as working electrode), a reference electrode (Ag/AgCl electrode) and a counter electrode (Pt wire). The tip was positioned at a distance of 10 µm (equal to the tip diameter) from the sample surface. This was detected with a vertical line-scan in feedback mode as the height at which a 25% reduction of the current was measured by the probe respect to the value in bulk solution. Acquisitions were performed through a scan rate of 30 µm/s and a step size of 10 µm. The tip was set at a potential of $+0.5$ V with respect to the Ag/AgCl reference electrode; the current that is measured between working and counter electrodes is due to two possible oxidation reactions inside the solution related to the electrochemical mediator (eq. 4.1) and to the corrosion reaction of the steel substrate (eq. 4.2), respectively:

$$Fe(CN)_6^{4-} \longleftrightarrow Fe(CN)_6^{3-} + e^- \tag{4.1}$$

$$Fe^0 \longrightarrow Fe^{2+} + 2e^- \tag{4.2}$$

Being that the sample is non-conductive, as long as the coating covers and protects the surface, the only signal is given by the mediator oxidation reaction (eqn. 4.1). Thus the value of current that is measured depends on the distance between the tip and the sample surface: approaching the surface, oxidation reactions are limited by hindered diffusion of new species near the tip, so the measured current decreases. The SECM measurements, performed on areas of 500 µm $\times$ 500 µm, were used to obtain morphological information about samples surface when immersed in the electrolytic solution.

Final morphological characterizations were performed by means of a Field Emission Scanning Electron Microscope (FESEM Supra 40, ZEISS) using an acceleration voltage of 15 kV and and aperture of 20 µm to take high magnification images." [71] ©2018 Società Italiana di Fisica

4.3 Results and discussion

"Visual appearance of the coated samples can be observed in Fig. 4.1. All coatings show a good transparency; the finishing is slightly glossy, but it does not modify the aesthetic appearance of the metallic substrate. The use of a draw-down rod for coating deposition allows one to obtain a constant thickness, but turns out in a not perfectly flat coating which sometimes appears as a wavering on the images. However this drawback can be easily overcome when the coating is applied not manually but using an automatic tool." [71] ©2018 Società Italiana di Fisica

In the following, results from different characterization techniques will be presented.

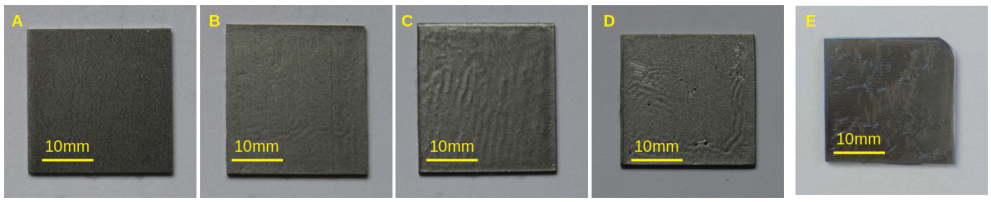

Figure 4.1: Picture of the samples under study: A) Steel without coating B) Epoxy coating C) Epoxy coating with addition of silica nanoparticles D) Epoxy coating with addition of graphene oxide nanoplatelets E) Epoxy coating with addition of silver nanoparticles.

4.3.1 Electrochemical characterization

Coatings protective effectiveness has been assessed by means of Electrochemical Impedance Spectroscopy. All formulations have been compared to the bare epoxy resin in order to better highlight the effect of the different fillers and results are reported in Fig. 4.2 as Bode diagrams.

It is possible to see that all coatings exhibit a capacitive behaviour, reaching phase values close to $90°$, at high frequencies, demonstrating a good protective effectiveness against the electrolytic solution. At lower frequencies, in all cases the modulus of impedance reaches a plateaux and the phase shifts to a resistive behaviour, that is values close to $0°$.

As far as the coatings containing silica nanoparticles are concerned, it is possible to observe the beneficial effect of the nanofiller. Actually, the modulus of impedance increases from about $10^6\ \Omega \cdot \text{cm}^2$ to $10^7\ \Omega \cdot \text{cm}^2$ for the two formulations containing TEOS. A higher concentration of TEOS does not lead to an improvement of the material barrier properties, probably due to an inhomogeneous dispersion of the precursor in the epoxy resin. Actually, silica domains of bigger dimension can act as local defects in the coating and have a less significant effect on its protective capabilities. All formulations containing TEOS show a stable behaviour during the immersion in the 0.1 M NaCl solution. Only a slight increase in the impedance modulus can be observed, which could be related to a slight oxidation of the steel at the interface between the coating and the metal.

Best corrosion protective behaviour was found for coatings containing graphene oxide nanoplatelets. Actually, the addition of a minimal concentration of nanofiller leads to an increase of the impedance modulus to $2 \cdot 10^7\ \Omega \cdot \text{cm}^2$, which remains almost stable during the 96 hours of immersion. This behaviour can be related to the lamellar shape of the nanofiller, which is characterized by a thickness lower than 10 nm and a lateral dimension in the order of some micrometers [77,78]. Actually, thanks to the high specific surface, it is able to decrease the water diffusion rate inside the the coating. This point will be better clarified using SECM measurements.

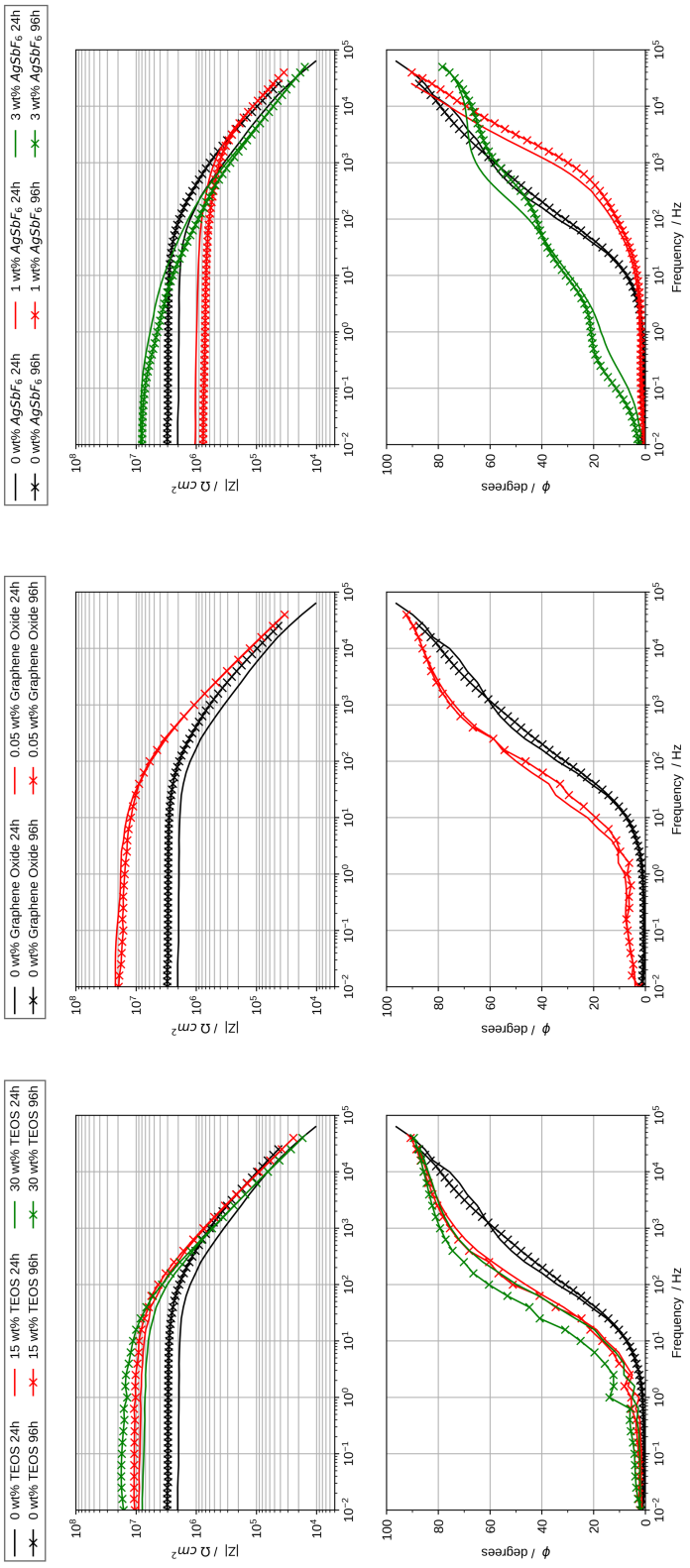

Figure 4.2: Bode plots recorded on the three typologies of coating after 24 hours and 96 hours of immersion in 0.1 M NaCl aerated solution

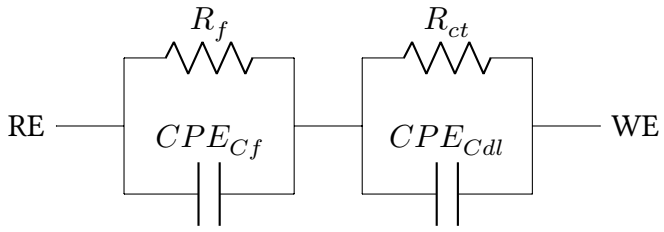

Figure 4.3: Equivalent circuit model used for fitting the EIS spectra.

Coatings containing silver nanoparticles showed an heterogeneous behaviour. Actually the addition of 1 wt% of $AgSbF_6$ did not have an effect on the protective effectiveness of the coating; as it is possible to see, modulus of impedance is lower that that of the bare epoxy resin. Probably silver nanoparticles act more as point defects than as a reinforcement for the polymeric matrix. On the other hand, the addition of 3 wt% of $AgSbF_6$ leads to an increase of the impedance modulus, that reaches values close to $10^7\ \Omega \cdot cm^2$.

"EIS spectra have been modelled through the equivalent circuit model shown in Fig.4.3, typically used in the case of organic coatings that undergo a degradation, where R_s is the resistance of the electrolytic solution which has been assumed fixed at the value of 100 Ω, R_f is the film resistance, in parallel with CPE_{Cf} (Constant Phase Element) representing the capacitance of the film and eventually R_{ct} is the Charge Transfer resistance, in parallel with another CPE (CPE_{Cdl}), that models the double layer capacitance at the interface with the metal.

The physical meaning of the CPE in the equivalent circuit model is correlated to the surface heterogeneity of the coatings [79, 80]; the CPE impedance value is represented by equation:

$$Z = \frac{C}{(i \cdot \omega)^{\alpha}} \tag{4.3}$$

where C is a constant related to the specific system under investigation, $\omega = 2\pi f$ takes into account the frequency, $i = \sqrt{-1}$ is the imaginary unit and α is a coefficient independent from frequency that ranges between 0 and 1 [79]. This element is a generalization of a classic capacitor, which becomes a specialized case of a CPE, when α = 1; when α = 0 the CPE is equivalent to a resistor, while when α= -1 is equivalent to an inductor.

R_{ct} and CPE_{Cdl} values obtained by fitting the EIS spectra by means of the equivalent circuit model of Fig.4.3 are reported in Table 4.1. In Fig. 4.4 EIS data are presented as Nyquist plot, superimposing the measured spectra after 96 hours of immersion with the one modelled through the equivalent circuit.

For the steel sample, R_{ct} is of about $350\ \Omega \cdot cm^2$ and CPE_{Cdl} is of about $2.64 \cdot 10^{-3}$ with $\alpha = 0.8$, thus indicating the poor corrosion resistance of the low carbon steel in the aggressive electrolyte. A significant increase in the charge transfer resistance can

Table 4.1: R_{ct} and CPE_{Cdl} values obtained by fitting the impedance spectra by the equivalent circuit model of Fig. 4.3

	R_{ct} ($\Omega \cdot cm^2$) 1 hour	CPE_{Cdl}, 1 hour
Epoxy	2.5×10^6	6.5×10^{-5} (α = 1)
Epoxy + 15 wt% TEOS	1.1×10^7	3.8×10^{-6} (α = 0.7)
Epoxy + 30 wt% TEOS	8.9×10^6	8.9×10^{-7} (α = 0.7)
Epoxy + 0.05 wt% Graphene Oxide	2.4×10^7	3.3×10^{-7} (α = 0.8)
Epoxy + 1 wt% $AgSbF_6$	1.2×10^6	1.5×10^{-6} (α = 0.8)
Epoxy + 3 wt% $AgSbF_6$	6.6×10^6	9.7×10^{-8} (α = 0.8)
Low Carbon Steel	3.56×10^2	2.64×10^{-3} (α = 0.8)
	R_{ct} ($\Omega \cdot cm^2$), 96 hours	CPE_{Cdl}, 96 hours
Epoxy	3.8×10^6	4.2×10^{-5} (α = 0.7)
Epoxy + 15 wt% TEOS	1.2×10^7	8.2×10^{-8} (α = 0.8)
Epoxy + 30 wt% TEOS	1.9×10^7	2.3×10^{-7} (α = 0.8)
Epoxy + 0.05 wt% Graphene Oxide	1.9×10^7	3.6×10^{-7} (α = 0.7)
Epoxy + 1 wt% $AgSbF_6$	8.8×10^5	4.3×10^{-6} (α = 0.8)
Epoxy + 3 wt% $AgSbF_6$	6.5×10^6	8.4×10^{-8} (α = 0.7)

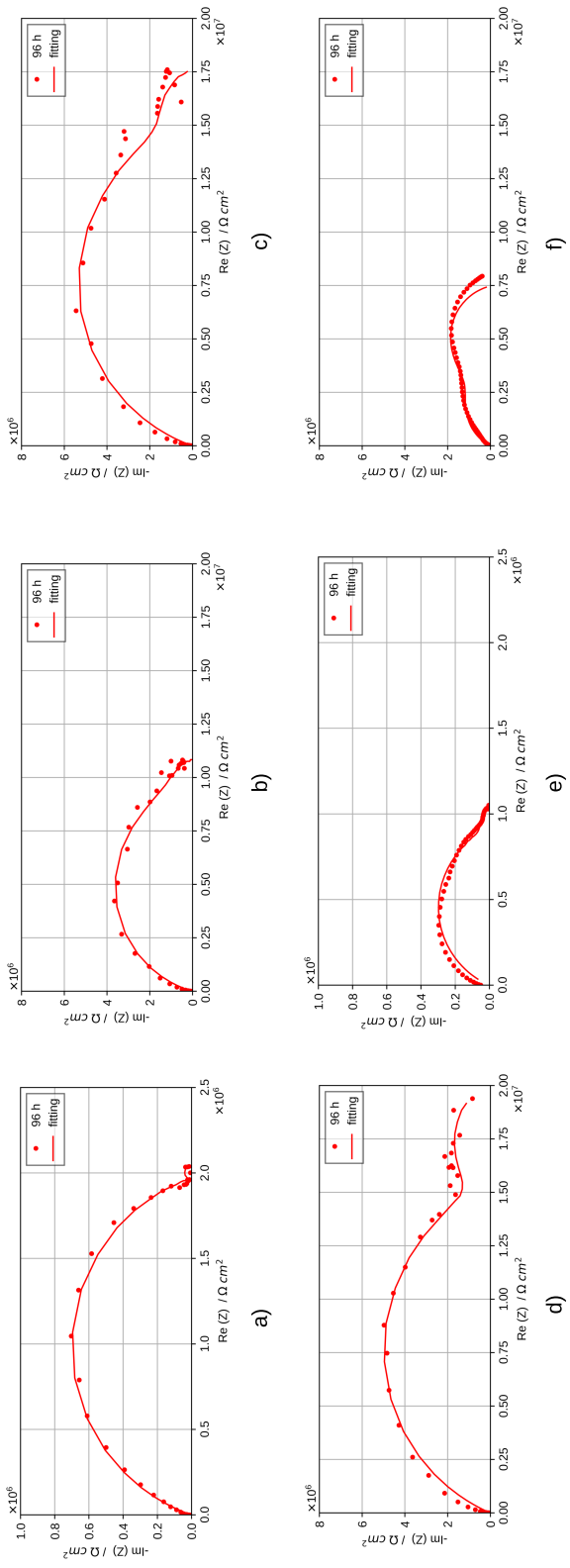

Figure 4.4: Nyquist plots recorded on the different coatings after 96 hours of immersion in 0.1 M NaCl solution and results from fitting: a) Epoxy coating b) Epoxy coating + 15 wt% of TEOS c) Epoxy coating + 30 wt% of TEOS d) Epoxy coating + 0.05 wt% of graphene oxide e) Epoxy coating + 1 wt% of $AgSbF_6$ f) Epoxy coating + 3 wt% of $AgSbF_6$

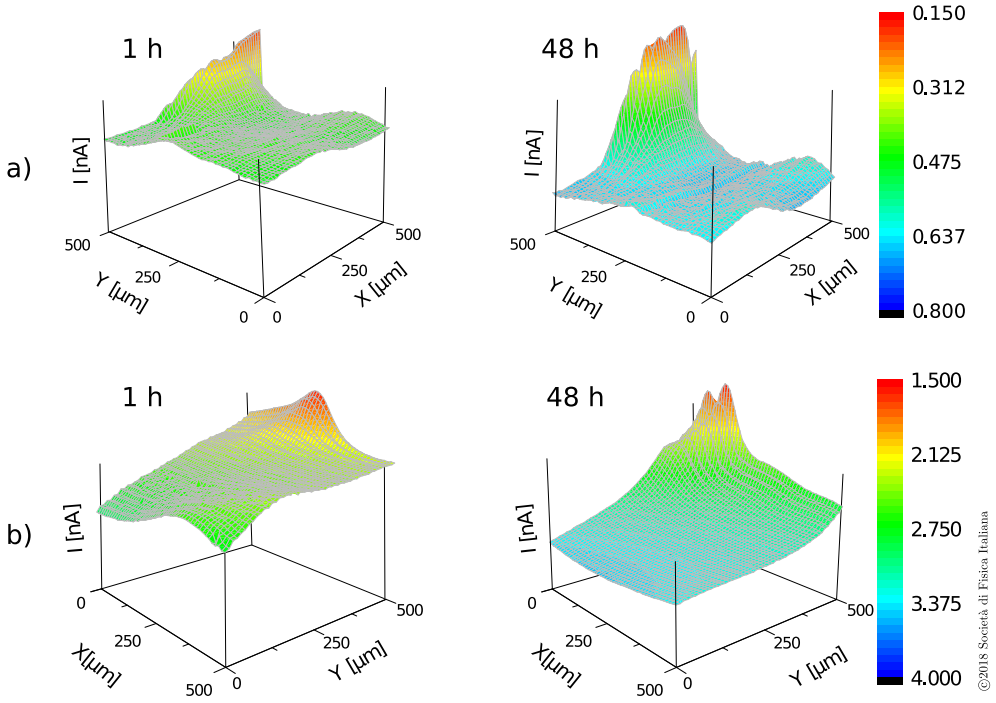

Figure 4.5: SECM measurement on a) Epoxy-TEOS and b) Epoxy-Graphene Oxide coatings after 1 hour and 48 hours. [71]

be observed for the three hybrid coatings with respect to the bare metal, but also when compared to the bare Epoxy Coating. The highest R_{ct} value is found for the formulation containing graphene oxide, while the sample containing 1 wt% of $AgSbF_6$ is the only one that does not exhibit a beneficial effect for the addition of the filler. Moreover, during the 96 hours of exposure to the electrolytic solution, no significant changes could be observed for all the coatings.

From the fitting of the impedance spectra, α values close to the unity were obtained for all samples, indicating a behavior similar to a capacitor. High values of the CPE_{Cdl} are expected for bare low carbon steel substrates, while lower values are recorded onto coated samples not affected by degradation. Moreover, such CPE values remain almost constant for the Graphene Oxide Coating over the 96 hours of exposure inside the electrochemical cell, while decreases for the formulation containing TEOS, probably due to the water uptake by the coating exposed to the electrolytic solution.

In order to better understand the degradation mechanism of the different coatings when immersed in the electrolytic solution, the SECM technique was used. In particular, the aim was to compare the different water absorption analysing the modification in the superficial morphology. So the same area was scanned at different immersion times, in order to detect changes in its roughness or defects being formed. Results for Epoxy-TEOS and graphene oxide samples are presented in Fig. 4.5.

SECM graphs have been plotted with the z axis (representing the current) inverted, so as to give a direct topographical representation of the surface [81]. Specimens appear not perfectly flat since the beginning of the test, due to the manual procedure to spread the coating on the metal surface. Epoxy-TEOS specimens show a higher roughness (respect to grafene oxide samples), characterized by peaks that protrude from the surface. Moreover, this kind of defects increases their dimension with the immersion time in the electrolyte, even if this does not influence the protective capabilities of the coating (as seen through the EIS measurements). The reason for this changes can be attributed to water uptake by the polymer, discovered in an early stage through SECM technique, but still difficult to detect through EIS. Actually, in order to have a significant decrease in the impedance modulus, a longer ionic conductive path would be necessary, so longer immersion time are required. In the case of graphene oxide coatings, the surface is smoother, even if still characterized by the presence of peaks. A notable point is that in this case the surface is less deteriorated by the immersion in the electrolytic solution, both considering the peaks and the mean roughness of the surface.

This behaviour can be explained in a twofold way. First of all, the shape of the filler inside the polymeric matrix plays an important role, as the lamellar shape of graphene oxide nanoplatelets is particularly suited to obstacle the diffusion of electrolyte through the coating [82, 83]. Actually, as it can be seen also from FESEM micrographs, silica nanoparticles have a spherical shape, which leads to lower tortuosity if compared to the effect of lamellar fillers [84]. Moreover, also the different hydrophilicity of the two coatings must be taken in account. As reported in scientific literature for analogous materials, TEOS-containing coatings are characterized by lower contact angles with water respect to graphene oxide ones [72, 76]. The role of the filler, if compared to graphene oxide coatings, is less effective in preventing absorption of water from the environment. Thus SECM measurements are an additional evidence of the different behavior of the two materials, which is in good agreement with previous literature [85, 86].” [71] ©2018 Società Italiana di Fisica

4.3.2 Morphological characterization

After immersion in the electrolytic solution, samples superficial morphology was characterized using electron microscopy. In agreement with EIS measurements, no signs of corrosion could be observed on the metallic surface and the metal was still coated by the polymeric coatings. In all samples, only a slight degradation of the polymer could be observed.

Fig. 4.6 shows the “FESEM micrographs of the Epoxy-TEOS coating before and after 96 hours of immersion in the NaCl solution. The same morphology described in literature for Epoxy-TEOS coatings can be observed. Some silica nanoparticles, characterized by size in the range of 100 nm — 200 nm, are visible near the surface of the coating already after deposition. Actually, this can be explained because the inorganic phase

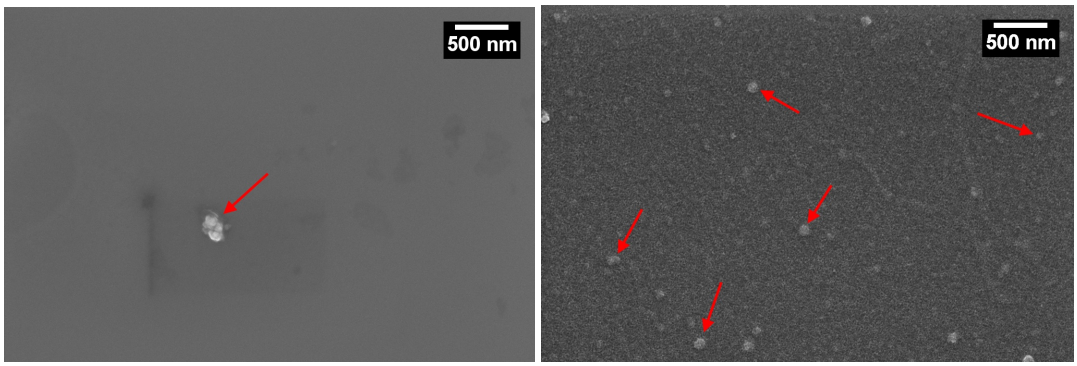

©2018 Società di Fisica Italiana

Figure 4.6: FESEM micrographs of the Epoxy-TEOS coating as deposited (on the left) and after 96 hours of immersion in 0.1 M NaCl aerated solution in the electrochemical cell used for the EIS measurements (on the right). [71]

(more polar than the organic one) tends to enrich superficial layers of the material. After permanence inside the electrochemical cell, a slight degradation of the resin occurs and it leads to the exposure of silica nanoparticles directly to the surface. Nanoparticles appear well distributed and dispersed in the organic matrix, without a major segregation of the silica phase. In the case of graphene oxide coatings, it was not possible to distinguish the filler inside the matrix, due to the same chemical composition and to the shape of the lamellae. This can also be interpreted as a sign of good dispersion of the nanofiller inside the polymer." [71] ©2018 Società Italiana di Fisica

Samples containing silver nanoparticles had a morphology similar to that of Epoxy-TEOS coatings. At lower magnification, a slight degradation of the polymer could be observed, even if the coating was still adherent to the substrate. At higher magnification, silver nanoparticles could be seen, having a diameter ranging between 30 nm and 80 nm. Also in this case, it is possible to notice the good dispersion of the nanofiller inside the polymeric matrix, that can be related to the process route used for the production of the nanocomposite.

4.3.3 Antimicrobial behaviour of Ag-doped organic coatings

Bacteriostatic properties of the silver nanocomposites have been evaluated immersing the samples in raw wastewater. Using such electrolytic solution guarantees to have a large variety of bacteria strains and thus to have a condition that aims at reproducing a real environment. The test had a duration of 240 hours and was carried out at a temperature of 30 ± 3 °C. Protective effectiveness of coatings containing silver nanoparticles has been evaluated first by means of EIS measurements during immersion in the electrolytic solution and then through morphological characterization of the sample surface after the immersion test.

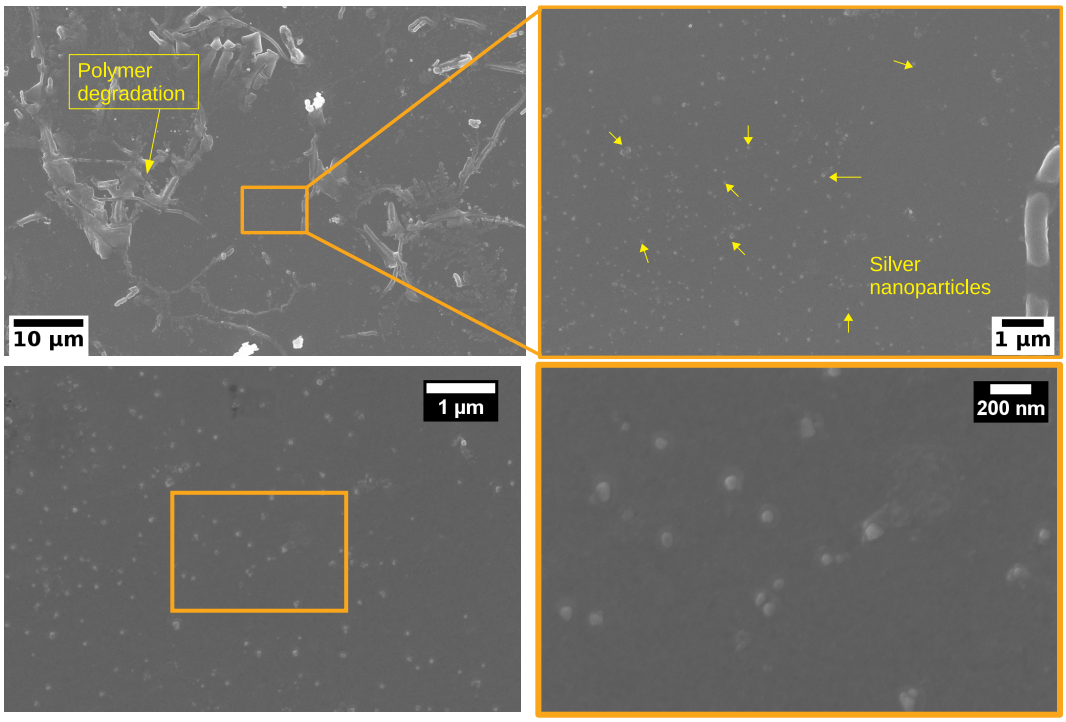

Figure 4.7: Silver-Epoxy nanocomposite (1wt% $AgSbF_6$) after 96 hours of immersion in the 0.1 M NaCl solution.

Results from EIS measurements have been plotted in Fig. 4.9 as Bode diagrams, comparing the two formulations containing silver nanoparticles to the bare epoxy coating. All three samples exhibit a less protective behaviour against the aggressive electrolyte, as can be seen from impedance modulus, which is more than one order of magnitude lower than for the tests in NaCl solution. Moreover it does not remain stable during immersion, but decreases in the course the tests. The less effective protective behaviour can also be deduced analysing the phase values, that remain close to 0° in a large part of the frequency range. The behaviour is similar for the two formulations with silver nanoparticles; the sample containing 3 wt% of $AgSbF_6$ has a higher modulus of impedance at the beginning of test, but then it stabilises to about $10^5\ \Omega \cdot cm^2$.

Also in this case, EIS spectra have been modelled through the equivalent circuit model shown in Fig. 4.3. Results are reported in Table 4.2 , while in Fig. 4.8 the impedance spectra recorded after 240 hours of immersion are plotted as Nyquist diagrams superimposing them with the model obtained from the equivalent circuit.

For all samples, resistance to charge transfer is one order of magnitude lower than in the tests in NaCl solution. Moreover it does not remain stable but decreases during the test, indicating an increase in the corrosion rate for the steel substrate due to exposure to the solution containing bacteria. Higher values are found for the Constant Phase

Table 4.2: R_{ct} and CPE_{Cdl} values obtained by fitting the impedance spectra by the equivalent circuit model of Fig. 4.3

	R_{ct} ($\Omega \cdot cm^2$) 1 hour	CPE_{Cdl}, 1 hour
Epoxy	1.3×10^5	3.8×10^{-4} (α = 0.7)
Epoxy + 1 wt% $AgSbF_6$	1.1×10^5	1.4×10^{-5} (α = 0.7)
Epoxy + 3 wt% $AgSbF_6$	4.6×10^6	9.5×10^{-6} (α = 0.9)
	R_{ct} ($\Omega \cdot cm^2$), 96 hours	CPE_{Cdl}, 96 hours
Epoxy	4.2×10^4	7.0×10^{-4} (α = 0.8)
Epoxy + 1 wt% $AgSbF_6$	6.7×10^4	2.1×10^{-5} (α = 0.7)
Epoxy + 3 wt% $AgSbF_6$	8.7×10^4	5.7×10^{-5} (α = 0.7)

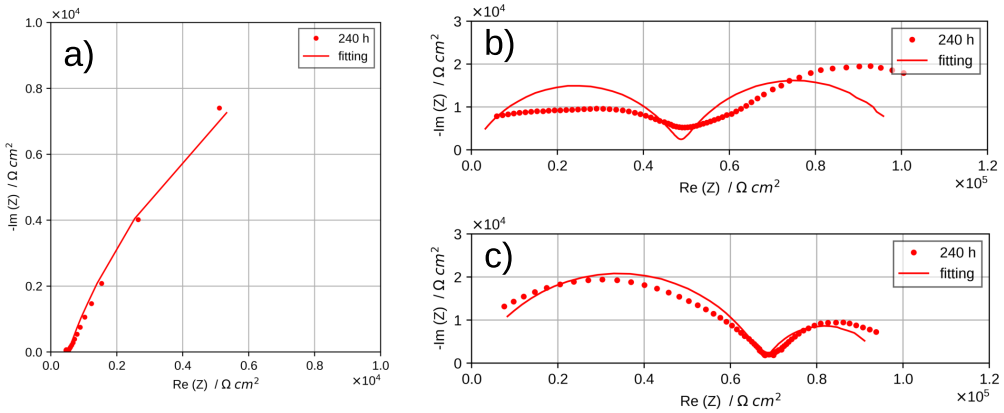

Figure 4.8: Nyquist plots recorded on the different coatings after 240 hours of immersion in raw wastewater and results from fitting: a) Epoxy coating b) Epoxy coating + 1 wt% of $AgSbF_6$ c) Epoxy coating + 3 wt% of $AgSbF_6$

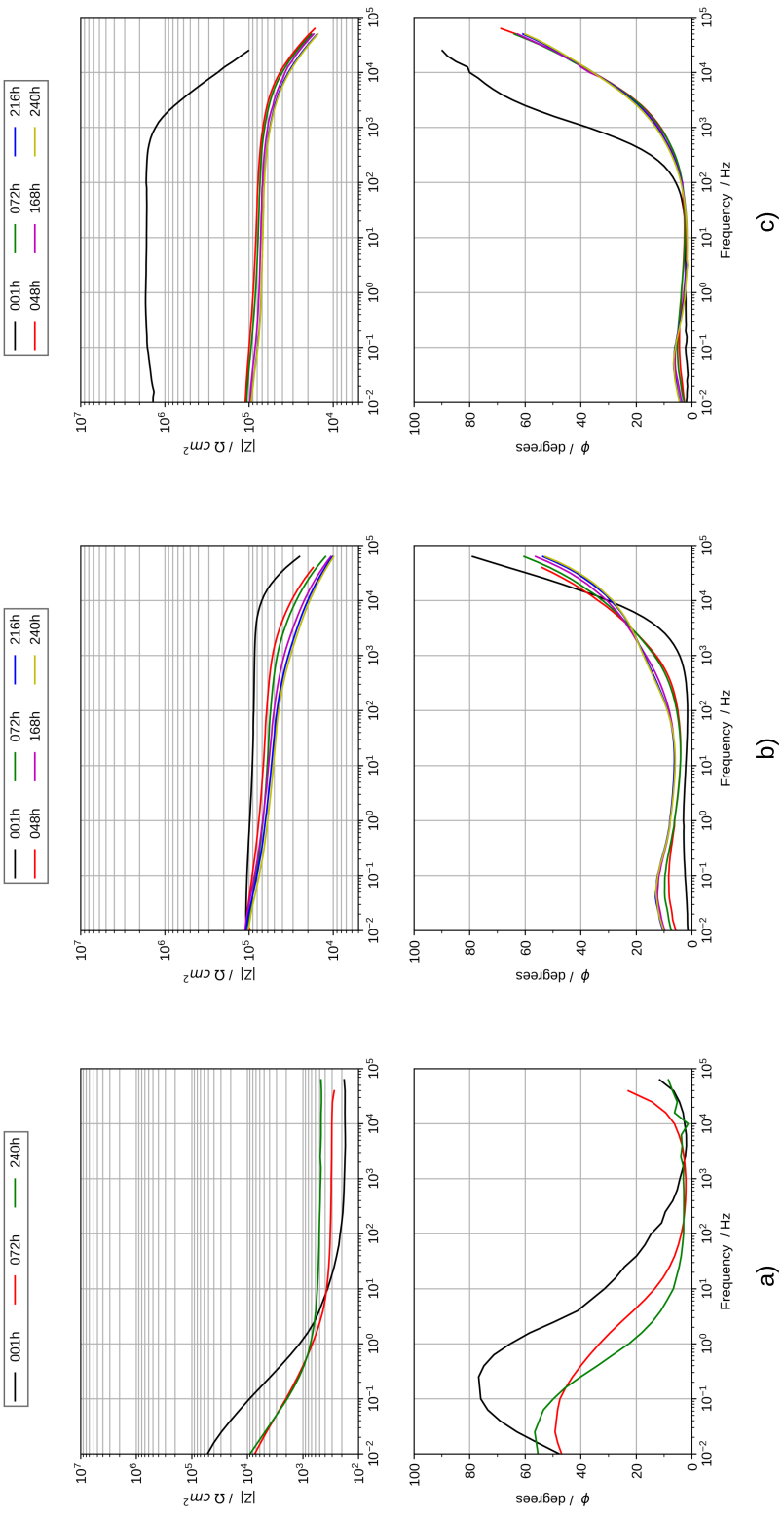

Figure 4.9: Bode plots recorded on the coatings containing silver nanoparticles during immersion in raw wastewater: a) Epoxy coating b) Epoxy coating + 1 wt% of $AgSbF_6$ c) Epoxy coating + 3 wt% of $AgSbF_6$

Element modelling the double layer capacitance, with α of about 0.7.

At the end of the immersion test, bacteriostatic behaviour of the silver nanocomposites was evaluated by means of morphological characterization of samples surface. Using electron microscopy it was possible to assess the bacteria attachment on the coating surface and evaluate the effectiveness of the nanofiller in preventing bacteria adhesion. SEM micrographs for the three samples are shown in Fig. 4.10.

As can be seen from the images, a completely different condition is found for the three coatings. As far as the bare epoxy coating is concerned, it is possible to see that bacteria are able to colonize the sample surface, forming a biofilm made of large aggregates. Even if a failure of the coating could not be observed during these tests, this condition is the most dangerous, as chemical compounds produced by bacteria metabolism can accelerate the coating degradation. In the case of the formulation containing 1 wt% of $AgSbF_6$, bacteria are still able to attach on sample surface, forming a biofilm that covers almost uniformly the coating. Large bacteria clusters are not present, but the morphology is that of singly attached bacteria. Moreover, to better understand the information gained from this characterization, it should be noticed that using electron microscopy it is possible to evaluate only the bacteria attachment on sample surface, without assessing if they were still living at the end of the test. To have this additional information, staining techniques would be required.

Increasing the concentration of silver precursor to 3 wt%, even better results could be observed. Actually, bacteria adhesion on the coating surface is almost completely inhibited and only few microorganisms are present on it.

FESEM micrographs have been analysed using the imaging algorithm presented in Section 3.4, in order to quantify the biofilm coverage for the different samples. Fig. 4.11 shows three micrographs representing the sample surface of the three coatings after immersion in wastewater and the results from the bacteria identification. The software is able to identify bacteria in virtually all cases, even if, as discussed in Section 3.4, the low contrast between the microorganisms and the coating surface, makes the identification more problematic than in cases involving a metallic sample.

Using the imaging algorithm it is possible to assess both the biofilm coverage (that is the ratio between the number of image pixels occupied by bacteria and the total number of pixels in the image) and the dimensional distribution of bacteria aggregates. Biofilm coverage is about 21% for the bare epoxy coating and 17% and 3% for the coatings containing respectively 1 wt% and 3 wt% of $AgSbF_6$. Moreover, looking at dimensional distribution of bacteria aggregates, reported in 4.12 as histograms, it is possible to assess the different morphology of bacteria clusters. In the bare epoxy samples aggregates dimension reaches 100 μm^2, while in the other two cases it is limited to about 20 μm^2, that is the size of singly attached bacteria. It is thus possible to conclude that, even if a similar biofilm coverage is found for the epoxy coating and the samples containing 1 wt% of $AgSbF_6$, the presence of large aggregates is a more dangerous condition for applications involving microbial corrosion.

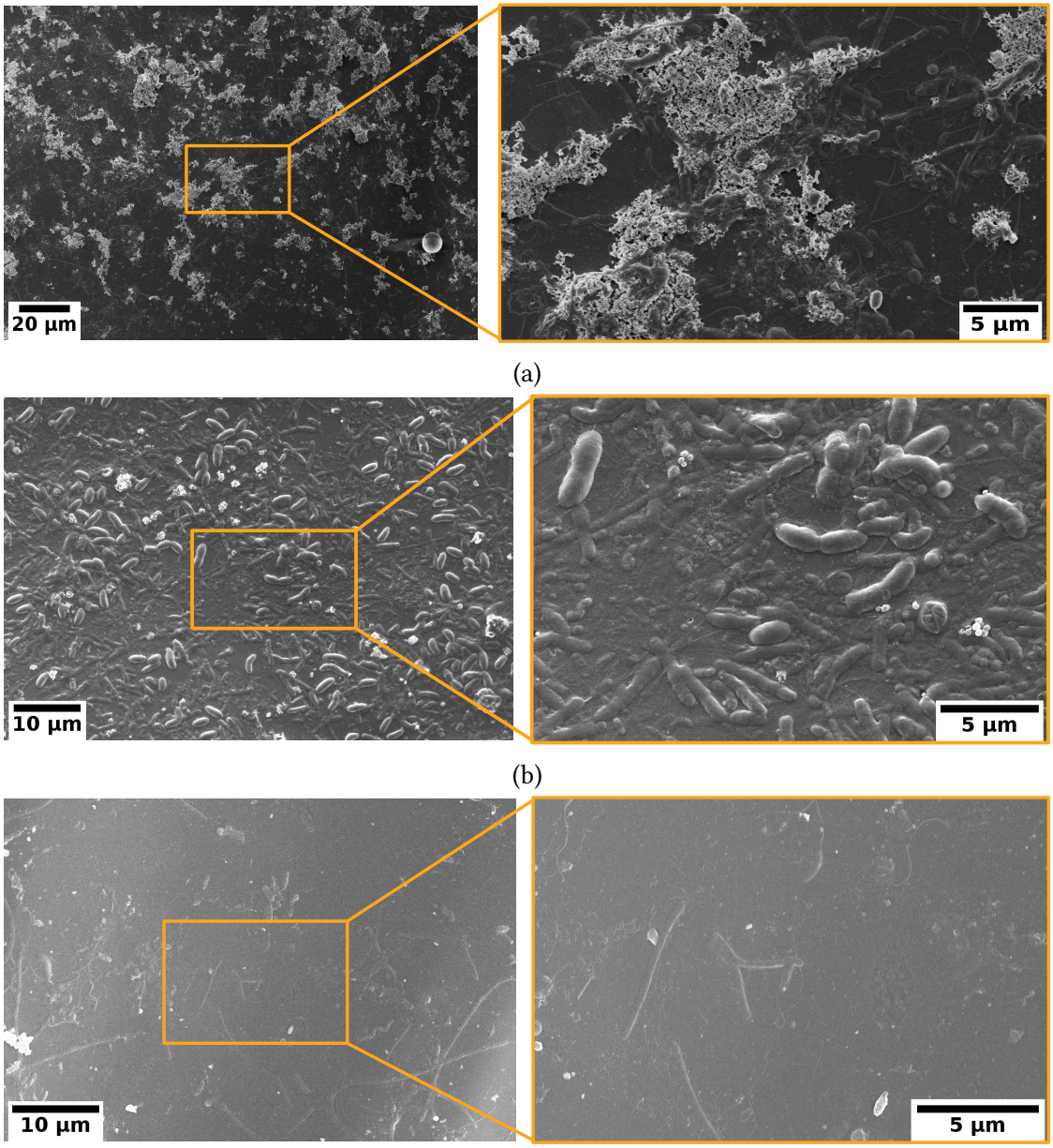

Figure 4.10: SEM micrographs showing samples surface after immersion in raw wastewater: a) Epoxy coating b) Epoxy coating + 1 wt% of $AgSbF_6$ c) Epoxy coating + 3 wt% of $AgSbF_6$.

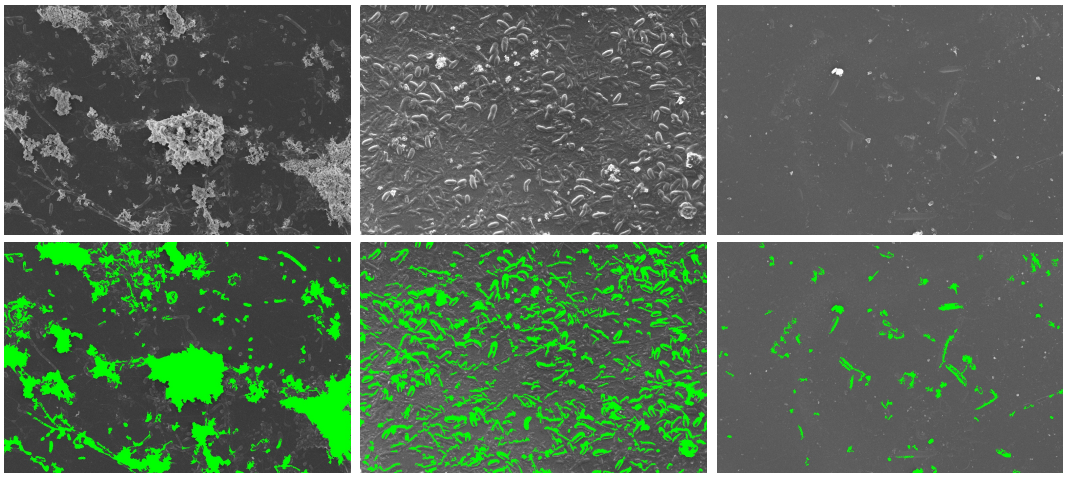

Figure 4.11: SEM micrographs and identified bacteria on three samples after immersion in wastewater: a) Epoxy coating b) Epoxy coating + 1 wt% of $AgSbF_6$ c) Epoxy coating + 3 wt% of $AgSbF_6$.

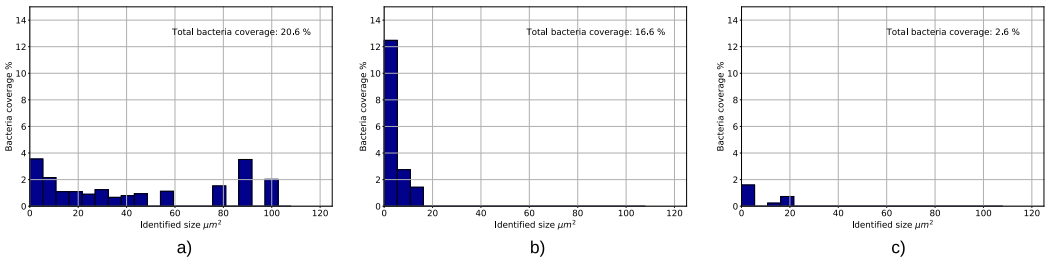

Figure 4.12: Histograms showing dimensional distribution of bacteria aggregates on different samples: a) Epoxy coating b) Epoxy coating + 1 wt% of $AgSbF_6$ c) Epoxy coating + 3 wt% of $AgSbF_6$.

4.4 Conclusions

This study presented the characterization of three typologies of hybrid organic coatings. As could be assessed by means of electrochemical measurements, the three different nanofillers are able to significantly improve the barrier properties of the epoxy resin against an aggressive electrolyte. Best corrosion protection performance was found for coatings containing Graphene Oxide. Actually, thanks to the lamellar structure and low hydrophilicity of the filler, they exhibit a good protective behaviour even using a very low filler content. Moreover, SECM measurements showed the lower water uptake of

this kind of coatings if compared to the formulation containing silica nanoparticles. Finally, antimicrobial properties of coatings containing silver nanoparticles has been evaluated immersing the samples in wastewater. Electrochemical measurements showed a similar behaviour for the two formulations containing $AgSbF_6$, but a completely different superficial morphology was found at the end of the immersion test. In samples without silver nanoparticles, formation of large bacteria clusters could be observed, which is the most dangerous condition. The addition of silver nanoparticles had a beneficial effect already using 1 wt% of $AgSbF_6$ and showed the best performance in the samples containing 3 wt% of $AgSbF_6$, which were almost not colonized by bacteria.

Chapter 5

Conclusions

This dissertation presented the results obtained in the study of innovative measurement techniques for microbial corrosion assessment. This topic was addressed focusing both on the development of a new experimental setup for MIC testing and on the use of imaging techniques for characterization of microbial colonization of sample surface.

As discussed in Chapter 2, the use of Microbial Fuel Cell as environment to carry out a microbial corrosion test has several advantages if compared to a traditional immersion test. Actually, it is possible to monitor many test parameters avoiding specific and costly analysis, but simply measuring the currents flowing in the MFC electrical circuit. Before the beginning of the test, it is possible to verify the presence of bacteria in the electrolytic solution measuring the current flowing between the anode and the cathode of the MFC. Actually, without bacteria activity no current could flow between the two electrodes, as they are made of the same material. Then, during the test it is possible to track the presence of nutrients in the solution monitoring the MFC power output. This is a great simplification, because it can avoid the use of chemical analysis to measure nutrients concentration. When the sample under study is connected the the MFC electrical circuit, it is possible to monitor the gradual colonization of sample surface by bacteria. Actually, the current flowing between the sample and the cathode can be associated to the biofilm growth on the metal surface and to the corrosion reactions occurring on it. Thus it is possible to compare the microbial corrosion resistance of different materials and the different biofilm growth rate. Moreover, the sample polarization in the MFC allows one to have more aggressive conditions if compared to a simple immersion test without altering bacteria metabolism. This technique can thus be considered as an additional tool for researchers in the microbial corrosion field, in order to study and compare the behaviour of different materials in an environment containing bacteria.

In the second part of the thesis, an imaging algorithm was presented. It aims at quantifying bacteria attachment on sample surface at the end of a corrosion test analysing micrographs taken using electron microscopy. The choice of this specific microscopy technique was due to its widespread use in many Materials Science studies; so it does

not require additional skills or expertises. Moreover, it does not require staining techniques, so it simplifies part of the sample preparation. Bacteria are identified in the micrograph relying on the contrast due to the different conductivity between the bacteria and the metal surface. So it is possible to binarize the image choosing a brightness threshold value to discriminate between pixels occupied by bacteria and by the metal substrate. The following identification of the microorganisms present on the sample surface permits to obtain a dimensional distribution of bacteria aggregates, which is an important information in order to assess their influence on the sample surface reactivity. Moreover, the computation of different parameters, such as the biofilm coverage or the average size of bacteria aggregates allows to compare the behaviour of a specific material in different electrolytic solution.

Traditional techniques and some of the proposed ones have been used to characterize the corrosion resistance properties of different materials. In Chapter 2, the microbial corrosion resistance of two stainless steels has been investigated using both electrochemical techniques and morphological characterizations. This allowed to highlight an interesting case of corrosion inhibition due to the oxygen consumption caused by bacteria metabolism. Eventually, in Chapter 4 the characterization of innovative hybrid coatings for corrosion protection has been presented. Electrochemical measurements permitted to compare the protective effectiveness of the different nanofillers dispersed in the polymeric matrix. Then, the bacteriostatic behaviour of the hybrid coatings containing silver nanoparticles was assessed using the proposed imaging algorithm. The use of SEM micrographs allowed to quantify the bacteria attachment as a function of the silver content inside the material, highlighting the good antimicrobial behaviour of the Ag-doped epoxy coating.

The studies presented in this dissertation can be considered as a contribution in the field of measurements for microbial corrosion. In particular, one of the main purposes was the simplification of some of the issues related to the biological part of the experiments, and this was achieved both through the new experimental setup and through the imaging system, that does not rely on staining techniques. Further developments of this research can be pursued in the study of new configurations for the MFC setup in order to study different experimental conditions. In this way, not only anaerobic, but also aerobic conditions could be reproduced, enabling researchers to investigate different environments using a single experimental setup.

Bibliography

[1] Gaines, R. H. (1910). "Bacterial Activity as a Corrosive Influence in the Soil". The Journal of Industrial and Engineering Chemistry, vol. 2, pp. 128-130. doi: 10.1021/ie50016a003

[2] Mattson, E. (1989). Basic corrosion technology for scientists and engineers. John Wiley and Sons, New York.

[3] Javaherdashti, R. (2017). "Microbiologically Influenced Corrosion: An Engineering Insight". London, UK. Springer.

[4] De Romero, M. F., Urdaneta, S., Barrientos, M., Romero, G. (2004). "Correlation between desulfovibrio sessile growth and OCP, hydrogen permeation, corrosion products and morphological attack on iron". Paper presented at the NACE Meeting Papers

[5] Little, B., Wagner, P., Mansfeld, F. (1991). "Microbiologically influenced corrosion of metals and alloys". International Materials Reviews, vol. 36 no. 1, pp. 253-272. doi: 10.1179/imr.1991.36.1.253

[6] Videla, H. A., Herrera, L. K. (2005). "Microbiologically influenced corrosion: Looking to the future". International Microbiology, vol. 8, no. 3, pp. 169-180.

[7] Jia, R., Unsal, T., Xu, D., Lekbach, Y., Gu, T. (2019). "Microbiologically influenced corrosion and current mitigation strategies: A state of the art review". International Biodeterioration and Biodegradation, vol. 137, pp. 42-58. doi:10.1016/j.ibiod.2018.11.007

[8] Li, Y., Xu, D., Chen, C., Li, X., Jia, R., Zhang, D., Gu, T. (2018). "Anaerobic microbiologically influenced corrosion mechanisms interpreted using bioenergetics and bioelectrochemistry: A review". Journal of Materials Science and Technology, vol. 34, no. 10, pp. 1713-1718. doi:10.1016/j.jmst.2018.02.023

[9] Little, B. J., Lee, J. S. (2014). "Microbiologically influenced corrosion: An update". International Materials Reviews, vol. 59, no. 7, pp. 384-393. doi:10.1179/1743280414Y.0000000035

[10] Xu, D., Gu, T. (2014). "Carbon source starvation triggered more aggressive corrosion against carbon steel by the desulfovibrio vulgaris biofilm". International Biodeterioration and Biodegradation, vol. 91, pp. 74-81. doi:10.1016/j.ibiod.2014.03.014

[11] Little, B., Wagner, P., Mansfeld, F. (1992). "An overview of microbiologically

influenced corrosion". Electrochimica Acta, vol. 37, no. 12, pp. 2185-2194. doi:10.1016/0013-4686(92)85110-7

[12] Wade, S. A., Javed, M. A., Palombo, E. A., McArthur, S. L., Stoddart, P. R. (2017). "On the need for more realistic experimental conditions in laboratory-based microbiologically influenced corrosion testing". International Biodeterioration and Biodegradation, vol. 121, pp. 97-106. doi:10.1016/j.ibiod.2017.03.027

[13] Loto, C. A. (2017). "Microbiological corrosion: Mechanism, control and impact—a review". International Journal of Advanced Manufacturing Technology, vol. 92, no. 9-12, pp. 4241-4252. doi:10.1007/s00170-017-0494-8

[14] Mansfeld, F., Little, B. (1991). "A technical review of electrochemical techniques applied to microbiologically influenced corrosion". Corrosion Science, vol. 32, no. 3, pp. 247-272. doi:10.1016/0010-938X(91)90072-W

[15] Trif, L., Shaban, A., Telegdi, J. (2018). "Electrochemical and surface analytical techniques applied to microbiologically influenced corrosion investigation". Corrosion Reviews, vol. 36, no. 4, pp. 349-363. doi:10.1515/corrrev-2017-0032

[16] Gerchakov, S. M., Little, B. J., Wagner, P. (1986). "PROBING MICROBIOLOGICALLY INDUCED CORROSION". Corrosion, vol. 42, no. 11, pp. 689-692. doi:10.5006/1.3583042

[17] Licina, G. J. (2001). "Monitoring biofilms on metallic surfaces in real time". CORROSION. pp. 11-16.

[18] Angell, P., Luo, J., White, D. C. (1995). "Microbially sustained pitting corrosion of 304 stainless steel in anaerobic seawater". Corrosion Science, vol. 37, no. 7, pp. 1085-1096. doi:10.1016/0010-938X(95)00016-D

[19] Chen, G., Palmer, R. J., White, D. C. (1997). "Instrumental analysis of microbiologically influenced corrosion". Biodegradation, vol. 8, no. 3, pp. 189-200. doi:10.1023/A:1008229419434

[20] Little, B. J., Lee, J. S., Ray, R. I. (2006). "Diagnosing microbiologically influenced corrosion: A state-of-the-art review". Corrosion, vol. 62, no. 11, pp. 1006-1017. doi:10.5006/1.3278228

[21] Wang, W., Wang, J., Xu, H., Li, X. (2006). "Some multidisciplinary techniques used in MIC studies". Materials and Corrosion, vol. 57, no. 7, pp. 531-537. doi:10.1002/maco.200503951

[22] Heydorn, A., Nielsen, A. T., Hentzer, M., Sternberg, C., Givskov, M., Ersboll, B. K., Molin, S. (2000). "Quantification of biofilm structures by the novel computer program COMSTAT". Microbiology, vol. 146, no. 10, pp. 2395-2407. doi:10.1099/00221287-146-10-2395

[23] Larimer, C., Winder, E., Jeters, R., Prowant, M., Nettleship, I., Addleman, R. S., Bonheyo, G. T. (2016). "A method for rapid quantitative assessment of biofilms with biomolecular staining and image analysis". Analytical and Bioanalytical Chemistry, vol. 408, no. 3, pp. 999-1008. doi:10.1007/s00216-015-9195-z

[24] Heuer, W., Elter, C., Demling, A., Neumann, A., Suerbaum, S., Hannig, M.,

Stiesch-Scholz, M. (2007). "Analysis of early biofilm formation on oral implants in man". Journal of Oral Rehabilitation, vol. 34, no. 5, pp. 377-382. doi:10.1111/j.1365-2842.2007.01725.x

[25] Demling, A., Heuer, W., Elter, C., Heidenblut, T., Bach, F., Schwestka-Polly, R., Stiesch-Scholz, M. (2009). "Analysis of supra- and subgingival long-term biofilm formation on orthodontic bands". European Journal of Orthodontics, vol. 31, no. 2, pp. 202-206. doi:10.1093/ejo/cjn090

[26] Vyas, N., Sammons, R. L., Addison, O., Dehghani, H., Walmsley, A. D. (2016). "A quantitative method to measure biofilm removal efficiency from complex biomaterial surfaces using SEM and image analysis". Scientific Reports, vol. 6. doi:10.1038/srep32694

[27] Iannucci, L., Parvis, M., Grassini, S., Angelini, E., Cristiani, P., Ferrero, R. (2018). "A microbial fuel cell measuring system for corrosion assessment". I2MTC 2018 - 2018 IEEE International Instrumentation and Measurement Technology Conference: Discovering New Horizons in Instrumentation and Measurement, Proceedings, pp. 1-5. doi:10.1109/I2MTC.2018.8409779

[28] Iannucci, L., Parvis, M., Cristiani, P., Ferrero, R., Angelini, E., Grassini, S. (2019). "A Novel Approach for Microbial Corrosion Assessment". IEEE Transactions on Instrumentation and Measurement, vol. 68, no. 5, pp. 1424-1431. doi:10.1109/TIM.2019.2905734

[29] Deshmukh, M.B., Akhtar, I., Srivastava, R.B., Karande, A.A. (1992). "Marine aerobic and anaerobic bacteria inducing corrosion of 304 stainless steel". Biofouling, vol. 6, no. 1, pp. 13-32. doi:10.1080/08927019209386206

[30] Jia, R., Yang, D., Xu, D., Gu, T. (2017). "Anaerobic corrosion of 304 stainless steel caused by the Pseudomonas aeruginosa biofilm". Frontiers in Microbiology, vol. 8, no. NOV, 2335. doi:10.3389/fmicb.2017.02335

[31] Yuan, S., Liang, B., Zhao, Y., Pehkonen, S.O. (2013). "Surface chemistry and corrosion behaviour of 304 stainless steel in simulated seawater containing inorganic sulphide and sulphate-reducing bacteria". Corrosion Science, vol. 74, pp. 353-366. doi:10.1016/j.corsci.2013.04.058

[32] Zhang, Q., Wang, P., Zhang, D. (2012). "Stainless steel electrochemical corrosion behaviors induced by sulphate-reducing bacteria in different aerated conditions". International Journal of Electrochemical Science, vol. 7, no. 11, pp. 11528-11539.

[33] Rousseau, R., Santaella, C., Bonnafous, A., Achouak, W., Godon, J.-J., Delia, M. L., Bergel, A. (2016). "Halotolerant bioanodes: The applied potential modulates the electrochemical characteristics, the biofilm structure and the ratio of the two dominant genera." Bioelectrochemistry, vol. 112, pp. 24-32. doi:10.1016/j.bioelechem.2016.06.006

[34] Rousseau, R., Santaella, C., Achouak, W., Godon, J.-J., Bonnafous, A., Bergel, A., Délia, M.-L. (2014). "Correlation of the electrochemical kinetics of high-salinity-tolerant bioanodes with the structure and microbial composition of the biofilm". ChemElectroChem, vol. 1, no. 11, pp. 1966-1975. doi:10.1002/celc.201402153

[35] Little, B. J., Wagner, P. A. (1994). "Advances in MIC testing". In *Microbiologically Influenced Corrosion Testing*. Philadelphia, PA, USA: ASTM STP, 1-11.

[36] Ilhan-Sungur, E., Çotuk, A. (2010). "Microbial corrosion of galvanized steel in a simulated recirculating cooling tower system". Corrosion Science, vol. 52, no. 1, pp. 161-171. doi:10.1016/j.corsci.2009.08.049

[37] Little, B. J., Wagner, P. A. (2001). "Application of electrochemical techniques to the study of microbiologically influenced corrosion". In *Modern Aspects of Electrochemistry*, vol. 34, pp. 205-246.

[38] Rabaey, K., Verstraete, W. (2005). "Microbial fuel cells: Novel biotechnology for energy generation". Trends in biotechnology, vol. 23, no. 6, pp. 291-298. doi:10.1016/j.tibtech.2005.04.008

[39] Oliveira, V. B., Simões, M., Melo, L. F., Pinto, A. M. F. R. (2013). "Overview on the developments of microbial fuel cells". Biochemical engineering journal, vol. 73, pp. 53-64. doi:10.1016/j.bej.2013.01.012

[40] Merino-Jimenez, I., Santoro, C., Rojas-Carbonell, S., Greenman, J., Ieropoulos, I., Atanassov, P. (2016). "Carbon-based air-breathing cathodes for microbial fuel cells". Catalysts, vol. 6, no. 9. doi:10.3390/catal6090127

[41] Santoro, C., Lei, Y., Li, B., Cristiani, P. (2012). "Power generation from wastewater using single chamber microbial fuel cells (MFCs) with platinum-free cathodes and pre-colonized anodes". Biochemical engineering journal, vol. 62, pp. 8-16. doi:10.1016/j.bej.2011.12.006

[42] Santoro, C., Artyushkova, K., Babanova, S., Atanassov, P., Ieropoulos, I., Grattieri, M., Schuler, A. J. (2014). "Parameters characterization and optimization of activated carbon (AC) cathodes for microbial fuel cell application". Bioresource technology, vol. 163, pp. 54-63. doi:10.1016/j.biortech.2014.03.091

[43] Cristiani, P., Carvalho, M. L., Guerrini, E., Daghio, M., Santoro, C., Li, B. (2013). "Cathodic and anodic biofilms in single chamber microbial fuel cells". Bioelectrochemistry, vol. 92, pp. 6-13. doi:10.1016/j.bioelechem.2013.01.005

[44] Liu, H., Logan, B. E. (2004). "Electricity generation using an air-cathode single chamber microbial fuel cell in the presence and absence of a proton exchange membrane". Environmental Science and Technology, vol. 38, no. 14, pp. 4040-4046. doi:10.1021/es0499344

[45] Nam, J., Kim, H., Lim, K., Shin, H. (2010). "Effects of organic loading rates on the continuous electricity generation from fermented wastewater using a single-chamber microbial fuel cell". Bioresource technology, vol. 101, no. 1 SUPPL., pp. S33-S37. doi:10.1016/j.biortech.2009.03.062

[46] Guerrini, E., Grattieri, M., Trasatti, S. P., Bestetti, M., Cristiani, P. (2014). "Performance explorations of single chamber microbial fuel cells by using various microelectrodes applied to biocathodes". International Journal of Hydrogen Energy, vol. 39, no. 36, pp. 21837-21846. doi:10.1016/j.ijhydene.2014.06.132

[47] Rago, L., Cristiani, P., Villa, F., Zecchin, S., Colombo, A., Cavalca, L., Schievano,

A. (2017). “Influences of dissolved oxygen concentration on biocathodic microbial communities in microbial fuel cells”. Bioelectrochemistry, vol. 116, pp. 39-51. doi:10.1016/j.bioelechem.2017.04.001

[48] Iannucci, L., Parvis, M., Di Francia, E., Grassini, S. (2018). “IHomeX: An internet-enabled laboratory for long-term experiment management”. IEEE Transactions on Instrumentation and Measurement, vol. 67, no. 5, pp. 1142-1149. doi:10.1109/TIM.2017.2786740

[49] Grassini, S., Corbellini, S., Angelini, E., Ferraris, F., Parvis, M. (2015). “Low-cost impedance spectroscopy system based on a logarithmic amplifier”. IEEE Transactions on Instrumentation and Measurement, vol. 64, no. 5, pp. 1110-1117. doi:10.1109/TIM.2014.2371191

[50] Carullo, A., Ferraris, F., Parvis, M., Vallan, A., Angelini, E., Spinelli, P. (2000). “Low-cost electrochemical impedance spectroscopy system for corrosion monitoring of metallic antiquities and works of art”. IEEE Transactions on Instrumentation and Measurement, vol. 49, no. 2, pp. 371-375. doi:10.1109/19.843080

[51] Kuo, Y., Lee, C., Lee, Y. (2018). “Compact coating impedance detector for fast evaluation of coating degradation”. Measurement: Journal of the International Measurement Confederation, vol. 124, pp. 303-308. doi:10.1016/j.measurement.2018.04.041

[52] Iannucci, L., Lombardo, L., Parvis, M., Cristiani, P., Basseguy, R., Angelini, E., Grassini, S. (2019). “An imaging system for microbial corrosion analysis”. I2MTC 2019 - 2019 IEEE International Instrumentation and Measurement Technology Conference, Proceedings, pp. 1-6. doi:10.1109/I2MTC.2019.8826965

[53] Iannucci, L., Lombardo, L., Parvis, M., Angelini, E., Sangermano, M., Grassini, S. (2019). “An imaging approach to assess the antimicrobial behavior of Ag-doped organic coatings”. 2019 IEEE International Symposium on Medical Measurements and Applications (MeMeA), Proceedings, pp. 1-5. doi:10.1109/MeMeA.2019.8802128

[54] Caines, S., Khan, F., Shirokoff, J. (2013). “Analysis of pitting corrosion on steel under insulation in marine environments”. Journal of Loss Prevention in the Process Industries, vol. 26, no.6, pp. 1466-1483. doi:10.1016/j.jlp.2013.09.010

[55] Codaro, E. N., Nakazato, R. Z., Horovistiz, A. L., Ribeiro, L. M. F., Ribeiro, R. B., Hein, L. R. O. (2002). “An image processing method for morphology characterization and pitting corrosion evaluation”. Materials Science and Engineering A, vol. 334, no. 1-2, pp. 298-306. doi:10.1016/S0921-5093(01)01892-5

[56] Codaro, E. N., Nakazato, R. Z., Horovistiz, A. L., Ribeiro, L. M. F., Ribeiro, R. B., Hein, L. R. O. (2003). “An image analysis study of pit formation on Ti-6Al-4V”. Materials Science and Engineering A, vol. 341, pp. 202-210.

[57] Pereira, M. C., Silva, J. W. J., Acciari, H. A., Codaro, E. N., Hein, L. R. O. (2012). “Morphology characterization and kinetics evaluation of pitting corrosion of commercially pure aluminium by digital image analysis”. Materials Sciences and Applications, vol. 3, no. 5, pp. 287-293.

[58] Holme, B., Lunder, O. (2007). "Characterisation of pitting corrosion by white light interferometry". Corrosion Science, vol. 49, no. 2, pp. 391-401. doi:10.1016/j.corsci.2006.04.022

[59] Jang, P. R., Arunkumar, R., Lindner, J. S. (2007). "Evaluation of aluminium pit corrosion in oak ridge research reactor pool by quantitative imaging and thermodynamic modeling". Proceedings of the 11th International ICEM Conference.

[60] Li, H., Zhou, E., Zhang, D., Xu, D., Xia, J., Yang, C., Yang, K. (2016). "Microbiologically influenced corrosion of 2707 hyper-duplex stainless steel by marine pseudomonas aeruginosa biofilm". Scientific Reports, vol. 6, pp. 1-12. doi:10.1038/srep20190

[61] Mystkowska, J., Ferreira, J. A., Leszczyńska, K., Chmielewska, S., Dąbrowski, J. R., Wieciński, P., Kurzydlowski, K. J. (2017). "Biocorrosion of 316LV steel used in oral cavity due to desulfotomaculum nigrificans bacteria". Journal of Biomedical Materials Research - Part B Applied Biomaterials, vol. 105, no-1, pp. 222-229. doi:10.1002/jbm.b.33518

[62] Heydorn, A., Nielsen, A. T., Hentzer, M., Sternberg, C., Givskov, M., Ersboll, B. K., Molin, S. (2000). "Quantification of biofilm structures by the novel computer program COMSTAT". Microbiology, vol. 146, no.10, pp. 2395-2407. doi:10.1099/00221287-146-10-2395

[63] Karygianni, L., Follo, M., Hellwig, E., Burghardt, D., Wolkewitz, M., Anderson, A., Al-Ahmad, A. (2012). "Microscope-based imaging platform for large-scale analysis of oral biofilms". Applied and Environmental Microbiology, vol. 78, no. 24, pp. 8703-8711. doi:10.1128/AEM.02416-12

[64] Thormann, K. M., Saville, R. M., Shukla, S., Pelletier, D. A., Spormann, A. M. (2004). "Initial phases of biofilm formation in shewanella oneidensis MR-1". Journal of Bacteriology, vol. 186, no. 23, pp. 8096-8104. doi:10.1128/JB.186.23.8096-8104.2004

[65] Hannig, C., Follo, M., Hellwig, E., Al-Ahmad, A. (2010). "Visualization of adherent micro-organisms using different techniques". Journal of Medical Microbiology, vol. 59, no. 1, pp. 1-7. doi:10.1099/jmm.0.015420-0

[66] Lombardo, L., Parvis, M., Angelini, E., Grassini, S. (2018). "An Optical Sampling System for Distributed Atmospheric Particulate Matter". IEEE Transactions on Instrumentation and Measurement, vol. 68, no. 7, pp. 2396-2403. doi:10.1109/TIM.2019.2890885

[67] Li, Q., Chen, X., Zhang, H., Yin, L., Chen, S., Wang, T., Zhang, R. (2012). "Automatic human spermatozoa detection in microscopic video streams based on OpenCV". 5th International Conference on Biomedical Engineering and Informatics, BMEI 2012, pp. 224-227. doi:10.1109/BMEI.2012.6513003

[68] Grassini, S., Pisano, R., Barresi, A. A., Angelini, E., Parvis, M. (2016). "Frequency domain image analysis for the characterization of porous products". Measurement: Journal of the International Measurement Confederation, vol. 94, pp. 515-522. doi:10.1016/j.measurement.2016.08.031

[69] Zelinsky, A. (2009). "Learning OpenCV—Computer vision with the OpenCV

library". IEEE Robotics and Automation Magazine, vol. 16, no.3, pp. 100. doi:10.1109/MRA.2009.933612

[70] Bradski, G. (2000). "The OpenCV Library". Dr. Dobb's Journal of Software Tools. Available at https://github.com/opencv/opencv, last checked on Nov. 3rd, 2018

[71] Iannucci, L., Ríos-Rojas, J. F., Angelini, E., Parvis, M., Grassini, S. (2018). "Electrochemical characterization of innovative hybrid coatings for metallic artefacts". European Physical Journal Plus, vol. 133, no. 12, pp. 1-7 doi:10.1140/epjp/i2018-12368-3

[72] Periolatto, M., Di Francia, E., Sangermano, M., Grassini, S., Spena, P. R. (2017). "Advanced epoxy-based anticorrosion coatings containing graphite oxide". doi:10.1007/978-3-319-50784-2 11

[73] Sangermano, M., Yagci, Y., Rizza, G. (2007). "In situ synthesis of silver-epoxy nanocomposites by photoinduced electron transfer and cationic polymerization processes". Macromolecules, vol. 40, no. 25, pp. 8827-8829. doi:10.1021/ma702051g

[74] Meng, Y., Xu, X., Li, H., Wang, Y., Ding, E., Zhang, Z., Geng, H. (2014). "Optimisation of carbon nanotube ink for large-area transparent conducting films fabricated by controllable rod-coating method". Carbon, vol. 70, pp. 103-110. doi:10.1016/j.carbon.2013.12.078

[75] Dan, B., Irvin, G. C., Pasquali, M. (2009). "Continuous and scalable fabrication of transparent conducting carbon nanotube films". ACS Nano, vol. 3, no. 4, pp. 835-843. doi:10.1021/nn8008307

[76] Amerio, E., Sangermano, M., Malucelli, G., Priola, A., Rizza, G. (2006). "Preparation and characterization of hyperbranched polymer/silica hybrid nanocoatings by dual-curing process". Macromolecular Materials and Engineering, vol. 291, no. 10, pp. 1287-1292. doi:10.1002/mame.200600216

[77] Stankovich, S., Dikin, D. A., Dommett, G. H. B., Kohlhaas, K. M., Zimney, E. J., Stach, E. A., . Ruoff, R. S. (2006). "Graphene-based composite materials". Nature, vol. 442, no. 7100, pp. 282-286. doi:10.1038/nature04969

[78] Stankovich, S., Piner, R. D., Nguyen, S. T., Ruoff, R. S. (2006). "Synthesis and exfoliation of isocyanate-treated graphene oxide nanoplatelets". Carbon, vol. 44, no. 15, pp. 3342-3347. doi:10.1016/j.carbon.2006.06.004

[79] Kahanda, G. L. M. K. S., Tomkiewicz, M. (1990). "Fractality and impedance of electrochemically grown silver deposits". Journal of the Electrochemical Society, vol. 137, no. 11, pp. 3423-3429. doi:10.1149/1.2086233

[80] Barsoukov, E., Macdonald, J. R. (2005). "Impedance spectroscopy: Theory, experiment, and applications". pp. 1-595. doi:10.1002/0471716243

[81] Souto, R. M., González-García, Y., González, S. (2009). "Characterization of coating systems by scanning electrochemical microscopy: Surface topology and blistering". Progress in Organic Coatings, vol. 65, no. 4, pp. 435-439. doi:10.1016/j.porgcoat.2009.03.008

[82] Hayatgheib, Y., Ramezanzadeh, B., Kardar, P., Mahdavian, M. (2018). "A comparative study on fabrication of a highly effective corrosion protective system based

on graphene oxide-polyaniline nanofibers/epoxy composite". Corrosion Science, vol. 133, pp. 358-373. doi:10.1016/j.corsci.2018.01.046

[83] Zheng, H., Guo, M., Shao, Y., Wang, Y., Liu, B., Meng, G. (2018). "Graphene oxide–poly(urea–formaldehyde) composites for corrosion protection of mild steel". Corrosion Science, vol. 139, pp. 1-12. doi:10.1016/j.corsci.2018.04.036

[84] Bharadwaj, R. K. (2001). "Modeling the barrier properties of polymer-layered silicate nanocomposites". Macromolecules, vol. 34, no. 26, pp. 9189-9192. doi:10.1021/ma010780b

[85] Sangermano, M., Periolatto, M., Signore, V., Russo Spena, P. (2017). "Improvement of the water-vapor barrier properties of an uv-cured epoxy coating containing graphite oxide nanoplatelets". Progress in Organic Coatings, vol. 103, pp. 152-155. doi:10.1016/j.porgcoat.2016.10.032

[86] Sangermano, M., Malucelli, G., Amerio, E., Priola, A., Billi, E., Rizza, G. (2005). "Photopolymerization of epoxy coatings containing silica nanoparticles". Progress in Organic Coatings, vol. 54, no. 2, pp. 134-138. doi:10.1016/j.porgcoat.2005.05.004

This Ph.D. thesis has been typeset by means of the TEX-system facilities. The typesetting engine was LuaLATEX. The document class was `toptesi`, by Claudio Beccari, with option `tipotesi =scudo`. This class is available in every up-to-date and complete TEX-system installation.